

The Messenger



No. 159 – March 2015

Science Verification of SPHERE
VISIR recommissioned
PIONIER study of exozodiacal dust
Polarised emission from the Galactic Centre



SPHERE Science Verification

Bruno Leibundgut¹
 Jean-Luc Beuzit²
 Neale Gibson¹
 Julien Girard¹
 Markus Kasper¹
 Florian Kerber¹
 Lars Lundin¹
 Dimitri Mawet¹
 Melissa McClure¹
 Julien Milli¹
 Monika Petr-Gotzens¹
 Ralf Siebenmorgen¹
 Mario van den Ancker¹
 Zahed Wahhaj¹

¹ ESO

² Institut de Planétologie et
 d'Astrophysique de Grenoble (IPAG),
 France

Science Verification (SV) for the latest instrument to arrive on Paranal, the high-contrast and spectro-polarimetric extreme adaptive optics instrument SPHERE, is described. The process through which the SV proposals were solicited and evaluated is briefly outlined; the resulting observations took place in December 2014 and February 2015. A wide range of targets was observed, ranging from the Solar System, young stars with planets and discs, circumstellar environments of evolved stars to a galaxy nucleus. Some of the first results are previewed.

The Spectro-Polarimetric High-contrast Exoplanet Research (SPHERE) is the new Very Large Telescope (VLT) extreme adaptive optics instrument (Beuzit et al., 2006; Kasper et al., 2012). SPHERE provides on-axis diffraction-limited observations (imaging, spectroscopy and polarimetry) from optical to near-infrared wavelengths in combination with various coronagraphic facilities. The common path and infrastructure (CPI) of SPHERE provides an adaptive optics (AO) corrected and coronagraphic beam to the three sub-instruments: the near-infrared integral field spectrograph (IFS); the infrared dual-beam imager and spectrograph (IRDIS); and the visible light Zurich Imaging Polarimeter (ZIMPOL).

Following the commissioning activities, as part of the transition to operations, all Paranal instruments undergo a Science Verification phase where scientific observations are carried out by a dedicated ESO team to test the end-to-end operations of a new instrument. The SPHERE SV took place from 4–11 December 2014 (eight full nights) and 9–12 February 2015 (four half nights). The SV runs were very successful, with some spectacular results, and one has already appeared in print (on the lack of a brown dwarf around V471 Tau, by Hardy et al. [2015]). We could complete 24 programmes and declared a further four programmes finished with sufficient data for a scientific analysis. Eight programmes received partial data — in several cases complete datasets on individual objects — although we could not obtain data for all the requested targets. The remaining four programmes were not observed. The total observed time expended for the approved programmes was 68 hours.

Proposal solicitation and submission

The call for SPHERE Science Verification proposals was issued on 19 September 2014¹ and was advertised through the ESO Science Newsletter issued on 22 September 2014². With the call, the SPHERE SV web page³ was launched. The deadline for observing proposals was 15 October 2014 and a total of 67 proposals was received.

The SPHERE SV team evaluated all proposals and the selection was discussed at a video conference. Care was taken to clarify any possible overlap with Guaranteed Time Observations (GTO) and proposed Period 95 (P95) observing programmes. For the latter, it was decided to reject all SV proposals which requested the same targets and observing modes as a P95 proposal, removing seven SV proposals. The cut-off line was defined at 88 hours of allocated time, which meant that 40 programmes received a time allocation. The approval of the selected proposals (announced 11 November 2014) was followed by a short and intensive Phase 2 period during which all principal investigators (PIs) had to prepare their observations in detail and submit them to the ESO User Support Department for

final review. By 3 December 2014 all 40 programmes were ready to go, awaiting their execution during the following week.

A wide range of science topics was proposed, including the imaging and spectroscopy of Solar System objects (companions of asteroids, shapes of asteroids, moons of Jupiter), exoplanetary systems, protoplanetary and debris discs around young stars, the binarity of brown dwarfs, the environment of evolved stars, SN 1987A and the nearby active galactic nucleus NGC 1068.

Observations

The observations were executed in service mode, giving priority to the programmes with the highest scientific ranking among those matching the required weather conditions. The target distribution was heavily concentrated in the right ascension (RA) range from 4 hours < RA < 6 hours with only few targets at the end of the night (see Figure 1). Modifications to the scientific ranking were necessary in regions where there were only a few Observing Blocks (OBs) available and hence lower ranked proposals were observed. Conversely, in RA regions with a high pressure, some higher ranked proposals could not be observed in the available time.

The weather conditions during the SV run were mostly good to excellent. Out of the eight nights in December 2014, there were two nights with cirrus and parts of two nights with wind restrictions. During the February 2015 run, two nights were lost to clouds and high humidity. The instrument worked without major faults and we experienced no major loss for technical reasons. The resulting data are of excellent quality and in almost all cases we were able to obtain unique high-contrast observations. All SPHERE modes were used during SV and all worked to expectation.

The complex SPHERE extreme AO (SAXO) / Standard Platform for Adaptive optics Real Time Applications (SPARTA) adaptive optics system proved to be reliable in operations and observational issues could be easily solved. Based on our SV experience, we can confirm that

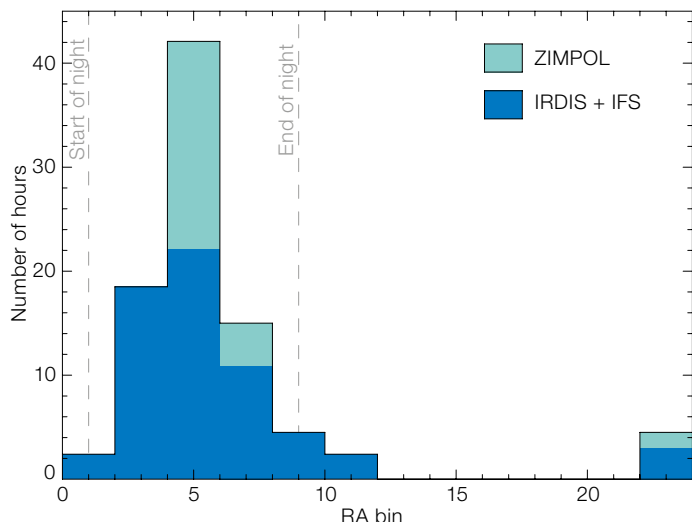
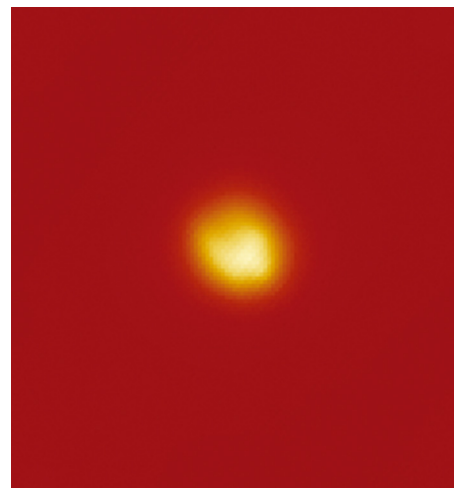


Figure 1. (Left) The distribution of the allocated SV targets in RA.

Figure 2. (Right) A SPHERE image of R Doradus — the largest star in the sky after the Sun. This V-band image taken with ZIMPOL shows R Dor, which has a diameter of 57 milli-arcseconds. The surface is clearly not smooth and shows large star spots.



the guide probe “seeing” is a good indicator for performance prediction and quality control (QC0). Above a full width half maximum (FWHM) of 1.2 arcseconds on the guide probe the AO system struggles. On the other hand, we managed to operate in photon-counting mode on rather faint natural guide stars, although with significantly degraded AO performance.

Archive and data processing

All raw data have been archived and are publicly available. The SPHERE SV webpage³ contains direct links to the SV raw data. A link to a pre-release of the SPHERE pipeline is also provided on the SV webpage. The pipeline is mostly functional.

First scientific results

The following provides a sample of some preliminary results obtained during SPHERE SV and demonstrates the scientific promise of SPHERE.

Resolving the surfaces of stars has not so far been possible with direct imaging. During SPHERE SV, the largest apparent diameter star in the sky after the Sun, R Doradus (diameter 57 milliarcseconds), was observed with ZIMPOL (Figure 2) and the V-band image displays large structures on the stellar surface. R-Dor is a Mira variable and one can easily imagine that monitoring the surface features

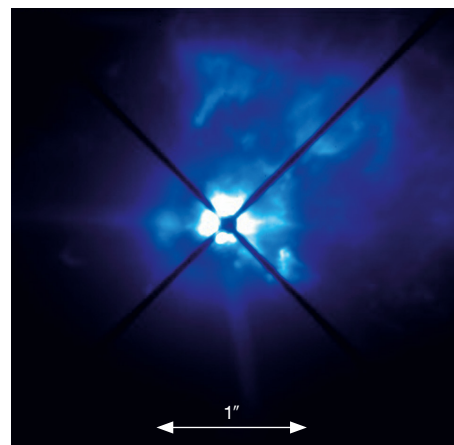
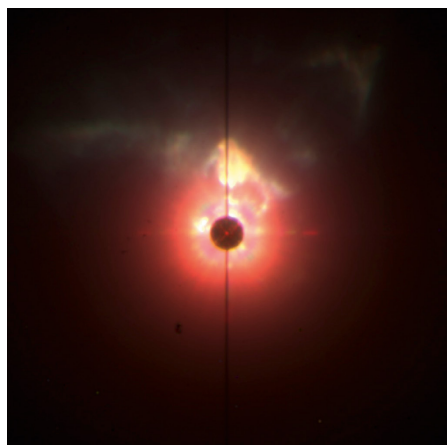
on R Dor, and similar giants, will yield further information on such evolved stars.

VY CMa, a red hypergiant star at a distance of 1.3 kpc, is one of the most massive ($18 M_{\odot}$) and most luminous ($2.7 \times 10^5 L_{\odot}$) nearby stars. VY CMa is losing the equivalent of 30 Earth masses per year. The ejected matter now constitutes the nebula seen in the high-contrast images of SPHERE (Figure 3; Scicluna & Siebenmorgen [2015] in prep.). The observations are key to understanding mass-loss phenomena in evolved stars. Mass loss in massive stars is thought to provide the interstellar medium with building blocks that have, are, and will eventually be, seeds of life in the Universe.

Figure 3 shows two images of VY CMa: on the left is an infrared multi-colour image obtained with IRDIS (field of view, 11 arcseconds on a side); the right-hand

image was obtained with ZIMPOL, the visible camera providing diffraction-limited images at scales as fine as 15 milli-arcseconds. Each feature in the image comes from a distinct mass-loss episode, similar to the Sun’s own coronal mass ejections, but on a much larger scale. The material visible in the images was ejected within the last 1000 years. Emission is only visible on the upper half of the image because dense matter blocks the rest. VY CMa is a candidate for a supernova: if the explosion occurs before the current nebula disperses a strong interaction between the supernova shock

Figure 3. Left: Colour-composite image of the out-flow around the evolved star VY CMa in the *JHK* filters. The image displays the full IRDIS field of view of 11 by 11 arcseconds. Right: Optical V-band image of VY CMa obtained with ZIMPOL. Note that the field of view is a fraction of the near-infrared image size (left) and shows nebular structure much closer to the star.



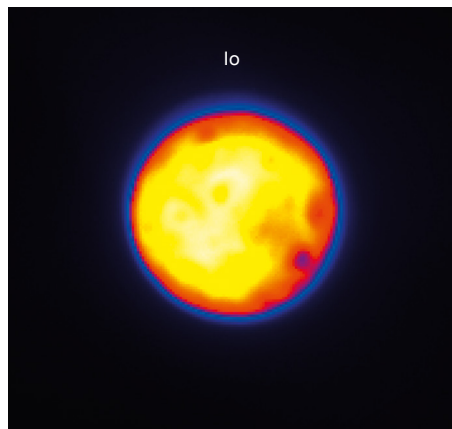
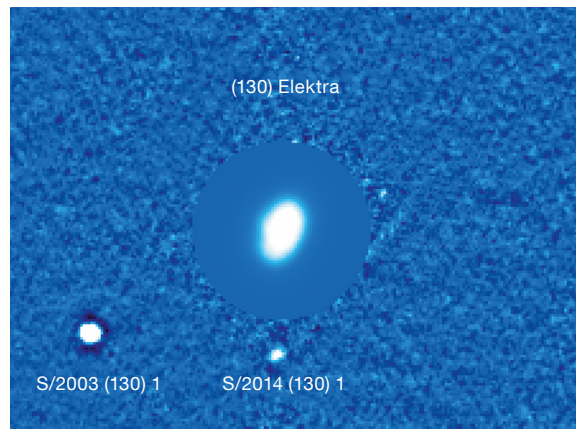


Figure 4. (Left) IRDIS *K* filter image of Jupiter's moon Io. The surface structure is clearly noticeable, with silica-rich hot spots attributed to geological activity. Using the IFS's capabilities, spectral mapping of these regions could be carried out.

Figure 5. (Right) The asteroid (130) Elektra with its satellites, observed with SPHERE IFS. The second (inner) satellite is a new discovery with SPHERE and received the preliminary designation S/2014 (130) S1. This represents the fifth known multiple system in the asteroid main belt.



Bin Yang, ESO

wave and the circumstellar material is expected, leading to a very bright super-nova due to the kinetic energy liberated in the shocks.

Within the Solar System, SPHERE can be used to map the surfaces of planets, moons or smaller bodies. Several Jovian moons were observed during SPHERE Science Verification at different times to obtain a full map of the surface of these objects. As an example, an image of Io is shown in Figure 4 and surface structures are easily visible. The full map of Io is being produced from a series of images at different rotational phases of the satellite (the rotational period is 1.77 days).

Two main belt asteroids with known satellites were observed in order to characterise the orbits. The observations of (130) Elektra yielded a new, second satellite to this asteroid, named S/2014 (130) S1 (Yang et al., 2014; see Figure 5). The image illustrates SPHERE's capability to observe faint objects close to bright sources. The adaptive optics correction was performed on the asteroids themselves, which are resolved at SPHERE's angular resolution, validating the effectiveness of the AO system for extended objects.

One of SPHERE's main goals is the direct observation of exoplanets. During SV this was demonstrated by observing the well-known planetary system around HR 8799. The planetary images could even be seen on the real-time display during the observations in the control room! The processed SPHERE *H*-band image displayed here (Figure 6) shows

the power of the instrument for high-contrast imaging. The removal of the fixed speckles reveals sources very close to the central (masked) star.

SPHERE also provides the option of high-contrast spectroscopy using a coronagraphic mask with IRDIS, covering in this case the *Y*- and *J*-bands. This capability was demonstrated by obtaining a spectrum of the brown dwarf companion to an M star (2MASS J01225093-2439505). The separation of the spectra is critical to allow the emission from the fainter source to be cleanly extracted without being swamped by the light of the bright primary star. The spectrum of the brown dwarf is displayed as the two-dimensional

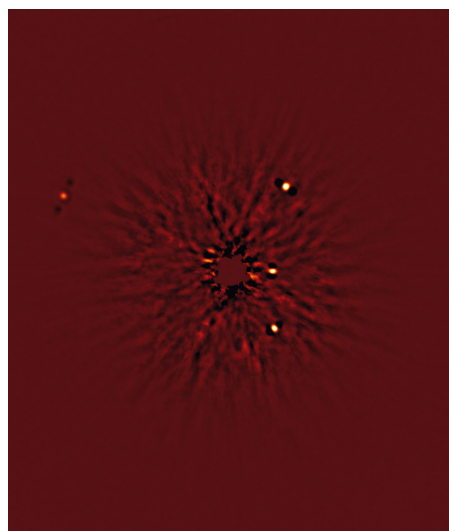


Figure 6. Four planets imaged with SPHERE around HR 8799. This is a processed image (in *H*-band), but the planets were also visible on the real-time display.

spectrum (wavelength runs vertically and the spatial direction is horizontal in the picture) in Figure 7.

Another popular application of SPHERE will be the direct imaging of discs around stars. We show here two very prominent examples of such discs. One is a face-on disc around the star MWC 758 where a strong spiral structure is detected in polarised light in the *Y* filter from the protoplanetary disc. The starlight has been suppressed by the coronagraph and the emission visible in Figure 8 stems from

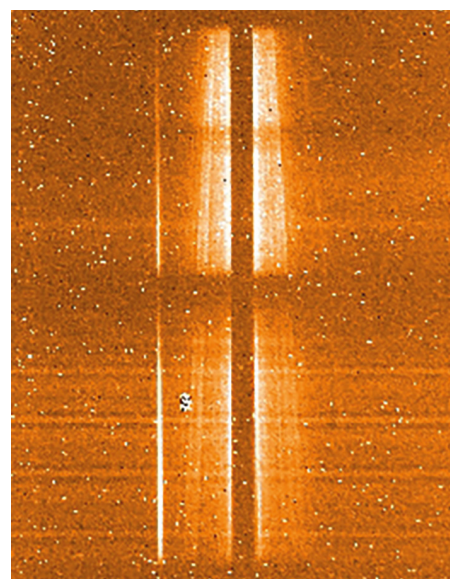


Figure 7. Spectrum display of a brown dwarf companion to the M star 2MASS J01225093-2439505 is shown. The spectrum is the bright, narrow, vertical line to the left of the M star spectrum. The coronagraph is the dark line covering the brightest parts of the M star spectrum.

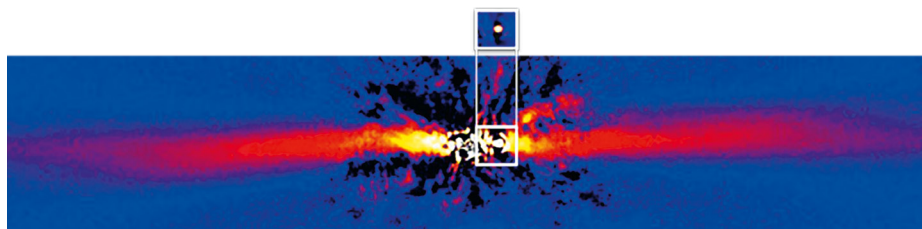
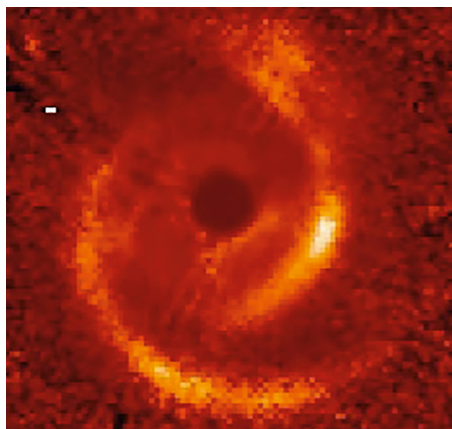


Figure 8. (Left) Spectacular spiral structure revealed around the star MWC758. This image shows the dust in the protoplanetary disc in polarised light, obtained with IRDIS in the Y filter.

Figure 9. (Above) The famous planetary system around β Pictoris imaged by SPHERE in a narrow K filter. The system harbours an edge-on debris disc with many asymmetries and distortions and a 10 Jupiter-mass planet currently at a projected separation of about 350 milliarcseconds from the star (shown by the different colour scale above). This image shows the full IRDIS field of view.

dust in the disc. The disc surface brightness is not uniform and probably indicates structure forming within the disc. The second example is the well-known massive disc around β Pictoris, shown in Figure 9. The detailed structure of the inner disc has been imaged with SPHERE and the (known) planet could be clearly observed. The narrowband K filter image of the debris disc reveals the warp and distortions in the inner disc.

Prospects

The above examples give only a small foretaste of the science we can expect

from SPHERE observations. The main topics will be exoplanet imaging and characterisation of planetary atmospheres. Circumstellar discs will also be favourite targets. But there are many other applications of high angular resolution and high-contrast imaging and spectroscopy that we can look forward to from SPHERE in the near future.

Acknowledgements

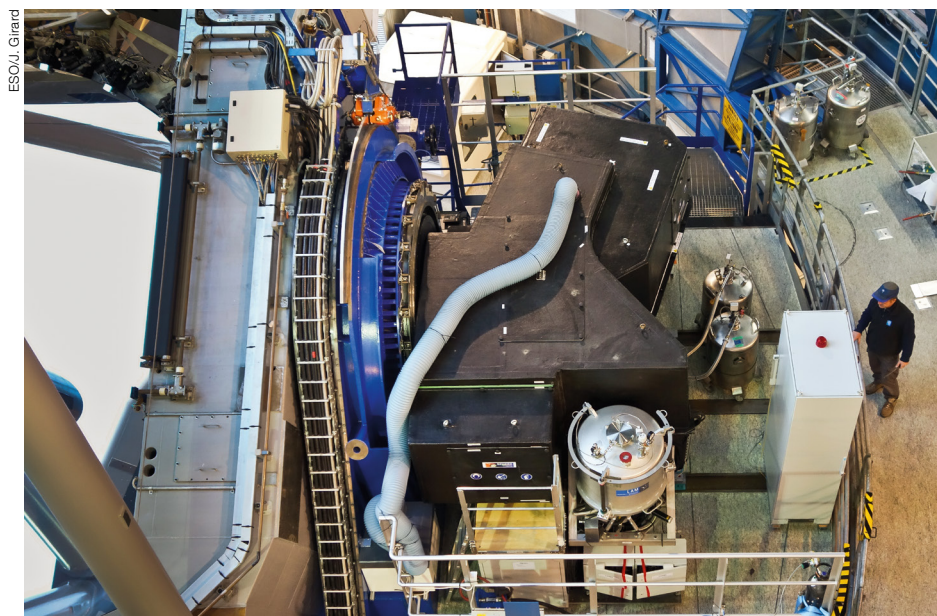
The team received extensive support from Alain Smette (VLT System Scientist) and the Telescope and Instrument Operators Claudia Reyes, Cristian Romero, Cristian Herrera, Sergio Vera and Ivan Aranda. The image for Figure 5 was kindly provided by Bin Yang.

References

- Beuzit, J.-L. et al. 2006, *The Messenger*, 125, 29
- Hardy, A. et al. 2015, *ApJ*, 800, L24
- Kasper, M. et al. 2012, *The Messenger*, 149, 17
- Yang, B. et al. 2014, *CBET*, 4035

Links

- ¹ Science announcement of SPHERE SV: <http://www.eso.org/sci/publications/announcements/sciann14047.html>
- ² SV announcement in Science Newsletter: <http://www.eso.org/sci/publications/newsletter/sep2014.html>
- ³ SPHERE SV webpage: <http://www.eso.org/sci/activities/vlts/spheresv.html>



The SPHERE instrument is shown shortly after it was installed on the VLT Unit Telescope 3 Nasmyth platform in May 2014. See Releases eso1417 and eso1506 for more detail.

Making FORS2 Fit for Exoplanet Observations (again)

Henri Boffin¹
 Guillaume Blanchard¹
 Oscar Gonzalez¹
 Sabine Moehler¹
 Elyar Sedaghati¹
 Neale Gibson¹
 Mario van den Ancker¹
 Jonathan Smoker¹
 Joseph Anderson¹
 Christian Hummel¹
 Danuta Dobrzycka¹
 Alain Smette¹
 Gero Rupprecht¹

¹ ESO

For about three years, it has been known that precision spectrophotometry with FORS2 suffered from systematic errors which made quantitative observations of planetary transits impossible. We identified the longitudinal atmospheric dispersion corrector (LADC) as the most likely culprit, and therefore engaged in a project to exchange the LADC prisms with the uncoated ones from FORS1. This led to a significant improvement in the depth of the FORS2 zero points, a reduction in the systematic noise, and should make FORS2 competitive again for transmission spectroscopy of exoplanets.

Over the last two decades remarkable progress has been made in understanding the diversity of planets in the Galaxy from the success of radial velocity and transit surveys. Transiting planets allow both their masses (if radial velocities are also available) and radii to be measured, leading to bulk densities and compositions. However, in order to truly understand planetary systems we need a method of obtaining the spectra of exoplanets, thereby probing the composition and structure of their atmospheres. Luckily, transiting systems allow such measurements, even though we cannot resolve the star and planet spatially; rather we can temporally resolve light from the star and planet during transits, when the planet passes in front of its host.

The transit depth obtained by transmission spectroscopy of the host star provides a direct measurement of the planet-to-star

radius ratio as a function of wavelength. The effective size of the planet varies due to wavelength-dependent opacities in the planet's upper atmosphere, and a transmission spectrum can therefore probe the atomic and molecular species in its atmosphere causing such radius variations (Seager & Sasselov, 2000; Brown, 2001; for a recent review, see Burrows, 2014). For many years, space-based observations with the Hubble Space Telescope (HST) and Spitzer Space Telescope were the only source of exoplanet spectra.

This all changed after pioneering observations of the exoplanet GJ 1214b using the Focal Reducer / low dispersion Spectrograph (FORS2) instrument proved that precise transmission spectra could be obtained from ground-based instruments (Bean et al., 2010). Their paper used the FORS2 multi-object spectroscopy capability with the mask exchange unit (MXU) to perform differential spectrophotometry, i.e., observing time-series spectra of the target star simultaneously with many comparison stars, thus correcting for variations in the Earth's atmospheric throughput. Since then, such observations have been performed routinely using different instruments and telescopes, and have even proved successful at infrared wavelengths (e.g., Snellen et al., 2010; Bean et al., 2011; Gibson et al., 2013a,b; Crossfield et al., 2013;

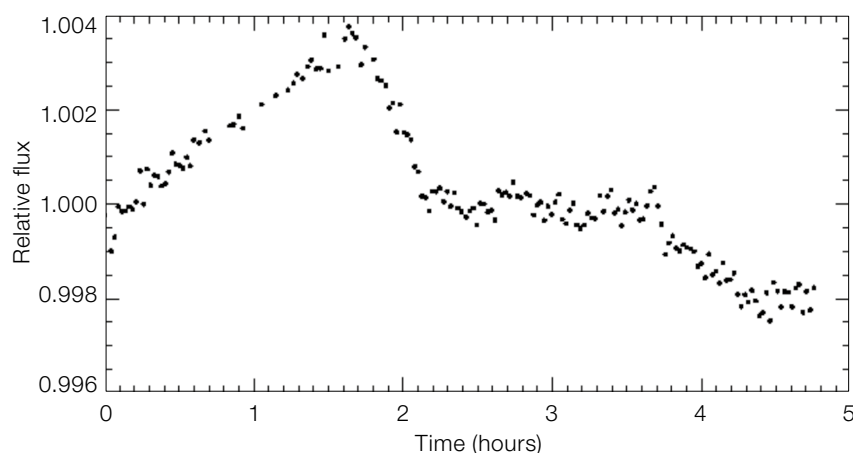
Stevenson et al., 2013; Schlawin et al., 2014). As future space-based observatories will focus on the infrared, ground-based instrumentation will be the only way to probe the optical transmission spectra of exoplanets. This is a crucial wavelength regime for the understanding of the physics of exoplanet atmospheres, and in particular for the determination of the mean molecular weight of the atmosphere and atmospheric scale height from measuring the Rayleigh scattering slope.

A cause for alarm

Despite the pioneering observations by Bean et al. (2010; re-analysed in Bean et al., 2011), no other exoplanet transit has been published so far from FORS2 data and it seems that there is a consensus in the community that FORS2 is no longer suited for the study of planetary transits. The fact that Bean et al. were successful in their observations is thought to be due to a combination of factors, i.e., short transit time, small variations in airmass during the observations, good weather, and more generally, the best of luck and great skill. This is of course a worrying situation, especially since the Gemini Multi-Object Spectrograph (GMOS) instruments on the Gemini telescopes, which are rather similar to FORS2, are among the most successful instruments to date for measuring transmission spectra from the ground (Gibson et al., 2013a, b; Crossfield et al., 2013).

The reason for this problem with FORS2 appears to lie with the unexpectedly high systematics in the differential light curves

Figure 1. Differential light curve of the source WASP 4 obtained in the z-band using FORS2 in MXU mode in December 2011. Most of the variations seen in this plot are attributed to variations in throughput within the FORS2 LADC.



that were obtained, which turned out to be impossible to calibrate out reliably (at least to the level of $\sim 10^{-4}$ as required in the transit depth precision for a hot Jupiter; see Figure 1). The main source of these instrumental systematics is most likely the LADC on FORS2. From visual inspection, the anti-reflection coating of this optical element is known to have degraded over time. Berta et al. (2011) reported these systematics: “Moehler et al. (2010) found that the LADC on the telescope has surface features that affect its sensitivity across the field of view. Because the LADC is positioned before the field rotator in the optical path and rotates relative to the sky, individual stars can drift across these features and encounter throughput variations that are not seen by the other comparison stars.”

The design of the FORS2 LADC consists of two prisms of opposite orientation that are moved linearly with respect to each other, between 30 mm (park position) and 1100 mm. The forward prism performs the dispersion correction, while the second prism corrects the pupil tilt, so that what remains is a variable image shift depending on the distance between the two prisms (Avila et al., 1997).

Exchanging the LADC prisms

The MgF_2 antireflection coatings of the FORS2 longitudinal atmospheric dispersion corrector prisms have degraded since 1999, following an attempt to clean them. They show a lot of scattering (see Figure 2). Since then, the LADC prisms have been cleaned several times in order to remove dust and paint (from the flat-field screen) that had led to further degradation. This degradation could be the cause of the systematics seen in the FORS2 transit data.

A damaged coating may introduce:

- transmission loss larger than an uncoated set of prisms;
- scattering, leading to a decreased signal-to-noise ratio on any photometric measurements;
- variability in the transmission caused by a change in the humidity level.

A project was started at Paranal to address this issue. One aspect was to

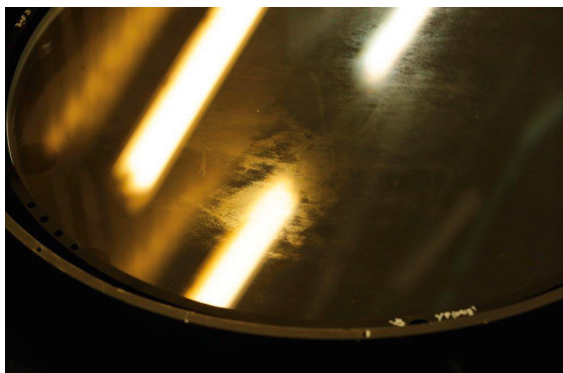


Figure 2. Photograph of the FORS2 LADC prism (with coating) after removal from the instrument. The damage to the coating in various places is obvious. Note that the bright regions are reflections of the neon lights on the ceiling.



Figure 3. Photograph taken during the removal of the coating on the FORS1 LADC prisms.

take advantage of the availability of spare parts from the twin instrument, FORS1, which is now decommissioned. We therefore decided to remove the coating from the prisms of the FORS1 LADC and exchange them with those previously in place in the FORS2 LADC. The removal of the damaged coating from the two prisms of the spare LADC was done by one of us (Blanchard; see Figure 3), using tools made of polyurethane and using cerium oxide (Opaline) for the polishing. The LADC prisms were then exchanged on 10 November 2014, while VLT Unit Telescope 1 (UT1) was undergoing maintenance.

A battery of tests

A set of test observations was performed according to a commissioning plan before (28–30 October 2014) and after (12–15 November 2014) the prism exchange. It is important to note that the coating of the primary mirror of UT1 had not been modified in the meantime,

so that any change detected should be due only to the LADC exchange. These tests have allowed us to conclude that the exchanged prisms did not affect the image quality of the instrument and confirmed that the LADC was still efficient at correcting the atmospheric dispersion up to an airmass of 1.6. On the other hand, the uncoated prisms led to an increase in the measured zero points (Figure 4): the implied gain in throughput is 0.12 (*B* filter), 0.08 (*V*), 0.06 (*R*) and 0.05 (*I*) magnitudes. This improvement was also confirmed by measurement of spectrophotometric standard stars before and after the prism exchange. The gain of the throughput can be explained by the scattering previously introduced by the damaged anti-reflective coating. The shortest wavelengths are more affected by the scattering, which is exactly what we see.

We have also measured the precision in the relative transmission between two stars as a function of time. For this measurement, we observed a given field of stars over about one hour (so that the

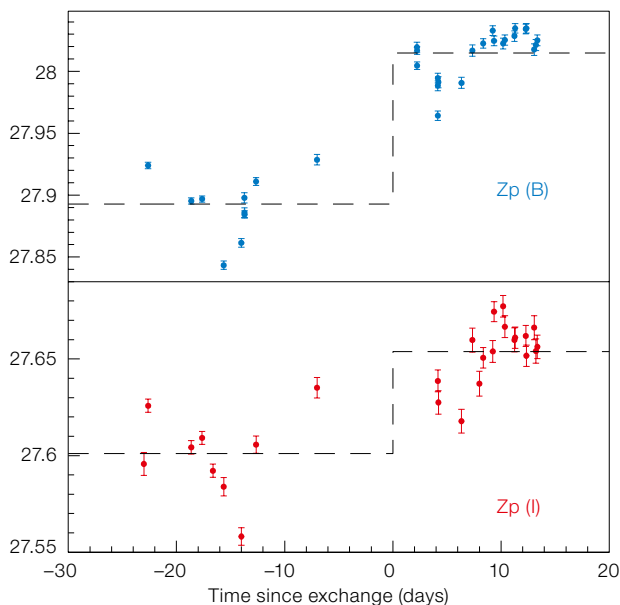


Figure 4. FORS2 zero points measured before and after the exchange of the prisms of the LADC in the *B*-band (upper) and in the *I*-band (lower). The figures clearly show the improvement in the zero points. The dashed curves indicate the mean values and highlight this improvement.

instrument rotator moved by more than 20 degrees). Observations were done in clear conditions in the *V*-band filter and the exposure time was 10 seconds. The magnitudes of some of the brightest non-saturated stars in the field were then measured for each frame, and we examined the dispersion in the light curves obtained of the stars (the sky variations were removed by subtracting the mean light curve of all stars and saturated stars were ignored). The fluxes of the selected stars were about 170 000–500 000 ADU. Sky flats were obtained close in time to the observations and the data were

reduced using the ESO FORS pipeline, with SExtractor being used for the photometry.

Before the LADCs were exchanged, on the night of 28 October 2014, we monitored the field around the standard star PG0231 for 50 minutes, during which time the rotator moved about 25 degrees. The airmass of the field was 1.0. After the LADC exchange, on the night of 13 November 2014, we monitored the standard star field around NGC 2298 for 78 minutes during which time the rotator moved 47 degrees; the airmass was 1.09.

Figure 5 shows that the dispersion of the points is clearly smaller after the LADC exchange, in comparison with the earlier measurements. The standard deviation of the light curves for a star with a signal-to-noise ratio (S/N) ~ 750 decreased from 3 milli-mag before the exchange to 1.9 milli-mag after the exchange. This is, however, still larger than we expected from the white noise, so there could still be some systematics in the data. The level of systematics would, however, need to be confirmed by a more detailed analysis, as the observations of the WASP-19b transit described below seem to indicate that the level is very small.

Back in business

The fact that the dispersion of points has decreased after the LADC exchange suggests that the removal of the coating has been beneficial and the study of exoplanet transits should once again be possible. However, this could only be checked on a real case to determine the achieved precision exactly. Thus, on the night of 15–16 November 2014, we observed the transit of WASP-19b between 2014-11-16 05:16 UT and 08:49 UT (Prog. ID: 60.A-9203(F); data publicly available in the ESO Science Archive) under thin cirrus, and with the LADC parked and in simulation, as is usually done for such observations. WASP-19b was chosen as previous observations with FORS2

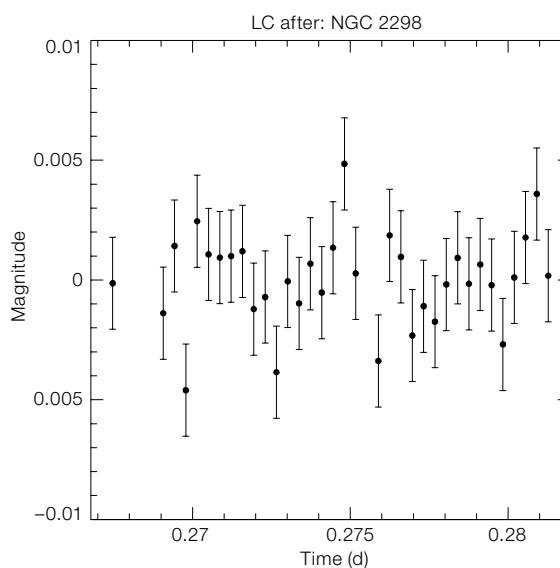
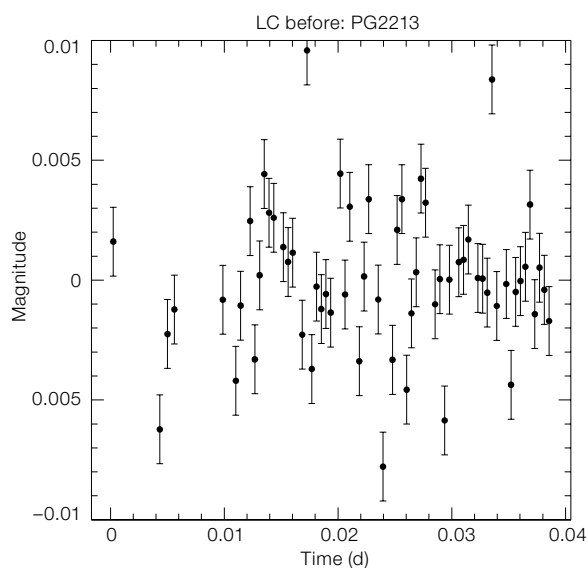


Figure 5. Light curves in the *V*-band for a relatively bright star with an $S/N \sim 750$ obtained before (left) and after (right) the LADC prisms were exchanged.

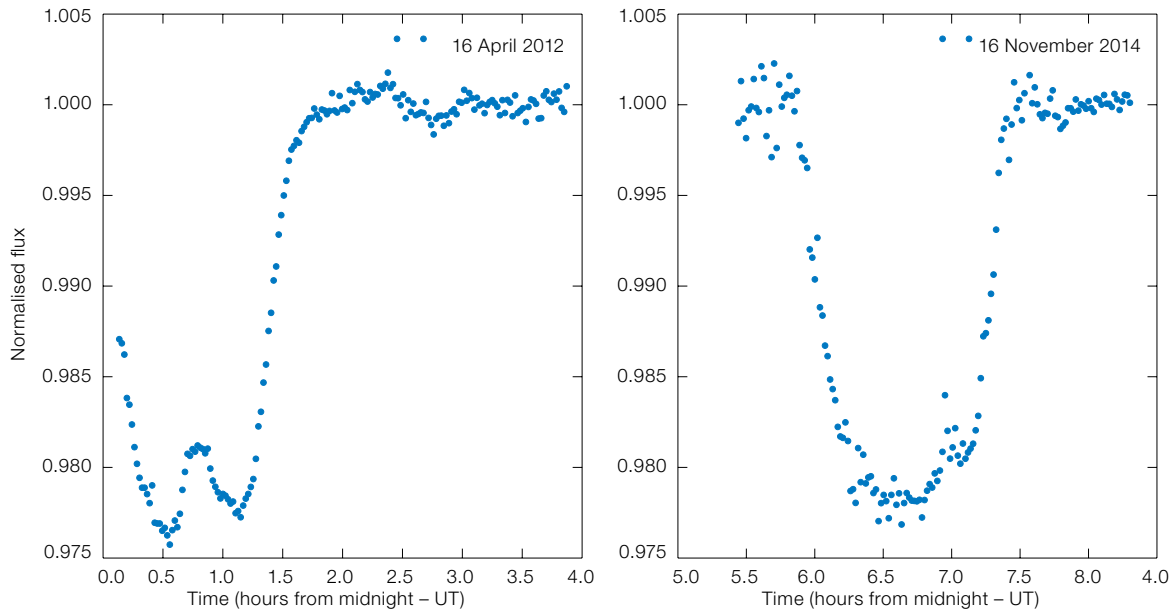


Figure 6. Light curve of WASP-19 obtained in April 2012, i.e., before the LADC prism exchange (left) and in November 2014, after the exchange (right), using the 600RI grism and integrating the spectra over the full wavelength domain (“white light”). Large systematics in the middle of the transit in 2012 are clearly visible.

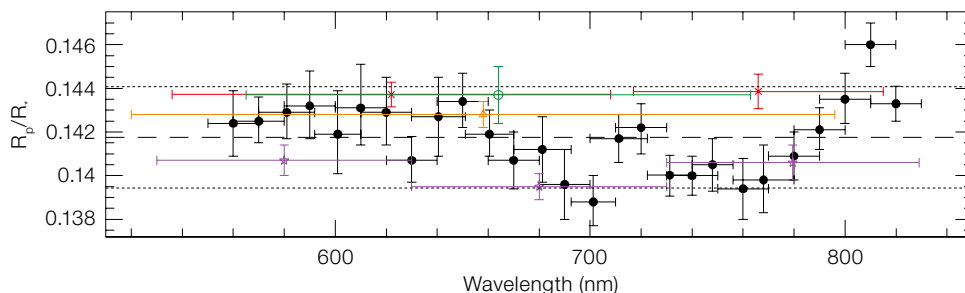


Figure 7. Transmission spectrum of WASP-19b based on our FORS2 data (with grism 600RI and 20 nm bin) from November 2014 (black, filled dots), compared to values from the literature (coloured points). The vertical error bars represent the errors in the fractional radius determination, while the horizontal bars are the FWHM of the passbands used. Note the high spectral resolution of the FORS2 data, compared to what has been available up until now. The dashed line represents the weighted mean, and the dotted lines the interval of plus and minus three scale heights.

existed (taken on 16 April 2012), thus allowing a direct comparison, while the transit duration of WASP-19b is also very short (1h 32m) and it is thus possible to cover it without expending too much observing time. Observations were done with the MXU, with 10-arcsecond-wide slits placed on several comparison stars, in the same configuration as for the 2012 observations. The grism 600RI (with the order sorting filter GG435) was used and the data were binned to a final 20 nm resolution.

The observations from 2012 reveal light curves with quite complex systematics (especially in the middle of the transit) that could not be removed even with high-order polynomial or extinction correction functions (see Figure 6). On the other hand, the new observations, performed after the exchange, show much smoother light curves, which can be

detrended using a second-order polynomial. The final, detrended light curve can be modelled, providing the parameters of the transit with good accuracy. The post-egress out-of-transit residuals in the light curve are 760 μ mag, very close to the value we expect from photon noise alone. This seems to indicate that the systematics that affected FORS2 have been significantly reduced.

The comparison of the planetary radius as a function of wavelength (the transmission spectrum) that we obtain with the new data and those from the literature is shown in Figure 7, highlighting the excellent agreement (see Sedaghati et al. [2015] for a more detailed analysis). The error bars of the dataset (due to the poor observing conditions and lack of suitable reference stars) do not allow us to distinguish yet between different models of the planetary atmosphere. Nevertheless,

these data represent the highest spectral-resolution transmission spectrum of WASP-19b and show the new potential of FORS2 in the study of the atmosphere of exoplanets. We hope this is thus the beginning of a new era for FORS2.

References

- Avila, G., Rupprecht, G. & Becker, J. M. 1997, SPIE, 2871, 1135
- Bean, J. L. et al. 2011, ApJ, 743, 92
- Bean, J. L., Kempton, E. M.-R. & Homeier, D. 2010, Nature, 468, 669
- Berta, Z. K. et al. 2011, ApJ, 736, 12
- Brown, T. M. 2001, ApJ, 553, 1006
- Burrows, A. S. 2014, Nature, 513, 345
- Crossfield, I. J. M. et al. 2013, A&A, 559, A33
- Gibson, N. P. et al. 2013a, MNRAS, 428, 3680
- Gibson, N. P. et al. 2013b, MNRAS, 436, 2974
- Moehler, S. et al. 2010, PASP, 122, 93
- Schlawin, E. et al. 2014, ApJ, 783, 5
- Seager, S. & Sasselov, D. D. 2000, ApJ, 537, 916
- Sedaghati, E. et al. 2015, A&A, submitted, arXiv:1503.04155
- Snellen, I. et al. 2010, Nature, 465, 1049

Improving the Quality of FORS2 Reduced Spectra

Sabine Moehler¹
C. E. García Dabo¹
Henri Boffin¹
Gero Rupprecht¹
Ivo Saviane¹
Wolfram Freudling¹

¹ ESO

The FORS2 instrument is one of the most widely used and productive instruments on the Very Large Telescope. This article reports on a project to improve the quality of the reduced FORS2 spectra that can be produced with the software provided by ESO. The result of this effort is that spectra of significantly higher quality can now be produced with substantially lower effort by the science user of the data.

Introduction

The two FOcal Reducer/low dispersion Spectrograph (FORS) instruments (Appenzeller et al., 1998; Rupprecht et al., 2010) are among the most popular instruments at the VLT. They are multi-mode instruments covering the optical wavelength range from 330 to 1100 nm, which have been in operation since 1 April 1999 (FORS1, decommissioned on 31 March 2009) and 1 April 2000 (FORS2), respectively. With their many modes, the FORS instruments are real Swiss Army knives. They support direct-imaging modes with narrow- and broadband filters, long-slit and multi-object spectroscopy, polarimetry and high time-resolution observations.

It is therefore not surprising that up until now, more than 1880 refereed papers have been published, based on data from FORS1 and FORS2. Among the scientific highlights discovered with the FORS instruments are conclusive evidence for the link between gamma-ray bursts and hypernovae (Hjorth et al., 2003) and the first ground-based transmission spectrum of a super-Earth planet (Bean et al., 2010). They have also enabled the discovery of the furthest quasar yet found, at redshift 7.1 (Mortlock et al., 2011) and the furthest gamma-ray burst at redshift 8.2 (Tanvir et al., 2009).

FORS2 observes objects closer to us as well, for example, allowing astronomers to find close binaries inside some magnificent planetary nebulae (Boffin et al., 2012), or permitting detailed studies of comets and asteroids, and even “rediscovered” life on Earth (Sterzik et al., 2012). For all these reasons FORS2 is still among the two most highly demanded VLT instruments. It is also behind some iconic astronomical pictures.

The FORS instruments produce a wide variety of complex data products that reflect their many different modes and options. Reducing these data, in particular spectroscopic data, is often quite a challenge. Since late 2006 ESO has provided pipeline software that can be used to process science data. Unfortunately, the products from the unsupervised reduction with that software did not always produce satisfactory results, and a variety of external software tools were necessary to produce science-ready results. In addition, using this pipeline required a significant effort of data organisation by the user. To remedy this situation, we embarked on a two-year effort to improve the FORS2 spectroscopic data products, looking at all aspects of the instrument operation that have an effect on the final data quality. In particular, we verified the current calibration plan, upgraded many aspects of the ESO pipeline, and produced a workflow in the ESO Reflex environment¹ that allows both “black box” and interactive execution of the FORS pipeline. The result of this effort is a major improvement in the quality of the spectra as they come out of the FORS pipeline. In this article, we summarise the most important aspects of these upgrades. The improved pipeline can be downloaded².

Spectroscopy with FORS2

FORS2 spectroscopy consists of three modes: classical long-slit spectroscopy with slits of 6.8 arcminutes length and predefined widths between 0.3 and 2.5 arcseconds (long-slit spectroscopy mode, [LSS]); multi-object spectroscopy with 19 slitlets of 20–22 arcseconds length each and arbitrary width created by movable slit blades (MOS mode); and multi-object spectroscopy using masks

with slitlets of almost arbitrary length, width, shape and angle (MXU mode). There are 15 grisms with resolutions (for a 1-arcsecond slit) from 260 to 2600, which may be combined with three different order-separating filters to avoid second-order contamination. More information about the instrument is available on the FORS web page³.

Reflex workflow

Like all other ESO pipelines, the FORS pipeline can be executed with the command line interface “esorex”. However, the organisation of FORS2 data for the various data reduction steps and the correct transfer of products from one recipe to the next can be cumbersome and error-prone. Automatic pipeline processing of FORS2 data will, in general, provide satisfactory results for a large fraction of all data. However, in many cases fine tuning of some parameters of the pipeline will further improve the results, and in some cases, such fine tuning is essential. For example, multi-object spectroscopy can sample very different parts of a dispersion relation, so that the default parameters for the dispersion relation may not be best suited for a specific observation.

In order to permit efficient processing of FORS2 data, including the interactive modification of pipeline parameters, we created a Reflex workflow (Freudling et al., 2013), which is shown in the screenshot in Figure 1. With this workflow, it is possible to reduce FORS2 spectroscopic data with the single push of a button. It also allows intermediate results to be inspected, parameters modified, and the impact of such modifications on the results to be assessed immediately.

This workflow organises the data according to configurable rules, allows the user to select the data to be processed and then performs the processing in the correct sequence, including the handover of products from one recipe to the next. Interactive windows like the one shown in Figure 2 allow the results to be checked and recipe parameters fine-tuned if necessary. It is also possible to switch off all interactivity and process large amounts of data in an automatic and unsupervised way.

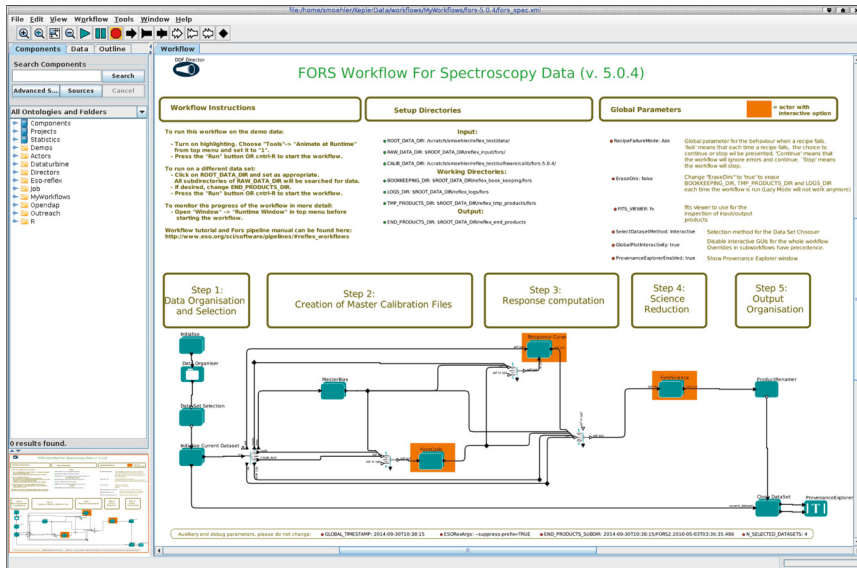
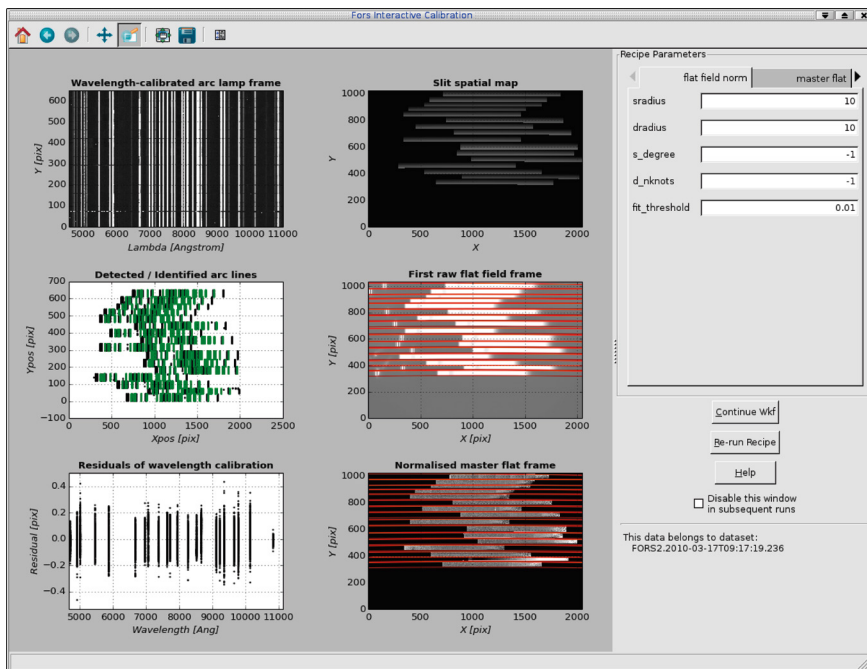


Figure 1. (Above) Screenshot of the FORS2 spectroscopy workflow. The upper part contains instructions and configuration settings, while the lower part contains the actual workflow.

Figure 2. (Below) Screenshot of one of the interactive windows of the FORS2 spectroscopy workflow. The windows provide information about the quality of the wavelength calibration, slit tracing and flat-field normalisation, while the tabs on the right allow the user to change parameters and rerun the recipe.



Error propagation

The full reduction chain has been retro-fitted with estimates of the uncertainties based on error propagation starting from the raw data. The initial uncertainties of all raw images are based on

the photon shot noise and the detector noise model. Subsequent propagation includes the uncertainties of the biases, flats and spectra extraction.

It should be noted that the systematic errors are not added to the statistical

uncertainties. The pipeline gives some idea of the systematic errors as quality control parameters, and they can be used for reference and comparison with the statistical errors.

Stability of biases and their noise

In the past the FORS2 detectors have sometimes shown significant variations of the bias level on periods of days. To safeguard against the negative effects of such changes, we implemented pre-/over-scan correction, using the median of the pre-scan region to scale the bias level. As FORS2 has only very narrow pre-/over-scan regions (five pixels in the default read-out modes) and some of those tend to be corrupt, we decided to use the median instead of more elaborate descriptions. Due to the small number of useful pre-/over-scan pixels, the read-out noise per frame cannot be determined from these regions. Instead the read-out noise is now determined from the full-bias frames and stored in the master bias. Assuming that it does not change between the bias and the other frames, this value is used as read-out noise for the error propagation along the full reduction chain. To take into account small slopes in the bias level we subtract the full master bias and not just the median of the pre-scan. To reduce the noise of the master bias, the number of bias frames taken during the day was increased from five per read-out mode to twenty. The errors of the master bias are stored in an error extension.

Wavelength and distortion calibration

The FORS2 spectroscopic pipeline processes the associated flat-field and arc-lamp frames simultaneously in order to provide a consistent description of the distortions along the spatial and dispersion axes respectively. Line identification is performed by pattern matching, and the dispersion relation is fitted by a polynomial, either row by row or using additional information along the spatial axis. We found that the algorithm is generally robust and gives good results for the dispersion relations with polynomial fits of degrees 3 to 5 (depending on the grism), if appropriate parameters and line

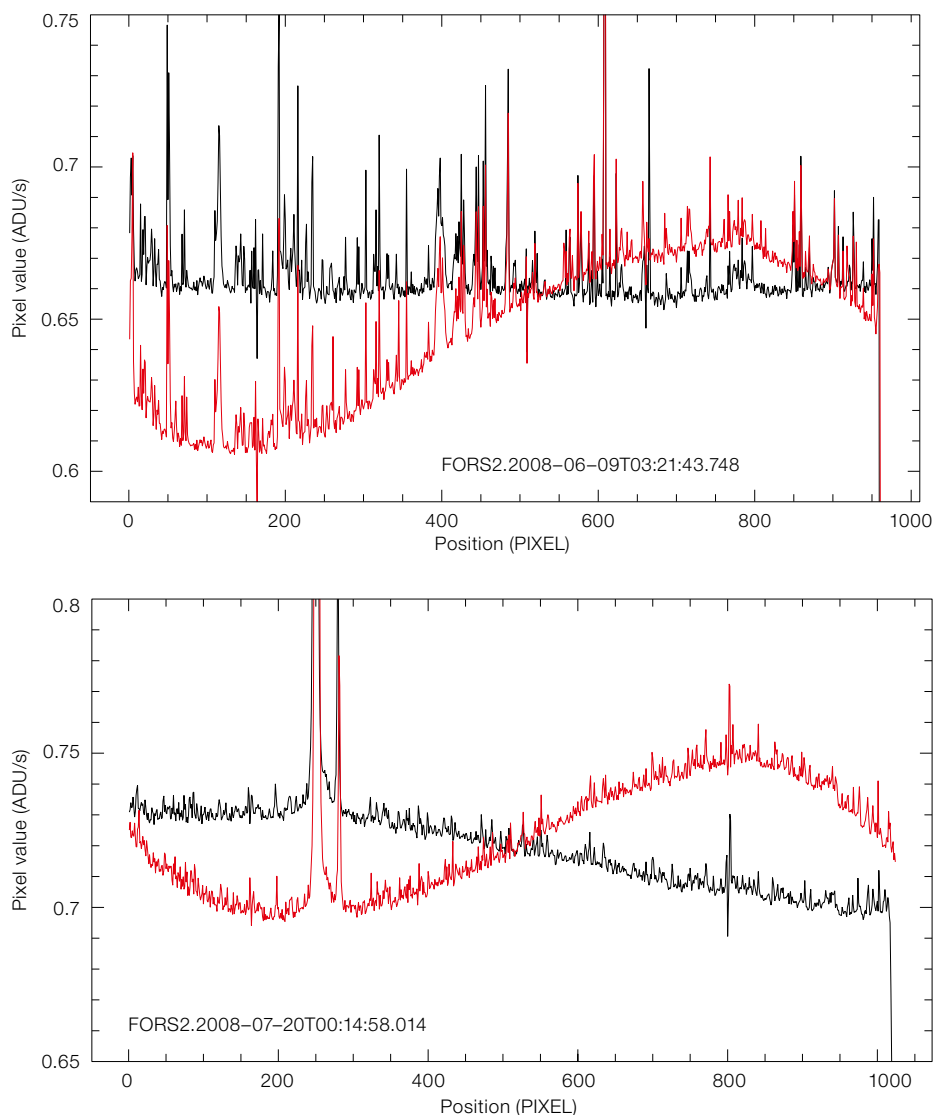
lists are used. Therefore we revised these ingredients and could thus reduce the random error of the wavelength calibration by about 25 %, or from 0.15 to 0.12 pixels on average.

A good quality and homogeneous wavelength calibration is especially important for multi-object observations, where the wavelength ranges covered may differ for different slit (and object) positions, but the results should be comparable across the field of view. The current arc lamps provide few lines at the edges of the FORS2 wavelength range, i.e., below 4000 Å (four lines only) and above 10 000 Å (two lines). In order to improve the situation for future data, we are searching for arc lamps that might provide more lines in these ranges (on the order of ten), while having sufficiently isolated lines to be suitable for low-resolution spectroscopy.

Flat fielding

Spectroscopic FORS2 flat fields use blue and red flat-field lamps to cover the full spectral range. The flux level and spectral energy distribution (SED) of the blue flat-field lamps can vary by 10 % on time scales of minutes, i.e., within one set of flat fields for a given setup, and of course also between such setups. These variations prevent meaningful flat-field stacking by median or sigma-clipping methods, unless the SED (and the flux level) are (at least roughly) normalised before the stacking. Such a normalisation has now been implemented and the average level and SED are put back into the stacked flat, which can then be normalised by smoothing or fitting along the dispersion and/or the spatial axes. The spectrum used to normalise the master flat field along the dispersion axis is retained and used for the flux calibration of volume-phase holographic (VPH) gratings (see below). The errors of the master flat field are derived from the raw flat fields and the master bias and stored in an extension.

Owing to the imperfect slit shapes, the illumination along the slit may vary, which can cause problems for sky correction and the analysis of extended objects. Such variations can amount to



about 10 % of the flux along the slit for long slits (see Figure 3, red lines). Some principal investigators (PIs) have therefore taken twilight flat fields to correct their observations and we have verified how the illumination gradients in these data compare to screen flat fields.

For that purpose the rectified flat fields (both twilight and screen) were averaged along the dispersion axis and the resulting profiles were compared to each other and to the slit illumination profile of the science data (the latter can be difficult to obtain for bright targets and/or extended objects). We found that the spatial illumination of LSS data is very similar for both kinds of flat fields and the science data. Keeping the spatial gradient of

Figure 3. The plots show two examples of the flux variation along the slit as derived by averaging the rectified long-slit spectroscopy science frame along the dispersion axis. The black profile shows the result by using flat fields which retain their spatial gradient, while the red one shows the results for which the spatial profile was eliminated during flat field normalisation.

long-slit spectroscopy flat fields (i.e., normalising only along the dispersion axis) will therefore allow the user to correct for the illumination gradient (see Figure 3, black lines).

Flux calibration

The spectrophotometric calibration of FORS2 data mostly uses flux standard

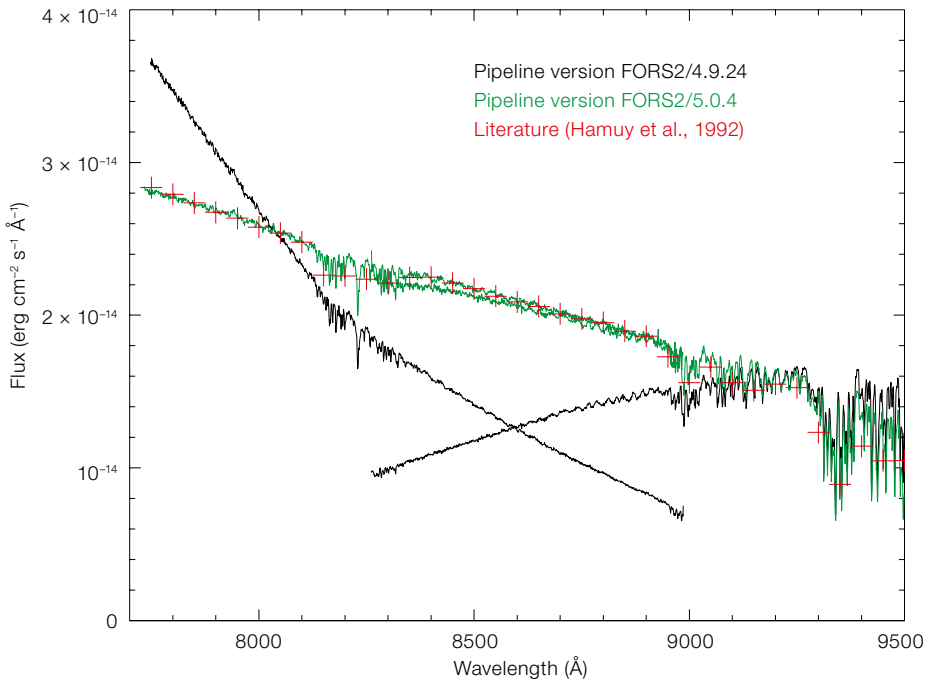


Figure 4. Plot showing the improvement in the flux calibration of data taken with VPH grisms. The spectrum of the standard star LTT3218 was observed with GRIS_1028z+OG590 at ± 150 arcseconds from the centre of the field of view, but calibrated with a response derived from observations taken at the centre of the field of view (as done with multi-object spectroscopy science data). The black spectra show the results without flat-field spectrum correction, where the slopes of the calibrated spectra differ for different positions. The green spectra were obtained with the newly implemented flat-field spectrum correction and show the correct slope irrespective of position. The red crosses mark the reference data from Hamuy et al. (1992).

of GRIS_1400V. One possible way of safeguarding multi-object spectroscopy taken with these grisms against lamp variations would be to place one slitlet at the centre of the field of view along the dispersion axis in order to have a reference flat-field spectrum to compare to the one used for the standard star.

Science processing

Given that long-slit spectroscopy is the mode of choice when observing extended objects, it was therefore rather annoying that the pipeline could not correct the spatial distortion along the slit. In order to enable this correction we took arc-lamp and flat-field frames for all available grisms using a dedicated MXU mask and derived global distortion tables, that can now be applied to LSS data to correct the distortion. One example is shown in Figure 5, where the effect of the distortion can be clearly seen at the top of the plot.

If the spatial illumination gradient is kept in the long-slit flat fields and thus corrected in the long-slit science spectra, it was found that the global sky subtraction (which utilises the oversampling of the sky spectrum due to the curvature of the sky lines) works better than the local one, which attempts to fit the spatial flux variations of the sky lines.

Implementation

The C/C++ MOSCA (MOS Common Algorithms) library has been used to implement most of the algorithms described here. It has been developed at ESO as a common library for MOS

star information from Hamuy et al. (1994). These were derived from low resolution ground-based spectra and binned to 50 \AA . The fact that they were observed from the ground means that they contain telluric absorption features, whose strength may not be the same as in the observed FORS2 spectra of these standard stars. In addition, the FORS2 grisms provide a wide range of resolutions, so that, even after binning to 50 \AA , the binned flux values for strong absorption lines (like those for white dwarfs) may differ from the tabulated values. We therefore calculated the ratios of observed vs. tabulated flux standard star spectra for all FORS2 flux standard stars (also those provided by other authors) and determined masking regions for stellar features (per star) and telluric features (per grism). These regions are now masked by default when fitting the response curve, but the user can change the masking via recipe parameters and also mask individual points. During this exercise we found that the Oke (1990) flux standard star tables had some problems (as already mentioned by their author) and we decided to remove them from the FORS2 calibration plan.

For the volume-phase holographic grisms, which are used for about 50% of the FORS2 spectroscopic data, the response

varies with the position on the detector along the dispersion axis. Therefore the flux standard star should be taken with a wide slit at the position of the science target. While this is easily done as part of the calibration plan for LSS data, this requirement poses an obvious problem for multi-object spectroscopy data. For such data the flux-standard star is observed at the centre of the field of view. If the position dependency of the response is not corrected, the flux-calibrated spectra will show systematically distorted slopes (see black lines in Figure 4).

We have fixed this problem by taking into account the response variation with position as seen in the flat-field spectra (Halliday et al., 2004; Milvang-Jensen et al., 2008) and applying it to both the flux-standard star and the science spectra. Then science spectra taken at a large distance from the centre of the field of view can be flux-calibrated using a standard star observed in the centre only (see green lines in Figure 4). This correction relies on the stability of the flat-field lamp in both flux level and spectral energy distribution. The instability of the blue flat-field lamp mentioned above therefore limits the accuracy of this correction at wavelengths below about 4800 \AA , i.e., for grisms GRIS_1200B and the blue part

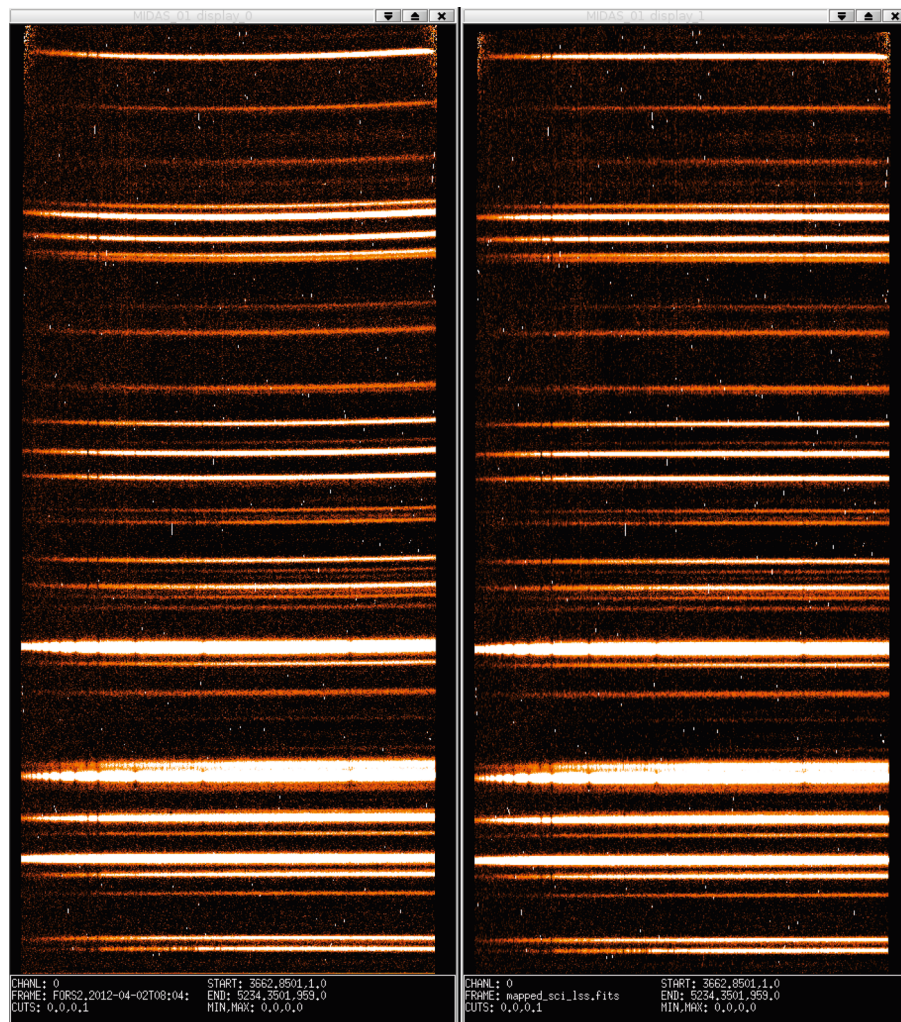


Figure 5. Wavelength calibrated long-slit spectroscopy science frame without (left) and with (right) distortion correction. The spectra are compressed along the dispersion axis to better illustrate the distortion. The position of the centre of the field of view along the y-axis is situated about 10 % from the bottom of the frame.

instruments (FORS and VIMOS for the time being) and is based on the concept of pattern matching. MOSCA is in itself based on two other ESO projects: CPL (Common Pipeline Library) and HDRL (High-level Data Reduction Library).

Verification

In order to verify that our changes in parameters and reference calibration do not cause any deterioration in the quality of the automatic processing, we

processed some 400 science datasets observed since 2008 and compared them to the results of the automatic processing by the Quality Control (QC) group, both for science and calibration products. We found that the accuracy of the wavelength calibration had improved by about 25 % as mentioned above and the accuracy of the flux calibration had improved by up to 50 % for VPH grisms. For the standard (non-VPH) grisms, the improvements were less striking, but there are some grisms here which also profit from more appropriate fit parameters (e.g., GRIS_600B). The signal-to-noise ratio could not be significantly improved as the FORS2 pipeline already uses the optimal extraction method (from Horne, 1986), which is well suited to these kind of data. We found no evidence for any systematic wavelength shift from sky lines above 0.05 pixels.

Conclusions

The improvements and new features described here will allow users to realise the full potential of their FORS2 spectra more easily. This project illustrates that the quest for improvements in data quality requires not just well-suited pipeline algorithms, but also appropriate calibration plans and reference data. One should therefore always try to look at the complete picture of data and software. The project also showed the inherent problems of working on an instrument with a long history — changes to the calibration plan will always be useful only for future data and will usually not allow existing problems to be fixed.

Acknowledgements

This research has made use of the NASA Astrophysics Data System Bibliographic Services, the National Institute of Standards and Technology database of atomic lines and the SIMBAD database, operated at CDS, Strasbourg, France. Thanks go to Joe Hennawi, Neil Crighton and Bo Milvang-Jensen for their assistance with the analysis of FORS2 twilight flats and to Alessandro Nastasi for his help with F-VIPGI. We are grateful to Mark Downing for his help with understanding the FORS2 detectors, to Hans Dekker for his explanations of the behaviour of VPH grisms and to Paul Bristow for his support of the physical model test. Special appreciation goes to the late Carlo Izzo, who wrote the original FORS pipeline.

References

- Appenzeller, I. et al. 1998, *The Messenger*, 94, 1
- Bean, J. L., Kempton, E. M.-R. & Homeier, D. 2010, *Nature*, 468, 669
- Boffin, H. M. J. et al. 2012, *Science*, 338, 773
- Freudling, W. et al. 2013, *A&A*, 559, A96
- Halliday, C. et al. 2004, *A&A*, 427, 397
- Hamuy, M. et al. 1994, *PASP*, 106, 566
- Hjorth, J. et al. 2003, *Nature*, 423, 847
- Horne, K. 1986, *PASP*, 98, 609
- Milvang-Jensen, B. et al. 2008, *A&A*, 482, 419
- Mortlock, D. J. et al. 2011, *Nature*, 474, 616
- Oke, J. B. 1990, *AJ*, 99, 1621
- Rupprecht, G. et al. 2010, *The Messenger*, 140, 2
- Sterzik, M. F., Bagnulo, S. & Palle, E. 2012, *Nature*, 483, 64
- Tanvir, N. R. et al. 2009, *Nature*, 461, 7268

Links

- ¹ ESO Reflex: <http://www.eso.org/sci/software/reflex/>
- ² Download of FORS2 pipeline: <http://www.eso.org/sci/software/pipelines/>
- ³ FORS web page: <http://www.eso.org/sci/facilities/paranal/instruments/fors.html>

The Return of the Mid-infrared to the VLT: News from the VISIR Upgrade

Hans Ulrich Käuffl¹
 Florian Kerber¹
 Daniel Asmus¹
 Pedro Baksai¹
 Nicola Di Lieto¹
 Philippe Duhoux¹
 Stephanie Heikamp²
 Christian Hummel¹
 Derek Ives¹
 Gerd Jakob¹
 Jean-Paul Kirchbauer¹
 Leander Mehrgan¹
 Yazan Momany³
 Eric Pantin⁴
 Eszter Pozna¹
 Miguel Riquelme¹
 Stefan Sandrock¹
 Ralf Siebenmorgen¹
 Alain Smette¹
 Jörg Stegmeier¹
 Julian Taylor¹
 Konrad Tristram¹
 Guillermo Valdes²
 Mario van den Ancker¹
 Ueli Weilenmann¹
 Burkhard Wolff¹

¹ ESO

² Leiden Observatory, the Netherlands

³ INAF–Osservatorio Astronomico di
Padua, Italy

⁴ Service d'Astrophysique/DAPNIA/DSM,
CEA Saclay, Gif-sur-Yvette, France

The VLT mid-infrared imager and spectrometer VISIR returns to science operations following an extended upgrade period. Among the most important modifications are: the imaging and spectroscopic detectors have been replaced with larger AQUARIUS (1024 by 1024 pixel) detector arrays; the *N*-band low-resolution grating has been exchanged; and support is now provided for precipitable water vapour monitoring, in order to select the best observing conditions. The AQUARIUS detectors stem from a development for very low background applications which result in excess noise under ground-based conditions. A series of interventions was needed to find a scheme that effectively exploits these detectors for ground-based use, involving the implementation of faster chopping. VISIR has been returned to service at the VLT with enhanced capabilities.

Introduction

The VLT Imager and Spectrometer for mid InfraRed (VISIR) is a combined imager and echelle spectrograph, providing access to the atmospheric *N*-band (7.7–13.3 μm) and *Q*-band (16–24 μm) with a great variety of observing modes¹. VISIR was originally built for ESO by the Service d'Astrophysique of the Commissariat à l'énergie atomique (CEA), Saclay, France, together with ASTRON, Netherlands Institute for Radio Astronomy in Dwingeloo. The instrument arrived at the Very Large Telescope (VLT) in 2004 (Lagage et al., 2004). VISIR was commissioned with small format detectors with less than excellent cosmetic quality and a low-resolution spectroscopy mode, which was not well matched to the science requirements.

Taking advantage of a detector development for the James Webb Space Telescope (JWST), new detectors (AQUARIUS) could be procured and were retrofitted in an upgrade intervention starting in mid-May 2012. The upgrade also included the integration of a water vapour radiometer, the Low Humidity And Temperature PROfiling microwave radiometer (LHATPRO) manufactured by Radiometer Physics GmbH (RPG), a new low spectral resolution prism mode and various means to enhance high-contrast and high spatial resolution imaging. Since late 2011, following a careful cross-calibration campaign, the radiometer is in full operation (Kerber et al., 2012). A first attempt to re-commission an optically and mechanically perfect VISIR in August 2012 was not successful, due to noise problems with the detector, which had not been diagnosed in laboratory testing. In August 2013 the path back to the telescope was finally established, which required enhancements to the Unit Telescopes (UTs) to allow for chopping at the original design frequency.

The status of the “new” VISIR after the second commissioning run in January 2015 is reported.

Scope of the upgrade

The main elements of the upgrade entailed:

- Change of both imager and spectrograph detectors from a 256×256 pixel device with 50 μm pixel pitch to the new AQUARIUS device (see Ives et al. [2014] for details). The AQUARIUS detectors have an area of 1024×1024 pixels and 30 μm pitch, so that the entire focal plane of ~ 25 mm by 25 mm, for which the VISIR optics had been designed, can be used. Since the new detectors dissipate typically an order of magnitude more power than the old ones below 10 K, an enhancement of the cooling harness was also required.
- Change of all detector cabling in the cryostat to connect the 2×64 detector outputs for signal frequencies up to ~ 10 MHz and addition of cold pre-amplifiers, just outside the spectro-meter structure, to reduce cable lengths, minimising detector artefacts and spurious signals.
- Integration of the detectors into the new ESO standard acquisition system, the new detector controller (NGC).
- Exchange of the *N*-band low-resolution grating in the VISIR low–medium-resolution spectral arm with a new prism manufactured from zinc selenide (ZnSe; Figure 1).
- Enhancement of the high-contrast imaging capabilities of VISIR by adding coronagraphy and aperture masking (sparse aperture masking [SAM]) capabilities; the lead on this part was taken by CEA, Saclay.
- Improvement of the image quality. VISIR depends on receiving images without aberration from the VLT (without adaptive optics) and the diffraction limit of the VLT at 10 μm is ~ 0.3 arcseconds. Observing with a frame rate as high as ~ 100 Hz showed that image distortions appear and disappear; the high rate of these changes rules out an atmospheric origin and suggested image quality problems within the VLT itself.
- Providing the means to measure atmospheric water vapour (precipitable water vapour [PWV]) along the line of sight. For certain operational modes, e.g., imaging in the *Q*-band (~ 20 μm), PWV is as important for good performance in the infrared as the seeing is for high-definition imaging; PWV has been introduced as a constraint parameter for service mode. PWV can be very low on Paranal, resulting in excellent atmospheric transmission (Kerber et al., 2014a).

- Substantial modifications to operating software to ensure standard data flow from Phase 2 proposal specification through to the science archive.

Spectro-polarimetry in combination with the new prism mode, although originally planned and reviewed, was, in the end, not implemented. Optomechanical problems mounting the Wollaston prism in the spectrograph fore-optics introduced a high risk to the schedule for the intervention and its success.

The upgrade was led by ESO-Garching in close collaboration with the Paranal Observatory and CEA provided the concept and optics for the new high-definition imaging modes. ASTRON also supported with expertise and some spare parts.

First intervention, 2012

To minimise downtime, an intervention of four months was planned, starting in May 2012. After a final check on-sky of the old configuration (close-out calibration), VISIR was moved to the instrument integration hall laboratory where the old detectors were checked and then the instrument was disassembled into its basic sub-units. The low and medium spectral resolution unit (carousel, Figure 2) was removed. After a complete disassembly of this very complex and delicate unit, a pocket was milled into the aluminum base part to create the space for the prism mount. After re-assembly and re-alignment of the spectrograph optics with the optical proxy, the prism was pre-aligned with a HeNe laser. The spectrograph detector mount and the imager detector mount were both modified to take the new AQUARIUS arrays. Some improvements to the baffling and the stray-light rejection of the imager for the larger optical field, accessible with the larger detector, were also made. Finally the aperture wheel was modified for the coronagraphic optics, and special filters and pupil masks were added to the imager filter wheel for coronagraphy and high-contrast imaging.

Alignment and testing of the re-assembled units was initially performed using optical light at room temperature with the bare detector multiplexer, thus avoiding

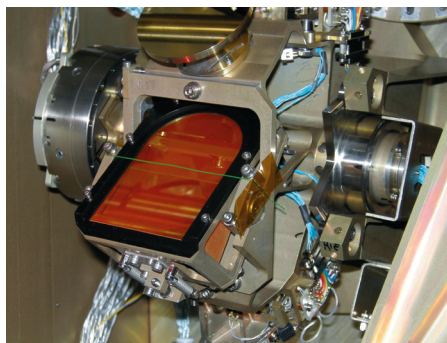


Figure 1. Close-up view of the new ZnSe prism. The prism was designed to disperse the $10\ \mu\text{m}$ window over ~ 900 pixels with a pupil size of approximately 50 mm. The green wire was used during alignment to mark the centre of the pupil.

the need to close and cool down the instrument. The tests were very successful, so that the “new” VISIR was integrated, evacuated and cooled down for the first time early in July 2012. The first infrared-light test in the laboratory indicated almost perfect optical quality, while the prism spectrum was also found to be well centred. Further tests showed perfect cosmetic quality and no signs of noise problems, so that by the end of July 2012 VISIR was ready, as planned, for re-commissioning on Unit Telescope 3 (UT3).

Re-commissioning, first attempt

The first night of re-commissioning began with the basic optical tests: the VISIR optical quality and the cosmetics of the detectors appeared to be quite impressive. However on the second night it became apparent that VISIR was substantially less sensitive in comparison to the situation before the upgrade. Moreover, it appeared that the conversion gain of the detector in the spectrograph was approximately three times higher than in the imager. After three more nights of testing the detectors, optics, software, etc., VISIR was dismounted from the telescope and brought back to the integration laboratory, in order to investigate this (quite confusing) situation further.

After lengthy investigations, which excluded optical problems with VISIR, it was ascertained that the detector material, developed for the low-background location of JWST operating at the Lagrange point, L2, was optimised for

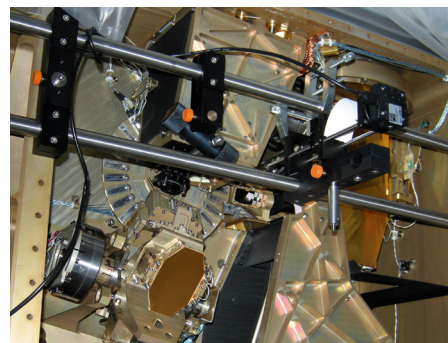


Figure 2. Close look at the VISIR low- and medium-resolution assembly. The unit in the lower left is the carousel, a precision rotary stage used to scan the gratings. At the top right is an optical bench with a CMOS camera rigged as proxy for the infrared optical axis. Slightly above the carousel the mount of the special prism can be seen, which compensates the alignment for the change in refractive index between the HeNe laser and the desired central wavelength ($10.5\ \mu\text{m}$) and the thermal shift between room temperature and the operating temperature of VISIR ($\sim 28\ \text{K}$).

extremely low dark currents. This introduced an excess low-frequency noise (ELFN) in the high-flux applications relevant to ground-based astronomy. This phenomenon was described 30 years ago by Stapelbroek et al. (1984). The ELFN is a form of correlated noise caused by fluctuations in the space charge induced by ionisation/recombination in the blocking layer. It manifests as a memory of photons in subsequent frames. It appears that this effect was not properly accounted for in the design of the Si:As detector material hybridised on the AQUARIUS multiplexer for the ESO detectors (see Ives et al. [2014] and references therein). Careful analysis of the spectral energy distribution of the detector noise indicated that the ELFN can be filtered out, if the chopper frequency is increased from fractions of a Hertz to the original specification of the VLT secondary mirror (M2) of 4–5 Hz.

In addition it was also found that the detector material in the spectrograph stemmed from a different batch to the one of the imager, and under nominal bias there was avalanche gain in the spectrograph, mimicking a higher conversion gain, which, in turn, manifested as an optical problem with the imager. The energy to create a charge in a photoconductor sensitive to $28\ \mu\text{m}$ is of order of $1/25\ \text{eV}$, so a typical detector bias of

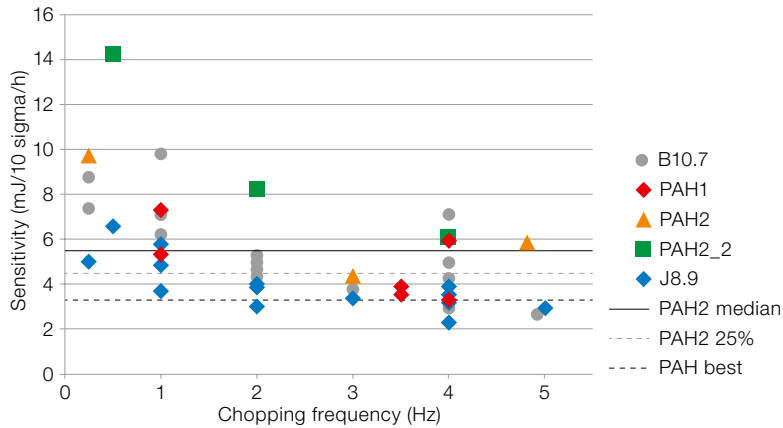


Figure 3. The on-sky sensitivity performance of VISIR is shown as a function of the M2 chopping frequency. The horizontal black lines give the performance of the “old” VISIR at the nominal chopping frequency (~ 0.25 Hz): the best-ever value, the 25th percentile and the median. The various symbols denote measurements taken during commissioning runs in November 2014 and January 2015, referring to the respective filter names of VISIR: the trend with chopping frequency is obvious. There is some scatter in these data that result from variable sky conditions, but once routine operations have started better statistics will soon become available.

1.5 V is some 40 times higher. The charge diffusing through the photoconductor can be accelerated sufficiently to create, via impact ionisation, secondary charges and so on. In the VISIR spectrometer case, there were of order three charges generated per detected photon; as this is a very noisy process, avalanche gain needs to be avoided. Strong fringing was observed in echelle spectroscopy and it was evident that the antireflection coating of the AQUARIUS detectors was not optimised for $10.5\ \mu\text{m}$, as specified by ESO, but for $\sim 6\ \mu\text{m}$ — again a JWST value.

Since there was no option for a new detector design, the only way to improve performance was to investigate faster chopping with M2. The VLT’s tracking precision, however, relies on vernier corrections using M2, normally referred to as fast guiding. The original implementation for VISIR was that each chopper state lasted substantially longer than the fast guiding time constant. Thus fast chopping was incompatible with the requirements for having a diffraction-limited telescope. With the ongoing replacement of obsolete elements, such as the technical CCDs in the VLT adaptors, the controllers and the network, this

incompatibility could be re-addressed and using the art, or the tools, of control engineering the control loop could be tuned as well, providing the capability for simultaneous diffraction-limited imaging and high chopping frequency.

A test in August 2013 confirmed that VISIR can indeed achieve sensitivities close to the theoretical limit (background-noise-limited performance, BLIP; see Käufl et al., 1991), provided that fast image modulation is applied, be it by chopping or by drift scanning; the latter being now the preferred method in submillimetre and radio astronomy. Then, in a series of three short technical test runs, the necessary changes to the VLT operation were implemented and verified. The status of the upgrade is summarised in Kerber et al. (2014b).

Meanwhile, in the context of the laboratory testing of more AQUARIUS detectors for the MATISSE instrument, the second generation VLT interferometer mid-infrared instrument (Lopez et al., 2014), it was found that some of the leadless chip carriers into which the detectors are integrated are warped so badly that the mount designed for VISIR could damage them. This concern led to another intervention in the summer of 2014, in which both detector mounts were checked. The imager detector carrier was found to be flat without blemishes. However the mount was changed to a new design compatible with the

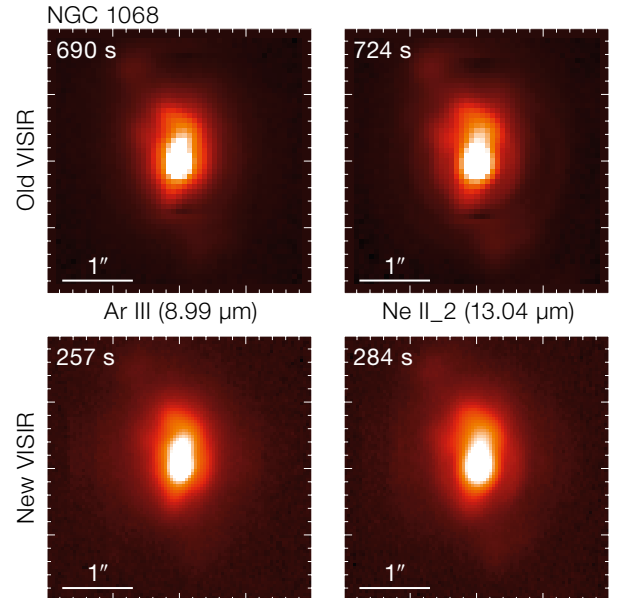


Figure 4. Comparison of images of the active galactic nucleus of NGC 1068 taken with the “old” and the “new” VISIR. After the upgrade, the same quality can be achieved in substantially less time, while having much finer spatial sampling, relevant for all image processing involving deconvolution.

warped carriers. The spectrograph detector had no significant damage either, but was replaced anyway with a device not showing avalanche gain and the mount was upgraded. Thereafter VISIR was ready to go back to the telescope and a first commissioning took place in November 2014.

The progress in 2014 and the long and unplanned interruption of observations led to a joint decision between the project team and Paranal science operations to have VISIR included in the call for proposals for Period 95, albeit with some restrictions, even though commissioning had not even started. In total 27 proposals were received for VISIR and 21 were awarded observing time.

Re-commissioning of VISIR

The focus of the commissioning was: to verify the fast chopping with field stabilisation using VISIR as a test camera; integrate the new detector controllers into the operations software to allow for robust synchronisation in fast chopping; modify and verify templates for the modes offered in Period 95; and establish the

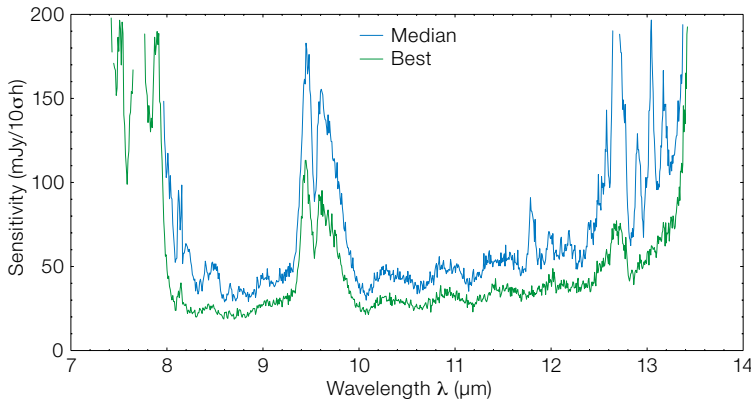


Figure 5. Sensitivity samples for the *N*-band low-resolution mode, as observed during the re-commissioning of VISIR in January 2015. This plot shows how many mJy a source needs to emit at a certain wavelength to be detected with a signal-to-noise ratio of ten in one hour. The plots retrace atmospheric radiance, i.e., the inverse of the transmission.

Special attention is drawn to the region around 12.8 μm , the wavelength of the [Ne II] emission line: the difference between the two graphs is largely due to changes in water vapour above the telescope so that selection of low-PWV periods will pay off when observing the [Ne II] transition in HII regions.

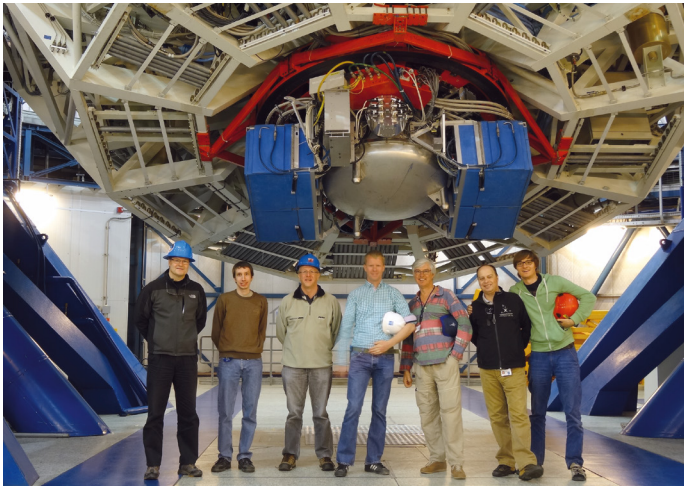


Figure 6. The re-commissioning team in front of the upgraded VISIR in January 2015. The signature of the upgrade is clearly visible between the blue boxes containing the electronics: to accommodate the connectors for the detector cabling required grafting in a new flange, almost a factor of two larger in diameter. To the left of this enlarged flange is an extra electronics box to adapt the AQUARIUS detectors to the standard voltage range of the ESO-NGC acquisition system.

data flow from the Phase 2 Proposal Preparation tool (P2PP) to the pipeline and science archive. The sensitivities of the image and low-dispersion spectrograph modes were then determined. For imaging, the sensitivities generally exceed those of the “old” VISIR (Figure 3), but for some filters the full field may be truncated to ~ 20 by 38 arcseconds for high-flux filters. Figure 4 shows, as an example, images in two emission-line filters for NGC 1068, before and after the upgrade. For *N*-band low-resolution spectroscopy, the sensitivity is generally up to a factor of two higher (correcting for the increased dispersion), while the throughput has been increased by a factor of four (c.f., Figure 5).

Performance and outlook

The main characteristics of VISIR after the upgrade can be summarised as follows:

- Imaging with sampling 0.045 arcseconds per pixel and field of view 38 by 38 arcseconds;
- Low-resolution prism spectroscopy over the complete *N*-band (7.7–13.3 μm) in one exposure at a spectral resolution ($\lambda/\Delta\lambda$) of 70 (8.0 μm) to 180 (13.3 μm) for a 1.0-arcsecond slit at a spatial scale of 0.076 arcseconds per pixel (slit length ~ 32 arcseconds).

Up-to-date information on the characteristics of the offered modes is available in the User Manual².

The *N*- and *Q*-band echelle spectroscopy will be commissioned in time for Period 95 with improved performance and 2.3 times the spectral coverage. It is then expected that for the call for proposals for Period 96 a variety of restrictions on the modes will be lifted.

VISIR, a true multimode instrument, is back in basic operation (see Figure 6). In the coming commissioning periods, several additional modes will be tested:

- coronagraphy;
- burst mode, and thus high speed photometry;
- imaging with sparse aperture masks;
- medium-resolution spectroscopy, especially in the *Q*-band and wavelengths beyond 20 μm .

Operations will support burst mode, offering the opportunity for frame selection and bringing background-limited performance within reach for most filters. Sub-aperture masking and coronagraphy will provide new scientific capabilities in terms of high-resolution, high-contrast imaging. We invite users to regularly check the VISIR upgrade web page³ and follow the progress on VISIR towards full science operations.

One important aspect for the future will be exploring options to address the shortcomings of the AQUARIUS detectors, especially since other instrument activities at ESO would profit as well.

References

- Ives, D. et al. 2014, *Proc. SPIE*, 9154, 91541J
- Käufl, H. U. et al. 1991, *Experimental Astronomy*, 2, 115
- Kerber, F. 2012, *The Messenger*, 148, 9
- Kerber, F. et al. 2014a, *MNRAS*, 439, 247
- Kerber, F. et al. 2014b, *Proc. SPIE*, 9147, 91470C
- Lagage, P. O. et al. 2004, *The Messenger*, 117, 12
- Lopez, B. et al. 2014, *The Messenger*, 157, 5
- Stapelbroek, M. G. et al. 1984, *Proc. IRIS Detector*, No. 2

Links

- ¹ VISIR instrument page:
<http://www.eso.org/instruments/visir/>
- ² VISIR User Manual: <http://www.eso.org/sci/facilities/paranal/instruments/visir/doc.html>
- ³ VISIR upgrade project news:
<http://www.eso.org/sci/facilities/paranal/instruments/visir/upgradeproject.html>

The SPEED Project: SPEEDing up Research and Development towards High-contrast Imaging Instruments for the E-ELT

Patrice Martinez¹
 Olivier Preis¹
 Carole Gouvret¹
 Julien Dejongue¹
 Jean-Baptiste Daban¹
 Alain Spang¹
 Frantz Martinache¹
 Mathilde Beaulieu¹
 Pierre Janin-Potiron¹
 Lyu Abe¹
 Yan Fantei-Cujolle¹
 Sebastien Ottogalli¹
 Damien Mattei¹
 Marcel Carbillat¹

¹ Laboratoire Lagrange, UMR7293,
 Université de Nice Sophia-Antipolis,
 CNRS, Observatoire de la Côte d'Azur,
 Nice, France

An overview is presented of the Segmented Pupil Experiment for Exoplanet Detection (SPEED) testbench. This is an advanced facility in development at the Lagrange Laboratory that will address several of the most critical issues affecting high-contrast imaging for the next generation of optical/near-infrared telescopes. The SPEED testbed can be used to investigate practical solutions for broadband coronagraphy on asymmetric, unfriendly apertures, enabling algorithmic or optical approaches to be developed to minimise segment effects and pupil discontinuity.

In June of last year, a major step towards for the European Extremely Large Telescope (E-ELT) was achieved through the blasting of part of the peak of Cerro Armazones, opening the path towards the construction of the telescope. After completion, the E-ELT will be the world's largest optical/near-infrared telescope, opening up new parameter space in both spatial resolution and photon sensitivity. The E-ELT will provide significant advances over the Very Large Telescope (VLT), with a gain of a factor of five in spatial resolution, 25 in signal to noise, and 625 in exposure time to reach a given signal to noise. Such a giant telescope is expected to tackle the major challenges of contemporary astrophysics. Among the numerous open questions for which it is designed, hunting down

low-mass exoplanets in the habitable zones where life could exist is probably its more exciting ambition.

Nevertheless, there is a catch to being the “world's biggest eye on the sky”: the unavoidable run for spatial resolution and photon sensitivity leads to a telescope that by design is not optimal for the exoplanet search problem. While segmented telescopes offer dramatically enlarged telescope diameters from the ground, translating current technological advances into the domain of high-contrast imaging for monolithic apertures (e.g., SPHERE at the VLT; Beuzit et al., 2006) to the case of segmented apertures is far from trivial. On account of the segmented primary mirror and the increase in the number of mechanical structures making up the telescope, the resulting pupil is geometrically fairly complex: the pupil exhibits amplitude discontinuities created by the space between the segments, a large central obscuration, various secondary supports, unavoidable missing segments, and phase discontinuities resulting from imperfect alignment (phasing) between the segments. These effects significantly limit high-contrast imaging capabilities (speckles and diffraction), especially for the direct detection of exoplanets. In the area of high-contrast imaging, the only advantage offered by the ELTs is their gain in diameter, but this is accompanied by a large set of drawbacks that demands strong research and development (R&D) efforts on the optical effects. The complexity of the telescope pupil and the high-contrast imaging strategies are bound up with one another.

SPEED — the segmented pupil experiment for exoplanet detection — in development at the Lagrange Laboratory, aims at preparing strategies and technologies for high-contrast instrumentation with segmented telescopes. SPEED will offer an ideal environment in which to make progress in the domain of ELTs with complex/irregular apertures. SPEED combines wavefront control, including precision segment-phasing architectures, wavefront shaping for both phase and amplitude control, and advanced coronagraphy that is relevant to very close angular separation imaging.

Rationale

Different requirements exist for the various science programmes, but the telescope must comply with them all. This is very difficult to achieve, and the situation can be well paraphrased by the idiom “too many irons in the fire”. In a high-contrast imaging instrument, the match between the scientific requirements (performance) and the instrumental requirements is generally quite complicated. While the E-ELT aims at gaining a spectacular factor of 100 to 1000 in contrast compared to SPHERE on the VLT for instance, its optical and mechanical characteristics impose severe hurdles that contribute a large part of the error budget of static or quasi-static aberrations, and set the ultimate limit regardless of the integration time. In particular, segmentation is an essential characteristic of the E-ELT that strongly complicates the telescope pupil structure and degrades coronagraphic contrast.

The E-ELT exoplanet imaging camera EPICS (Kasper et al., 2010) phase A conceptual study highlighted the complexity of the error budget affecting the propagation of light in such a new class of instrument. As a result the technological limitations must be addressed through various development programmes (for high-order deformable mirrors, real-time systems, wavefront sensors, etc.). Notwithstanding these obstacles — some of which will probably require technological breakthroughs to surmount — several additional concerns affecting exoplanet detection require that brand new challenges must be tackled in the area of high-contrast imaging. In particular:

- ELTs will start to resolve stellar discs (0.5 milliarcseconds [mas] apparent radius for nearby stars) with a 39-metre telescope at 1.6 μm . The result is degradation of the coronagraphic contrast, in particular for small inner-working angle coronagraphy, since coronagraphic leakage is proportional to the square of stellar radii.
- The pupil of an ELT is made up of various discontinuities in both phase and amplitude: the primary (M1) large central obscuration, inter-segment spacing, island effect from the secondary (M2) support structures, imperfect phasing, etc. All these aspects are detrimental for high-contrast imaging.

- While the current specification for E-ELT segment phasing can reasonably be considered to be achievable, it is uncertain whether the high-precision phasing requirements deemed appropriate for a high-contrast instrument can be achieved. The solution may require dedicated solutions at the instrument level.
- Missing segments are of the utmost concern. Since the segment reflectivity coating will have a lifetime of about 18 months, up to three segments will need to be re-coated on a daily basis. As for now, three to seven segments in total may be expected to be missing per observing run at the E-ELT. The effect of missing segments is dramatic and can be easily understood from classical Fraunhofer diffraction theory following Babinet's theorem: the far-field pattern of an obscuration is equal to that of an aperture of similar dimensions. Thus the width of the diffraction halo in the image plane is inversely proportional to the missing segment diameter, while its maximum intensity is proportional to the segment surface.
- Both the gain in spatial resolution offered by the E-ELT, and new scientific targets (e.g., M stars) for planet detection, demand an observing mode with a small inner-working angle (IWA), typically 15 mas (!) in the near-infrared. As a result, this mode will be subject to difficulties due to stellar resolution, pointing stability, amplitude error effects, etc.
- The instrument design and control of contrast on such giant telescopes requires careful mastering of Fresnel/Talbot effects, which are an important class of perturbation affecting a high-contrast imager. A pure phase aberration on an optical surface mixes between phase and amplitude aberrations as light propagates, and this oscillation occurs over a distance called the Talbot distance. This distance is proportional to the square of the aberration spatial period and inversely proportional to the wavelength of light, and hence is a chromatic effect. While the E-ELT diameter is increased by a factor of five compared to the VLT, the instrument size is not, and the optical beam compression is crude so that Fresnel diffraction induced by out-of-pupil optics is of the utmost importance.

Following from these points, both specialised and efficient post-coronagraphic wavefront sensing and control solutions, as well as image post-processing, are of major importance. This is especially so for the case of observing modes at small IWAs where standard strategies, such as angular differential imaging, are likely inefficient.

Concept and features

The complications elucidated here require both prudence and pragmatism in translating the current concept (e.g., SPHERE) to the ELTs. In order to provide insights into these issues, the concept of SPEED (Martinez et al., 2014) was proposed in 2013 to study solutions for optimising high-contrast imaging with unfriendly telescope apertures. The SPEED concept is described in Figure 1, while the 3D optical/mechanical view of the SPEED bench is shown in Figure 2.

Star planet simulator

At the entrance of the testbed, a star planet simulator (SPS source; Hénault et al., 2011) will allow a bright and unresolved star with an exoplanet signal to be simulated with adjustable angular separation and flux ratio. Stellar resolution will be possible within the SPS module up to 0.5 mas. Within SPEED it is assumed that the atmospheric turbulence (short-lived and fast-evolving speckles) has already been pre-corrected by an upfront eXtreme Adaptive Optics (XAO) system, and thus we can concentrate on the quasi-static aberrations in the instrument. While the SPEED bench will mainly operate on the assumption that this virtual correction is perfect (i.e., no XAO residuals), it will be possible to generate uncorrected atmospheric residuals using exchangeable phase screens.

Segmented telescope simulator

The next subsystem is the segmented telescope simulator. This consists of the combination of an active segmented mirror (ASM) with 163 segments controlled in piston and tip-tilt (a surrogate of the E-ELT primary mirror) and an optical mask inserted into the beam to simulate the presence of the E-ELT secondary mirror, including the primary central obscuration. The E-ELT M4 residuals and

segmentation will be included at a later stage using a dedicated phase screen. Such a telescope simulator will allow several key aspects of the E-ELT architecture and error propagation to be investigated, as well as their impact for high-contrast imaging in the form of missing segments, gaps and the island effect. The island effect consists of the partial, or complete, coverage of the pupil by the dark zones created by the secondary mirror supports (spider arms), thus directly impacting the phasing sensor or wavefront sensor.

As part of the telescope simulator, a phasing system based on the Zernike contrast sensor principle (Dohlen et al., 2006) will be implemented, while alternative solutions, such as the asymmetric pupil Fourier wavefront sensor (Martinache et al., 2013), or the self coherent camera phasing sensor (Janin-Potiron et al., in preparation), will be compared. In this context, the purpose of the former ESO Active Phasing Experiment (APE) project (Gonté et al., 2009) was to explore, integrate and validate non-adaptive segment phasing schemes and technologies at the telescope level for an ELT. While the current specifications of the E-ELT segment phasing is assumed to be achievable by such means, high-contrast imaging might be much more demanding in terms of phasing requirements. Fine phasing at the instrument level will be treated within SPEED.

Wavefront-shaping module

Two sequential deformable mirrors of 952 actuators (DM1 and DM2), separated by free-space propagation, constitute the wavefront control and shaping module of SPEED, enabling efficient correction for both phase and amplitude errors, and/or remapping of the pupil discontinuities. The upfront correction of aperture irregularities by optical remapping in the geometric, and thus achromatic, regime is feasible for subsequent feeding into a coronagraphic stage. The difficulty is driven by the demand to derive mirror shapes (Pueyo et al., 2013) suitable to remove the structures introduced by spiders and gaps, without losing photons.

Coronagraphic module

Several small IWA-class coronagraphs are currently the subject of vigorous R&D to bring them to high technological

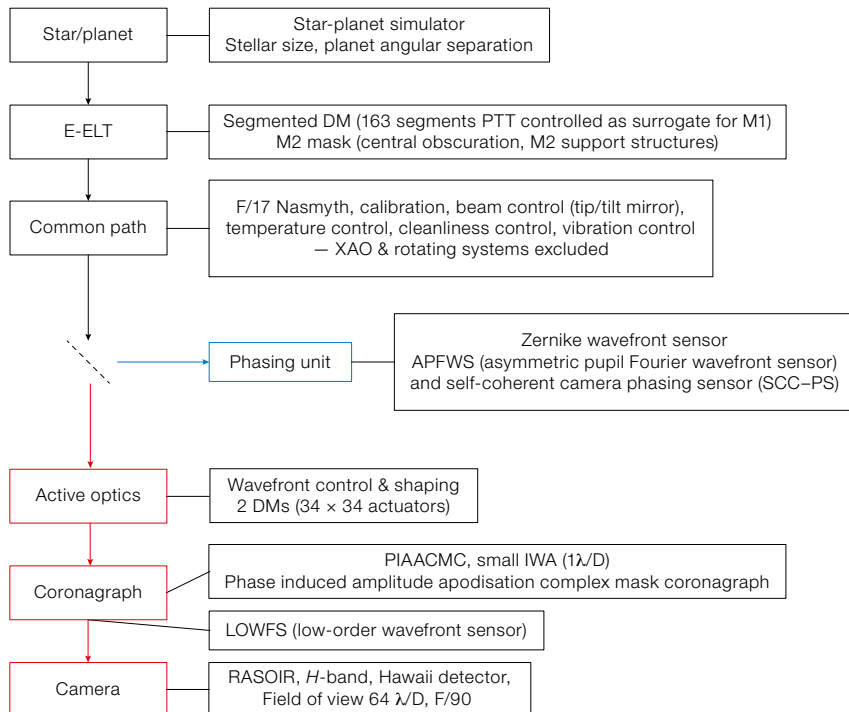


Figure 1. The general layout of SPEED is shown with optical/near-infrared paths differentiated by blue and red colours respectively.

maturity. In particular, PIAA (phase induced amplitude apodisation) uses beam remapping for lossless apodisation (Guyon et al., 2014), and can be combined with opaque masks (PIAAC and PIAALC), or partially transmissive phase-shifting (complex) masks (PIAACMC). PIAA theoretically offers complete starlight extinction, with high throughput and

sub- λ/D inner working angle, regardless of the aperture shape. PIAA offers nearly 100% throughput and approaches the fundamental coronagraph performance limits.

The technological maturity of PIAA benefits from ten years of R&D activities, from scratch to on-sky demonstration, and actual raw contrast reaches levels up to 10^{-8} at $2 \lambda/D$ and is expected to deliver 10^{-6} in H -band at $1 \lambda/D$ at the Subaru Telescope. The goal within SPEED is to develop a PIAACMC that can cope with $1 \lambda/D$ IWA, stellar angular size up to 0.5 mas, and correct for all or part of the telescope pupil discontinuities (secondary

support structures) with raw contrast of 10^{-7} at the IWA. The PIAACMC is shown in Figure 2 and is composed of three elements: the PIAA module (to create pupil apodisation by optical remapping without losing photons), a complex focal plane mask, and a PIAA^{-1} module (called PIAA inverse, to recover the translational invariance of the point spread function lost with the PIAA module). As the PIAACMC development will require intensive efforts in the manufacturing and testing process, a step 0 coronagraph based on conventional pupil apodisation will be considered in the early stage of the experiment.

Coronagraphic wavefront sensor

A low-order wavefront sensor is critical to ensure that starlight remains centred at the coronagraphic plane. Since the PIAACMC is part of a family of coronagraphs that is optimised for the detection of companions at very low angular separations, it is highly sensitive to low-order aberrations, especially tip-tilt errors (pointing errors). The SPEED bench therefore includes a robust and efficient wavefront sensor to measure tip-tilt as well as defocus, namely the coronagraphic low-order wavefront sensor (CLOWFS; Vogt et al., 2011). Since the PIAACMC is a phase-mask-based coronagraph, the light used for the analysis is taken at the Lyot-stop plane, i.e., reflected towards an optical element that re-focuses the light onto the LOWFS camera. A dedicated tip-tilt mirror upstream in the optical path will be used to correct for the tip-tilt estimation from the CLOWFS. As the PIAACMC has to cope with stellar angular size up to 0.5 mas, residual jitter (tip-tilt) must be no larger than the stellar angular size in the error budget, hence

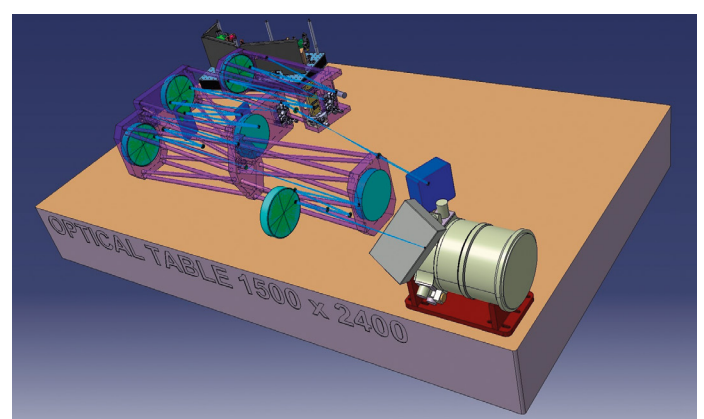
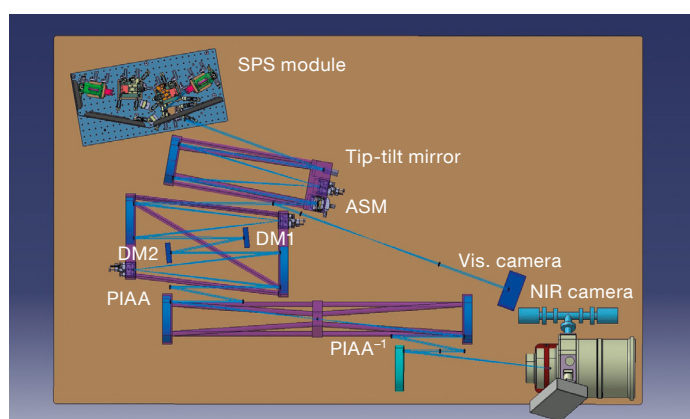


Figure 2. 3D optical/mechanical views of the SPEED bench are shown: from above (left) and inclined (right).

no larger than few $10^{-2} \lambda/D$ at $1.6 \mu\text{m}$. On top of that, in order to achieve point spread function raw contrast of 10^{-7} at such small IWA with the PIAACMC, quasi-static pointing should likely be accurate to about $10^{-3} \lambda/D$ at $1.6 \mu\text{m}$. Such tiny levels have already been demonstrated at the 10^{-2} level at the Paris Observatory (Mas et al., 2012) and at the 10^{-3} level at the Subaru Telescope (Vogt et al., 2011).

Imaging cameras

The infrared camera works at $1.65 \mu\text{m}$ with an internal *H*-band filter. Its read-out noise is 12 e- rms/pixel and quantum efficiency $> 60\%$. It is a 1k by 1k Hawaii array (engineering grade) from which we select only a quadrant of 512 pixels (enough considering the field of view of $64 \lambda/D$); it is read in double-correlated sampling mode. The optical camera for the phasing unit is an Apogee camera with 1024×1024 pixels with 2.2 e- rms/pixel read-out noise, and 92% quantum efficiency.

Current status

The SPEED testbed is temporarily installed at the Côte d'Azur Observatory and will be relocated to Nice University in early 2016 (in an ISO7 class room). It is placed on an optical table with air suspension, and reflective optics has been adopted for the whole design, except for the phasing unit arm. The testbed is located in a cleanroom in a nearly closed box to minimise internal turbulence and optimise stability. The bench environment is being intensively characterised. The stability of the whole system is one of the major concerns and will be characterised, monitored, pre-compensated by design as far as possible, and efforts will focus on developing actively controlled solutions to ensure the required level of stability for reaching the objectives of the project.

The finalisation of the SPEED optical design is underway pending extensive numerical simulation efforts. An end-to-end simulator code is nearly complete for adequately specifying the remaining parameters related to the Fresnel/Talbot effect. Mastering of these effects is mandatory for instrumental and contrast design. Integration is planned to start

in mid-2015. Most of the critical hardware is already in-house and under extensive test and characterisation.

The SPEED project: A step towards the ELT-PCS and a path toward PRIS²M

The overall objective of the SPEED project is to advocate R&D for the future generation of high-contrast imaging instruments. Devising a practical solution for broadband high-contrast capabilities operated at very small angular separation on unfriendly/complex apertures is an outstanding problem in high-contrast instrumentation. In particular, SPEED aims at increasing the technological readiness level of several subsystems to a satisfactory status for any high-contrast instrument for the E-ELT, especially for the E-ELT Planetary Camera and Spectrograph (PCS) instrument (Kasper et al., 2013). Although selected for construction, the ELT-PCS is subject to technical readiness, whereas it is considered mandatory for the E-ELT to achieve its primary science case (imaging and characterisation of exoplanets ideally down to Earth-like planets in the habitable zone). The technological requirements are ambitious and considered to be not yet ready for key components and subsystems, but with a clear R&D roadmap (Kasper et al., 2013) it should be possible to avoid any major showstopper. The primary objective of the SPEED project is therefore to provide a strong contribution to these efforts.

Together with this initial ambition, the SPEED project has been conceived as an initiator for a real instrument, likely in visitor mode, either dedicated to the VLT (or similar class of telescopes), or to an incentive demonstrator/precursor instrument for the E-ELT-PCS (assuming the presence of a visitor port with access to a single conjugated adaptive optics [SCAO] system). The recent two-phase approach to the E-ELT construction could foresee an early on-sky demonstration of PCS technologies on a 8-metre telescope as the optimal approach. Using an 8-metre telescope as test bed for E-ELT high-contrast imaging instrumentation could indeed be a major asset and could leverage significant scientific gain over the SPHERE instrument.


A large number of new ideas and know-how could be inherited from the SPEED experiment to build a simplified, single purpose, and thus efficient, instrument. For instance, a small IWA observing instrument to search areas very close to M-dwarfs could straightforwardly emerge from the SPEED project. This is the ambition behind the PRIS²M project (Planet Research Instrument at Small Separations from M-dwarfs) under exploration at the Lagrange Laboratory. Such an instrument could be seen as both a complementary programme for SPHERE (M-stars are not covered by the SPHERE science cases) and an exploratory programme for exoplanet direct imaging with the E-ELT-PCS, tackling an important science objective. It could bridge the gap between current exoplanet imaging instrumentation and the E-ELT-PCS slot, or alternatively anticipate by ten years the operation of a high-contrast imaging instrument at the E-ELT. The high density of M-dwarfs in the Solar Neighbourhood makes them good candidates for searches for young planets, ensuring a favourable contrast. M-dwarfs are important for understanding the mechanisms of planet formation and are currently the focus of several ongoing survey programmes.

Acknowledgements

The activity outlined in this paper is partially funded by the Région Alpes Côte d'Azur, the French Government, and by the European Union as part of the FEDER programme. The project also benefits from funding support from the Nice Sophia-Antipolis University, Côte d'Azur Observatory, Lagrange Laboratory, Airbus Defence and Space (Astrium), and CNES through a 2015 R&T programme. We are grateful to ESO for the loan of the near-infrared camera (the former ADONIS near-infrared wavefront sensing camera), and warmly acknowledge Sébastien Tordo, Jean-Louis Lizon, Markus Kasper and Norbert Hubin.

References

- Beuzit, J.-L. et al. 2006, *The Messenger*, 125, 29
- Dohlen, K. et al. 2006, *Proc. SPIE*, 6267, 34D
- Gonté, F. et al. 2009, *The Messenger*, 136, 25
- Guyon, O. et al. 2014, *ApJ*, 780, 171
- Hénault, F. et al. 2011, *Proc. SPIE*, 8151, 81510A
- Kasper, M. et al. 2010, *The Messenger*, 140, 24
- Kasper, M. et al. 2013, High-contrast imaging roadmap for the E-ELT-PCS, ESO internal document
- Martinez, P. et al. 2014, *Proc. SPIE*, 9145, 91454E
- Martinache, F. 2013, *PASP*, 125, 422
- Mas, M. et al. 2012, *A&A*, 539, 126
- Pueyo, L. & Norman, C. 2013, *ApJ*, 769, 102
- Vogt, F. P. A. et al. 2011, *PASP*, 123, 1434



FORS1 colour composite (*B*, *V*, *R* and $H\alpha$) image of the head of the cometary globule CG4 in the Gum Nebula. CG4 is a dusty star-forming globule with a long tail extending to the west (bottom of image) and pointing away from the Vela supernova remnant which may be responsible for compressing and shaping the globule. See Release eso1503 for more details.

An Unbiased Near-infrared Interferometric Survey for Hot Exozodiacal Dust

Steve Ertel^{1,2,3}Jean-Charles Augereau^{2,3}Olivier Absil⁴Denis Defrère⁵Jean-Baptiste Le Bouquin^{2,3}Lindsay Marion⁴Amy Bonsor⁶Jérémy Lebreton^{7,8}¹ ESO² Université Grenoble Alpes, France³ CNRS, Institut de Planétologie et d'Astrophysique de Grenoble, France⁴ Département d'Astrophysique, Géophysique et Océanographie, Université de Liège, Belgium⁵ Department of Astronomy, Steward Observatory, University of Arizona, USA⁶ School of Physics, H. H. Wills Physics Laboratory, University of Bristol, United Kingdom⁷ NASA Exoplanet Science Institute, California Institute of Technology, Pasadena, USA⁸ Infrared Processing and Analysis Center, California Institute of Technology, Pasadena, USA

Exozodiacal dust is warm or hot dust found in the inner regions of planetary systems orbiting main sequence stars, in or around their habitable zones. The dust can be the most luminous component of extrasolar planetary systems, but predominantly emits in the near- to mid-infrared where it is outshone by the host star. Interferometry provides a unique method of separating this dusty emission from the stellar emission. The visitor instrument PIONIER at the Very Large Telescope Interferometer (VLT) has been used to search for hot exozodiacal dust around a large sample of nearby main sequence stars. The results of this survey are summarised: 9 out of 85 stars show excess exozodiacal emission over the stellar photospheric emission.

Planetesimals and comets are a major component of the Solar System (in the Kuiper Belt and the asteroid belt), as well as of extrasolar planetary systems, where they occur in debris discs. Besides the planets, they are the main outcome of the planet formation process. Studying the

composition and distribution of the dust produced in debris discs through collisions and outgassing of these larger bodies is a powerful tool that can help to constrain the architecture, dynamics and evolution of extrasolar planetary systems. However, debris discs that are relatively easy to detect are located several astronomical units (au) to a few hundreds of au from their host stars, and thus only trace the outer regions of planetary systems. In order to study the inner regions close to the habitable zones, one has to study warm and hot dust closer to the star. This dust is called exozodiacal dust, or exozodi for short, by analogue with the Zodiacal dust in the Solar System.

The Zodiacal light can be observed on dark nights directly after dusk and before dawn as a cone of faint light stretching from the horizon in the west (after dusk) or in the east (before dawn). It is caused by sunlight scattered off small dust particles close to the orbit of the Earth. More generally, Zodiacal dust is distributed in a disc inside the asteroid belt, extending all the way down to the sublimation distance of the dust from the Sun, which corresponds to a few Solar radii. The dust temperatures range from about 100 K to about 2000 K, depending on the distance from the Sun. In the innermost regions it forms the Fraunhofer corona (F-corona) of the Sun, a region of the corona where the prominent absorption lines in the Solar spectrum are visible because the light seen there is nearly unaltered sunlight scattered by the dust particles. It is noteworthy that the Zodiacal light is the most luminous component of the Solar System after the Sun itself.

Not unlike the Zodiacal dust, exozodiacal dust is located in the inner regions of extrasolar planetary systems, within a few au of main sequence stars. This region often encompasses their habitable zone. Historically, this circumstance has brought it a lot of attention, because the presence of exozodi is expected to complicate the direct-imaging detection and characterisation of Earth-like planets in the habitable zones around other stars by future space missions. The faint light of these potential planets can be hidden in the extended emission of the dust disc. The structures created in the dust distribution due to planet-disc interaction may pro-

vide clues pointing towards the presence of a planet, but clumps in the dust distribution may also be misinterpreted as actual planets due to the limited resolution and sensitivity of current instruments. Thus, detecting and characterising exozodiacal dust systems provides critical input for the design of such space missions. However, detecting the dust itself with present instruments is complicated by the fact that the warm and hot emission peaks at near- to mid-infrared wavelengths where the dust emission is outshone by the host star. Thus, only a few very bright — and perhaps unrepresentative — systems can be detected photometrically.

Infrared interferometric detection of exozodi

Due to the small extent of exozodiacal systems — one au at a typical distance of 10 pc for nearby stars corresponds to an angular size of 100 milliarcseconds — only interferometry is currently able to spatially resolve them. When used at baselines of a few tens of metres, near-infrared interferometry is able to fully resolve the extended emission of the dust disc while the star still remains largely unresolved. The result is a small deficit in the measured squared visibilities (the main observable of infrared interferometry) compared to the values expected from the star alone (see Figure 1 for an explanation). Using this technique the disc can be spatially disentangled from the star, allowing the disc to be detected and the ratio between the disc and stellar emission measured. This method has so far been the most powerful and efficient tool in the search for faint exozodiacal dust.

However, the dust detected by this method in the near-infrared (NIR) is expected to be very hot, close to its sublimation temperature, and its relation to slightly cooler dust in the habitable zone is unclear. This habitable zone dust is brighter in the mid-infrared (MIR) where it can be detected by the VLTi MID-infrared interferometric instrument (MIDI) for a few bright systems (e.g., Smith et al., 2009) or more efficiently by nulling interferometry. With this latter method the stellar light from two telescopes is brought to destructive interference, while light

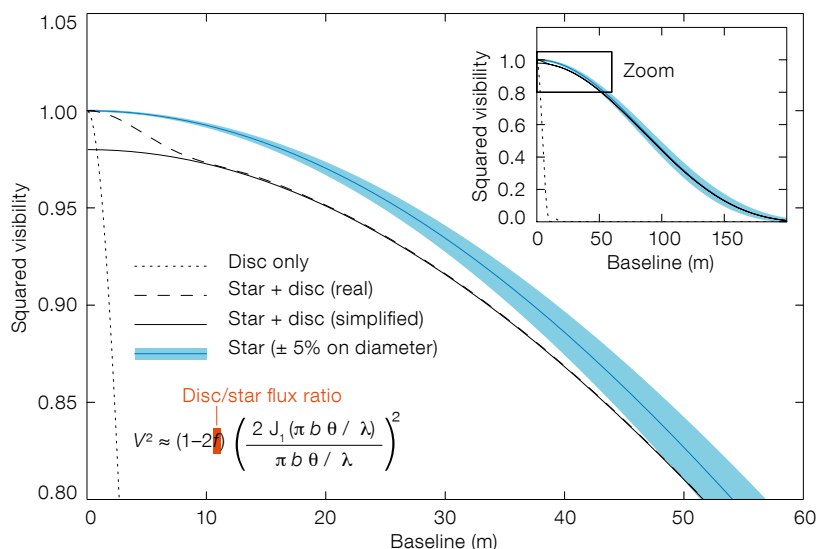


Figure 1. (Left) Illustration of the detection strategy for exozodis. The dashed curve shows a realistic case assuming a uniform disc for both the star and the flux distribution from the exozodiacal dust and a disc-to-star flux ratio of $f = 1\%$. For the simplified case, the solid curve shows the same assumptions, but with the approximation following the equation. Diameters of the star and (face-on) disc have been chosen to be 2.5 milliarcseconds (about an A-type star at 10 pc) and 500 milliarcseconds (5 au at 10 pc), but exact numbers are not relevant for this illustration.

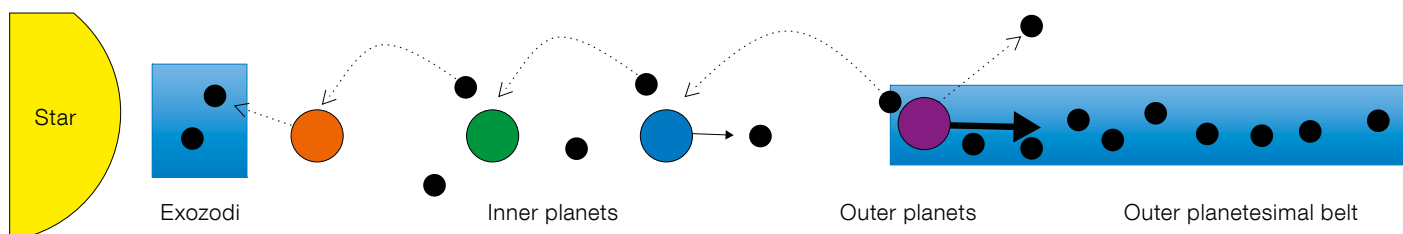


Figure 2. (Below) A diagram (not to scale) to illustrate the scattering of planetesimals by an outer planet, that leads to an exchange of angular momentum and the outward migration of that planet (Bonsor et al., 2014). Some of the scattered particles are ejected, whilst some are scattered into the inner planetary system, where they interact with the inner planets. This scattering leads to a flux of material into the exozodi region.

off-centre from the star is transmitted, which improves the dynamic range of the observations. Both methods have been used in parallel in the past to search for exozodiacal dust, mostly with the Fiber Linked Unit for Optical Recombination (FLUOR) instrument at the Center for High Angular Resolution Astronomy (CHARA) array (in the NIR; e.g., Absil et al., 2006) on Mt. Wilson, California and the Keck Interferometer Nuller (in the MIR; Mennesson et al., 2014) on Mauna Kea, Hawaii.

Due to the recent development of the visitor instrument PIONIER (Precision Integrated Optics Near Infrared Experiment; LeBouquin et al., 2011) at the VLTI, which operates in the H -band, the search for exozodis in the NIR has become more efficient and of similar accuracy to the previous surveys, allowing for a significant increase in the number of surveyed stars. The sensitivity of the available instruments is, however, only capable of detecting exozodis a couple of hundred times brighter (more massive) than the Zodiacal dust. This state-of-the-art exozodi sensitivity is approximately one order of magnitude larger than that

required to prepare future exoEarth imaging missions. The Large Binocular Telescope Interferometer (LBTI) is designed to achieve the required sensitivity and will soon start a MIR survey of 50 to 60 carefully chosen nearby main sequence stars (Weinberger et al., 2015).

Potential origins of exozodiacal dust

The fact that many exozodiacal systems have already been found, given the limited sensitivity of present instruments, is surprising (Absil et al., 2013). Such high levels of dust are difficult to sustain. The Zodiacal dust has two main origins: collisions of asteroids in the asteroid belt result in dust that is dragged inwards by the interaction with stellar radiation (Poynting–Robertson drag) and the evaporation of comets heated when they get close to the Sun supplies dust. While these scenarios might work for a few MIR-detected systems, they generally do not work well for more massive systems, as have been detected in the NIR around other stars. If the dust density in the disc is too high, the dust will further collide and be destroyed before being dragged

inwards to regions where it is detected. Furthermore, a higher dust mass would require a larger number of planetesimals which are colliding more often to produce the dust present; this process would in turn destroy the planetesimals faster, so that at the ages of the systems observed, few planetesimals would be left (Wyatt et al., 2007). The production of the observed amounts of dust through comet evaporation would require a large number of comets, approximately one thousand events per year similar to Hale–Bopp reaching its perihelion.

A potential scenario explaining such a large number of comets would be a connection to an outer debris disc where planetesimals are scattered inwards through gravitational interaction with an existing planetary system (see Figure 2). Considering the realistic interaction of these planets with the planetesimals (planetesimal-driven planetary migration), this scenario is able to produce detectable exozodis even if the outer debris disc were too faint to be detected with present instruments (Bonsor et al., 2014). However, such a mechanism puts strong constraints on the architecture of the

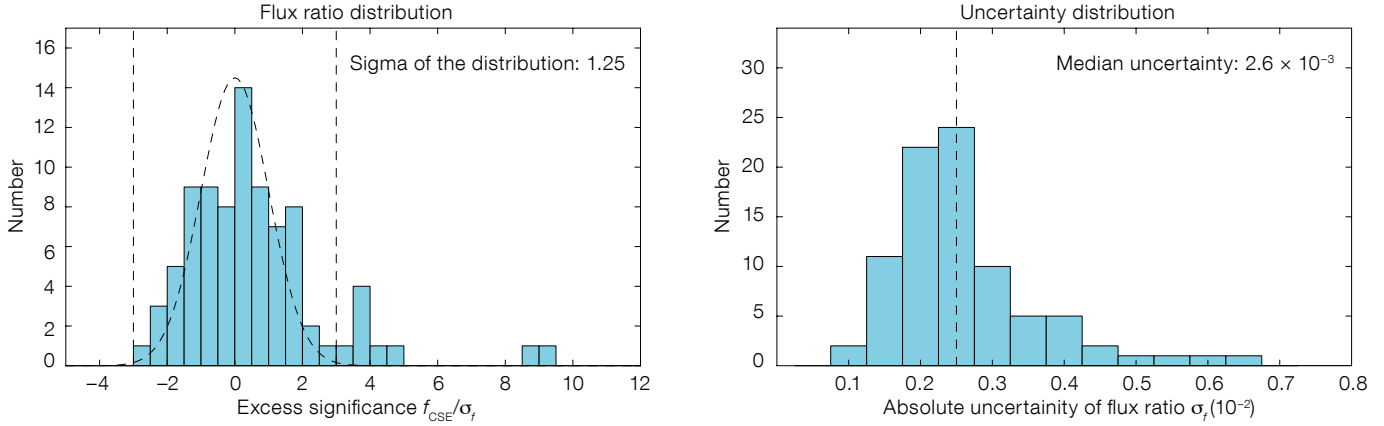


Figure 3. Excess distribution (left) and distribution of uncertainties (right) on the disc-to-star flux ratio are shown. The Gaussian overplotted on the excess distribution has a width of $\sigma = 1$ and is used to guide the eye, illustrating that the data are consistent with this ideal behaviour. Vertical dashed lines are plotted at $f = -3\sigma$ and $+3\sigma$ for the excess distribution and at the median uncertainty (2.6×10^{-3}) for the uncertainty distribution.

underlying planetary system. While this would be a very interesting scenario, it is questionable whether all systems observed are likely to meet these constraints. A combination of planetesimal-driven migration and dust trapping could explain the presence of the detected dust. Potential dust-trapping mechanisms are suggested from the realistic treatment of the dust sublimation (Lebreton et al., 2013) or the interaction of dust grains with the stellar magnetic field (Czechowski & Mann, 2010).

An unbiased near-infrared interferometric survey

Strong constraints on the potential origins of exozodiacal dust, described above, can be placed by a statistical analysis of the detection rate and excess levels of exozodiacal dust with respect to other properties of the systems, such as stellar spectral type, age of the system, or the presence of a detectable cool debris disc in the outer regions of the systems. A dependence on the stellar spectral type (i.e., stellar mass), similar to the one that has been found for debris discs and younger protoplanetary discs, would suggest a similar or even common origin of the material detected in these different dust populations. For these systems,

more massive discs are present around more massive stars. A strong dependence on the system's age (most exozodis are detected around very young stars) would suggest that the origin is a collisionally depleting planetesimal belt. Alternatively a strong correlation with the presence of an outer disc would suggest that the hot material is supplied through some mechanism from this outer reservoir.

Our team carried out the first large, NIR interferometric survey for hot exozodiacal dust in order to statistically address the questions on the origin and evolution of these enigmatic systems (Absil et al., 2013; Ertel et al., 2014). We started our search using CHARA/FLUOR, the first instrument to routinely provide the required accuracy of the measurements. However, FLUOR can only use two telescopes at a time, which results in a limited observational efficiency. Thus, in about seven years, only around 40 stars could be observed with sufficient accuracy, but this still allowed the first statistical conclusions to be drawn (Absil et al., 2013).

The development of the PIONIER instrument for the VLTI, which can use four telescopes simultaneously, allowed a significant increase in our observing efficiency, so that in only 12 nights during 2012 a total of 92 stars could be observed. A cumulative median 1σ accuracy per target of 0.26% on the disc-to-star flux ratio was reached (Figure 3). To increase our sample and thereby to improve our statistics we combined the results from the PIONIER survey with those from FLUOR, resulting in a total of about 130 stars observed and available

for the statistical analysis. The targets for both surveys were selected carefully in order to avoid any relevant selection bias that could affect the statistics.

In addition to the higher efficiency, PIONIER provides a few advantages over FLUOR. The simultaneous use of four telescopes allows the closure phase of the detected systems to be measured, which can only be achieved by combining the light from combinations of three telescopes. This quantity measures the deviation of the brightness distribution of an observed target from point symmetry, allowing a star surrounded by a dust disc and a star orbited by a faint, close companion, which otherwise have a very similar observed visibility deficit, to be distinguished. Another advantage is the fact that PIONIER data can be obtained with a small spectral resolution of three or seven spectral channels across the H -band. This information allows one to constrain the spectral slope of the detected excess and thus the emission mechanism and — in case of thermal emission — the temperature of the dust.

Survey results

From our PIONIER survey we have found that nine out of the 85 targets which proved to be suitable for our analysis ($\sim 11\%$) show a significant excess, typically around 0.5 to 1%, above the stellar photosphere. Five targets were found to have a faint, stellar companion and needed to be rejected as exozodis. These latter detections were analysed in a separate study and interesting implications for the formation of binary stars were

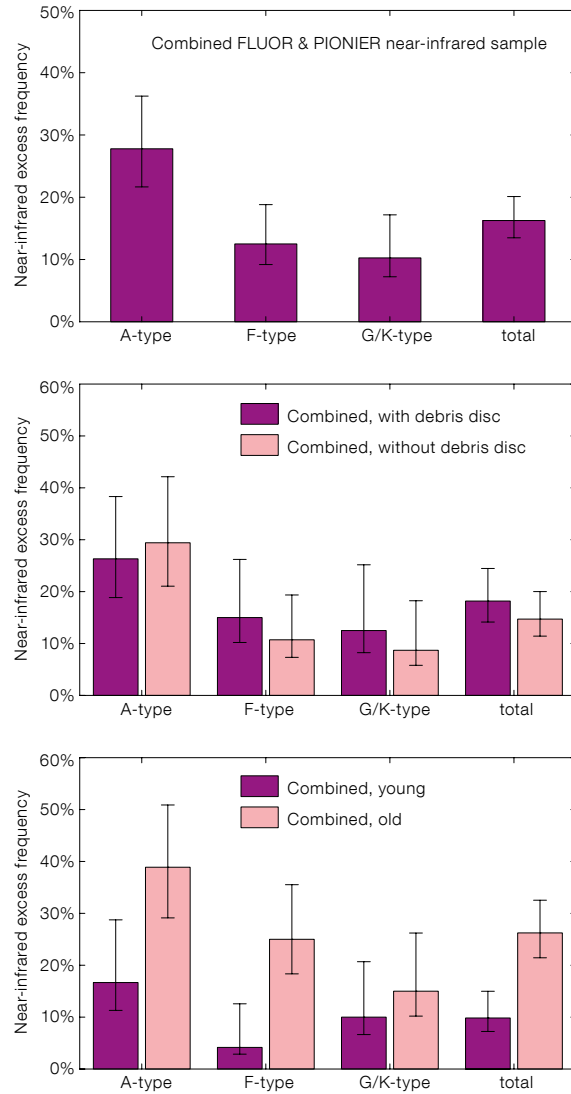
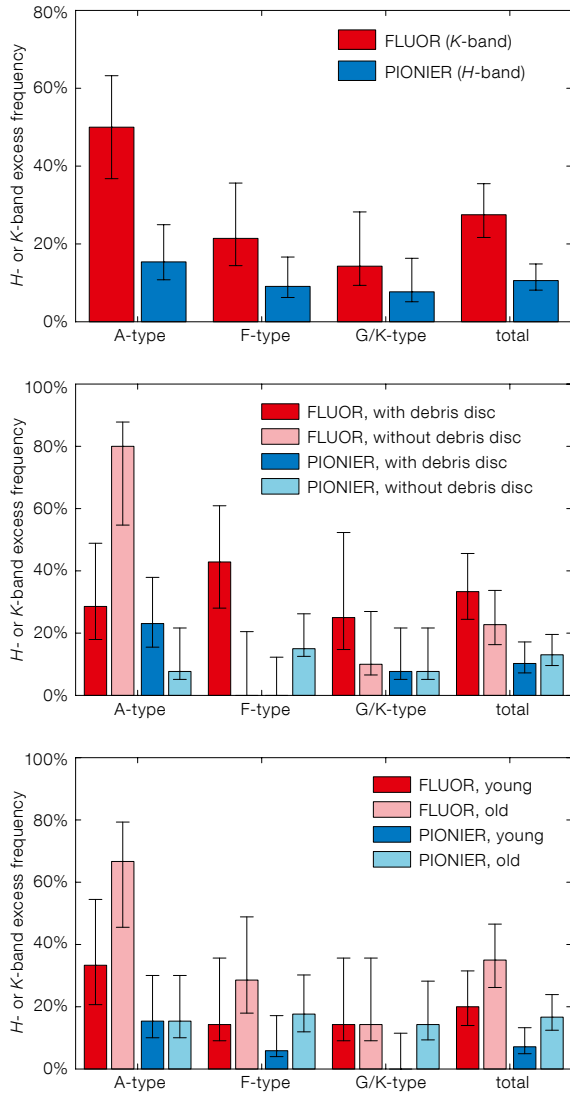


Figure 4. Single (left) and combined (right) statistics from the FLUOR (red) and PIONIER (blue) sample. The top row shows the excess fraction with respect to the stellar spectral type, the middle row shows the same, but, in addition, separated for stars with and without a debris disc detected, and the bottom row the excess fraction for different spectral types and separated for stars younger and older than the median age in each spectral type bin.

found (Marion et al., 2014). One more star was rejected from the analysis because it shows hints of post-main sequence evolution which could cause other effects, such as mass loss or strong stellar winds that might mimic an exozodi in our data.

A detailed statistical analysis of the combined PIONIER and FLUOR sample (Figure 4) shows that the distribution of the exozodiacal dust detection rate, with respect to the stellar spectral type, is similar to that of debris discs. This suggests that both kinds of dust discs are produced by circumstellar material originating in the protoplanetary disc during the planet formation process. However, there is no correlation between the presence of a debris disc and an exozodi

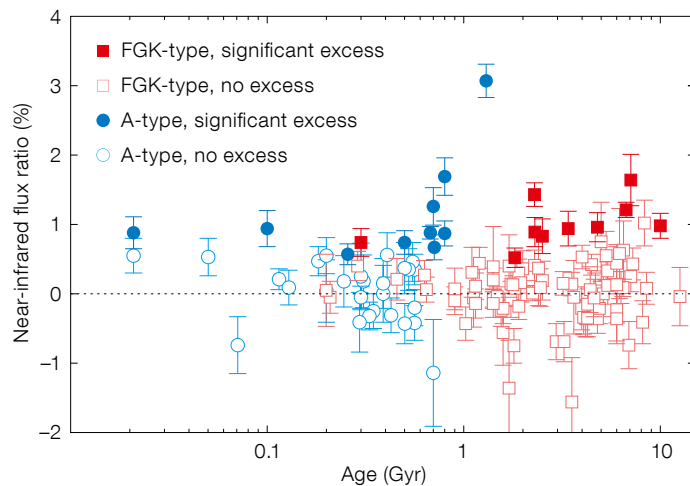


Figure 5. Excess levels for the stars in our sample shown against stellar age. Filled symbols are for stars with significant excess, while empty symbols are for stars without a significant detection. The sample is separated into A-type stars and stars of later spectral types, in order to account for the different main sequence lifetimes of these stars. The star with a 3% flux ratio is α Aql (see Absil et al. [2013] for details).

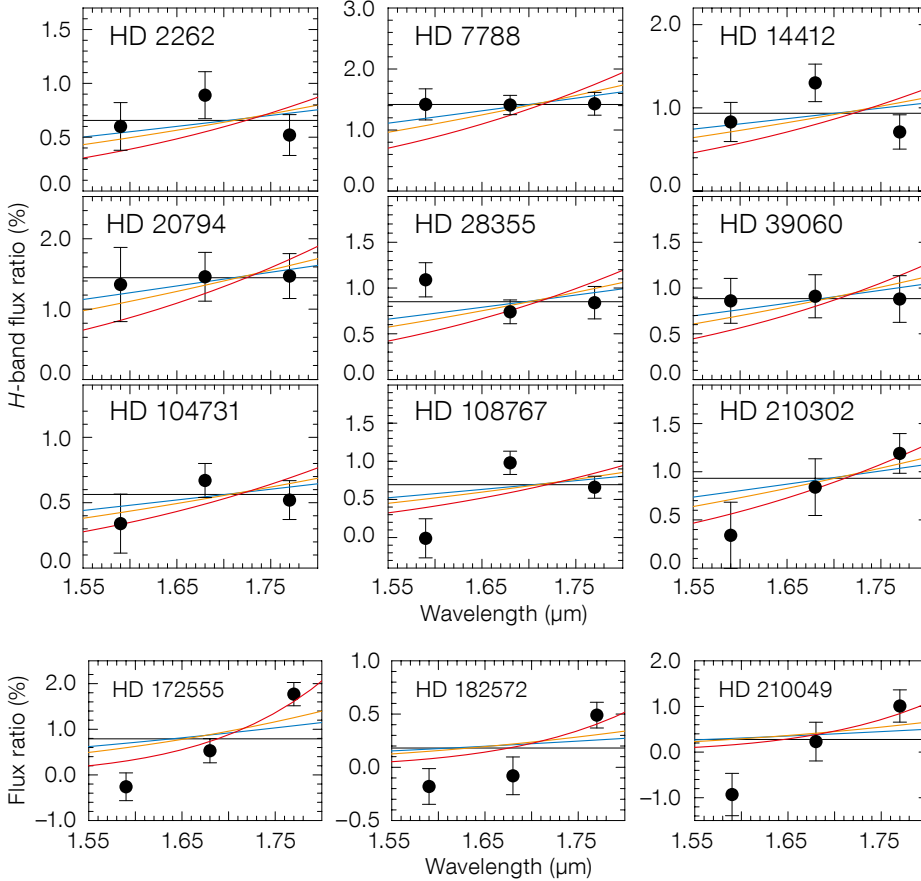


Figure 6. Spectral slopes of the excesses detected with PIONIER (first three rows) and some potential excesses only identified by their spectral slopes, considered tentative (fourth row). The horizontal, black line illustrates the case of purely (grey) scattered stellar light, while the coloured curves show the shapes expected from blackbody thermal emission at different temperatures. Error bars are 1σ .

very hot dust emitting significantly in the *H*-band needs to be very close to the star, in the case of scattered light the dust could be slightly more distant, closer to the habitable zone. At that location, the dust has a stronger impact on the detectability of habitable Earth-like planets.

Future prospects

Our sample of near-infrared bright exozodis provides an excellent basis for further studies. At the same time, our observations are very timely for the new VLTI instruments, GRAVITY and MATISSE, expected to arrive in 2015 and 2016, respectively. GRAVITY will enable us to observe the discs in the *K*-band, at slightly longer wavelengths than PIONIER, thereby better constraining the slope of the excess and thus the emission mechanism. From the increased emission in *K*-band compared to *H*-band, GRAVITY will also allow the excesses to be measured at very high significance. This will allow detection of small variations in the excess levels, indicative of variation in the mass and location of the dust, enabling strong constraints to be put on its evolution. MATISSE will cover the range of even longer wavelengths up to the *N*-band in the MIR, constraining very well the most relevant region in which the dust emits (Figure 7). Combining all VLTI instruments, we will be able to study in detail the dust distribution and composition in these systems. The strength of combined modelling of different interferometric data has — to some extent — already been shown by our team (Defrère et al., 2011; Lebreton et al., 2013).

One of the main questions to be answered concerns the nature of any connections between the hot dust detected in the NIR, the warm dust in the habitable zone and even the colder dust further out. So far there are indications that there might be an anti-correlation

visible in our data. This might suggest that there is indeed no physical correlation between the two phenomena. On the other hand, it is important to note that we are only able to detect the brightest, most extreme exozodis with current instrumentation, and the debris discs detectable so far are also at least a few times more massive than the Kuiper Belt in the Solar System. Thus, a significant fraction of both kinds of discs remain undetected and a correlation might be hidden by that fact.

A very surprising result is that the detection rate (Figure 4) and excess levels (Figure 5) of exozodis do not decrease with the ages of the systems. This would be expected for any phenomenon that evolves over time, such as a belt of colliding planetesimals. In contrast, the exozodis seem to be caused by a stochastic process or a process that can be triggered stochastically at any time during the evolution of the planetary system. One example could be a planetary colli-

sion; however, given the high detection rate of exozodis, the short lifetime of the dust and the expected scarcity of such events, this is not a likely explanation for the detected systems. Thus, the independence of the detection rate and excess levels from the ages of the systems surveyed remains enigmatic.

An important result from PIONIER derives from the spectrally dispersed data, enabling us to constrain, for the first time, the spectral slopes of a large number of excess detections (Figure 6). The thermal emission of even the hottest dust is increasing towards wavelengths longer than the *H*-band. A consequence of this thermal emission would be an increasing disc-to-star contrast with wavelength. However, we find for most of our detections that the contrast is rather constant with wavelength, indicating that the emission is dominated by starlight scattered off the dust grains. This unexpected result has important implications for the dust distribution in these systems. While

between the presence of NIR- and MIR-detected dust. This might suggest the presence of planets in the systems with MIR bright dust emission that prevents the dust from the outer regions migrating further in, where it would be detected in the NIR. Instead the dust would pile up near the orbits of those planets.

In the context of future observational perspectives, two instruments in the northern hemisphere will soon provide critical complementary information on exozodis: the CHARA/FLUOR instrument in the NIR and the LBTI in the MIR. A new mode at CHARA/FLUOR will provide spectrally dispersed observations of northern objects inaccessible from Paranal, while the LBTI will observe with unprecedented sensitivity a sample of 50 to 60 nearby main sequence stars to characterise the faint end of the exozodi luminosity function (see first LBTI results in Defrère et al. [2015]). However, the efficiency of both instruments is limited due to the use of only one interferometric baseline at a time and the need for a large number of observations to reach the nominal sensitivity. Furthermore, the LBTI exozodi survey is designed for broadband detection of faint levels of

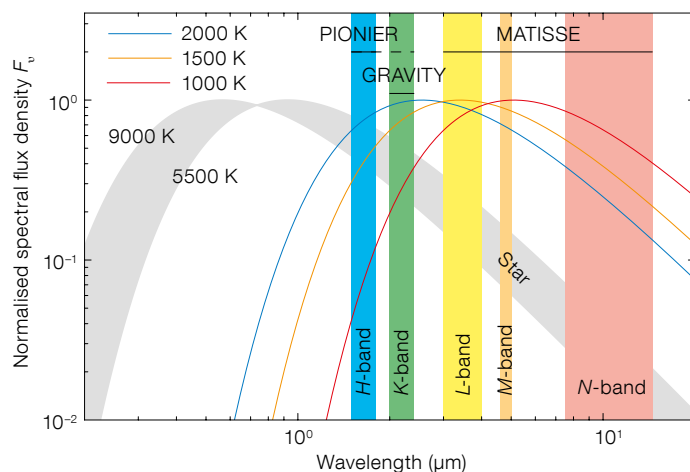


Figure 7. Illustration of the spectral coverage of PIONIER and the future VLT instruments GRAVITY and MATISSE. The shape of the stellar emission is shown in grey as the blackbody emission of two different, typical stellar temperatures. Dust blackbody curves are shown as coloured lines. The spectral coverage of the VLT instruments is illustrated by the coloured, vertical bars.

dust and will give limited constraints on the dust properties. Only a complete exploitation with both NIR and MIR observations, and in particular those of the near-future instruments at the VLT, will allow us to precisely characterise exozodiacal dust and study its origin and evolution, even if this is only possible for systems bright enough to be detected by our survey.

References

- Absil, O. et al. 2006, *A&A*, 452, 237
- Absil, O. et al. 2013, *A&A*, 555, 104
- Bonsor, A. et al. 2014, *MNRAS*, 441, 2380
- Czechowski, A. & Mann, I. 2010, *ApJ*, 714, 89
- Defrère, D. et al. 2011, *A&A*, 534, 5
- Defrère, D. et al. 2015, *ApJ*, 799, 1
- Ertel, S. et al. 2014, *A&A*, 570, 128
- Le Bouquin, J.-B. et al. 2011, *A&A*, 535, 67
- Lebreton, J. et al. 2013, *A&A*, 555, 146
- Marion, L. et al. 2014, *A&A*, 570, 127
- Mennesson, B. et al. 2014, *ApJ*, 797, 119
- Smith, R. et al. 2009, *A&A*, 503, 265
- Weinberger, A. J. et al. 2015, *ApJS*, in press
- Wyatt, M. C. et al. 2007, *ApJ*, 658, 569



VISTA VVV (the Variables in the *Via Lactea* Public Survey) near-infrared colour image (*JHKs*) of the centre of the Galactic H II region M20 (NGC 6514). At near-infrared wavelengths the line emission is weaker than in the optical and the dust extinction lower, so background stars are easily located. Two Cepheid variables on the other side of the Galactic disc at 11 kpc were detected in this field; see Release eso1504 for details.

An Astrophysical Laboratory: Understanding and Exploiting the Young Massive Cluster Westerlund 1

Simon Clark¹
 Ignacio Negueruela²
 Ben Ritchie¹
 Paco Najarro³
 Norbert Langer⁴
 Paul Crowther⁵
 Liz Bartlett⁶
 Danielle Fenech⁷
 Carlos González-Fernández⁸
 Simon Goodwin⁵
 Marcus Lohr¹
 Raman Prinja⁷

¹ Department of Physics and Astronomy,
 The Open University, Milton Keynes,
 United Kingdom

² Departamento de Física, Ingeniería
 de Sistemas y Teoría de la Señal,
 Universidad de Alicante, Spain

³ Departamento de Astrofísica, Centro de
 Astrobiología, (CSIC-INTA), Madrid,
 Spain

⁴ Argelander Institut für Astronomie,
 Bonn, Germany

⁵ Department of Physics and Astronomy,
 University of Sheffield, United Kingdom

⁶ Astrophysics, Cosmology and Gravity
 Centre (ACGC), Astronomy Department,
 University of Cape Town, South Africa

⁷ Department of Physics & Astronomy,
 University College London, United King-
 dom

⁸ Institute of Astronomy, University of
 Cambridge, United Kingdom

Westerlund 1 provides a unique opportunity to probe the physics of massive stars, from birth to death and beyond, as well as the formation and evolution of a super star cluster that appears destined to evolve into a globular cluster. We highlight the result of current studies of this cluster, its diverse stellar constituents and immediate environment, concluding with a summary of future research avenues enabled by ESO facilities.

Massive stars play a central role in the evolution of galaxies, from the early Universe through to the current epoch, via their intense radiation fields and the deposition of chemically enriched gas and solid-state material into the interstellar medium. Moreover they are ultimately responsible for the most energetic, tran-

sient high-energy phenomena in the Universe: supernovae, gamma-ray bursts and X-ray binaries. It is therefore somewhat unsettling that the mechanisms of their birth, the processes governing their subsequent evolution on and beyond the main sequence (MS) and the nature of their deaths and ultimate fate — neutron star or black hole — are shrouded in uncertainty.

Nevertheless, our current understanding is sufficient to enable us to identify the physical agents driving massive stellar evolution. A central theoretical tenet is that the evolutionary pathway of a star is dependent on its initial mass, but, for the most massive stars, powerful stellar winds and, in their latter evolutionary stages, violent instabilities act to continuously strip their hydrogen-rich outer layers away. The efficiency of such processes is likely to contribute to the dichotomy between type II (H-rich) and type Ibc (H-poor/depleted) supernovae (SNe). Since stellar winds are driven by radiation pressure, this in turn introduces an additional explicit metallicity dependence into massive stellar evolution.

Moreover, the internal dynamics of such stars, and hence the degree of mixing of chemically processed and unprocessed material they experience, will also play a profound role in their evolution. Since it is likely that both the (differential?) rotation of such stars and the presence (or absence) of an internal magnetic field will play key roles in determining the efficiency of such processes, these too must be incorporated into theoretical models.

Finally, it has recently been recognised that a large proportion of massive stars are born in binary systems, and that in many cases these are close enough to permit interactions on or beyond the MS (e.g., Sana et al. 2013; de Mink et al., 2014). Since this can lead to the removal of the outer layers of a mass donor, the rejuvenation/growth of the mass recipient and, in extreme cases, their merger, it is apparent that both the binary fraction as well as the physical properties (e.g., mass ratio and orbital separation) also profoundly impact stellar evolution.

One can thus readily envisage how the endpoints of the stellar lifecycle depend

on the interplay of these parameters. At a given stellar mass, do these factors combine to drive sufficient mass loss to permit a type Ibc rather than a type II SN? Is the pre-SN core rotating rapidly enough to permit a gamma-ray burst? Indeed, is the core massive and compact enough to form a black hole rather than a neutron star, and, if the latter, is it powered by the extraction of rotational or magnetic energy?

Observational tests

How, then, may one quantify the roles played by these various evolutionary agents? Ideally, one would like to study a homogeneous stellar population where the competing physical effects might be distinguished. An obvious solution is to employ massive stellar clusters or associations as laboratories, since both the age and metallicity of the stars may be expected to be well constrained and furthermore they furnish a statistically robust sample size.

With a mass likely $> 10^5 M_{\odot}$, the 30 Doradus star-forming complex (R136) within the Large Magellanic Cloud is a compelling target (Figure 1, bottom), more so because the low foreground extinction permits observations of traditional “blue-end” (400–500 nm) spectral diagnostics for massive stars. These factors drove the development and implementation of the VLT/FLAMES Tarantula survey (Evans et al., 2011), which encompasses ~ 800 O and B stars and, to date, has resulted in about 20 refereed publications on the properties and evolution of its members. Given this undoubted success, what is the motivation for additional studies?

We may identify a number of factors. Most importantly one would wish to study differing metallicity environments in order to determine the effect of chemical composition on stellar evolution. Secondly, star formation across the ~ 200 pc extent of 30 Dor appears to have proceeded in multiple bursts over ~ 10 Myr (Walborn & Blades, 1997). Therefore, identifying the co-eval populations ideally required to most effectively investigate stellar evolution is non-trivial, especially since the most likely locations to host them — dense individual clusters such as

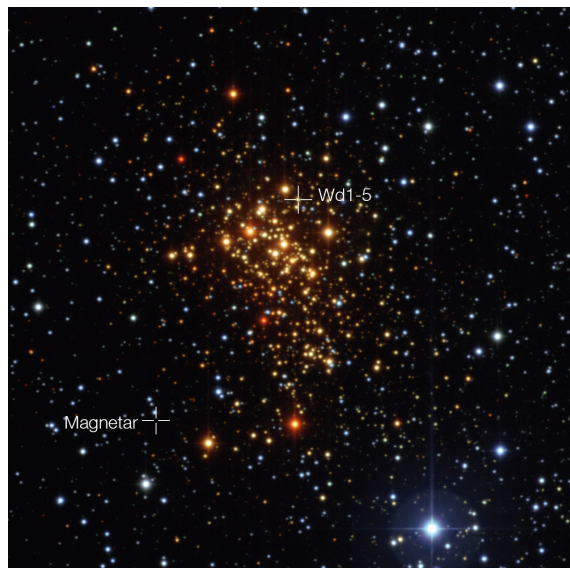


Figure 1. Top: Optical image of Westerlund 1 (~ 7.3 pc on a side) taken with the Wide Field Imager (WFI) on the MPG/ESO 2.2-metre telescope, with *BVR* filters, showing the position of both the magnetar and putative binary companion Wd1-5.

Middle: Wide-field optical image (~ 175 pc on a side) of the field centred on Wd1 (the fuzzy orange blob in the centre).

Bottom: HST composite-colour image of the star-forming complex 30 Doradus in the Large Magellanic Cloud (size 185 pc by ~ 146 pc), from a combination of Hubble Space Telescope Advanced Camera for Surveys/Wide Field Channel (ACS/WFC) and Wide Field Camera 3 (WFC3/UVIS) images (*I*-band) and WFI ([O III] and $H\alpha$ narrow-band filters).



R136 — are difficult to probe due to crowding. Despite this extended star formation history, 30 Dor appears to lack the cool hypergiants which help drive the extensive mass loss required to facilitate the formation of H-depleted Wolf–Rayet stars (WRs). Finally one might also wish to explore whether the environment in which the stars form affects their life cycle, e.g., via the dynamical formation, modification and disruption of binaries.

Historically, it was thought that the massive stellar aggregates required to enable such studies were absent from the Galaxy. However the advent of near- and mid-infrared surveys revealed an ever-expanding population of heavily obscured young massive clusters, alleviating this apparent deficiency. Nevertheless, given the effort expended in uncovering this population, it is frustrating that possibly the most massive cluster in the Galaxy appears to have been hidden in plain sight: in 1961 Bengt Westerlund simply characterised his discovery as a very young “heavily reddened” cluster, with Westerlund 1 (Wd1; Figure 1, top and middle) languishing in relative obscurity for the next forty years.

In retrospect the detection of an unprecedented cohort of cool, short-lived yellow hypergiants (YHGs) and red supergiants (RSGs) in the earliest observations of Wd1 obviously required a substantial population of massive progenitors; a clear indication that the cluster was worthy of follow-up observations. Motivated instead by the unusual radio properties of Wd1, the discovery that it hosted unprecedented numbers of both blue super- and hypergiants (BSG/BHGs) and WRs came as a complete surprise (Clark et al., 2005). Analysis of these populations implied a distance of ~ 5 kpc, a radius of < 2 pc (in comparison to the 200 pc extent of 30 Dor; Figure 1, bottom) and an apparent integrated mass of $\sim 10^5 M_{\odot}$, revealing that Wd1 was the first direct Galactic analogue of the super star clusters that characterise the young stellar population of starburst galaxies.

Intriguingly, the simultaneous presence of both WRs and RSGs was unexpected, suggesting that we either view Wd1 at a privileged point in its evolution, or that it comprises two or more stellar

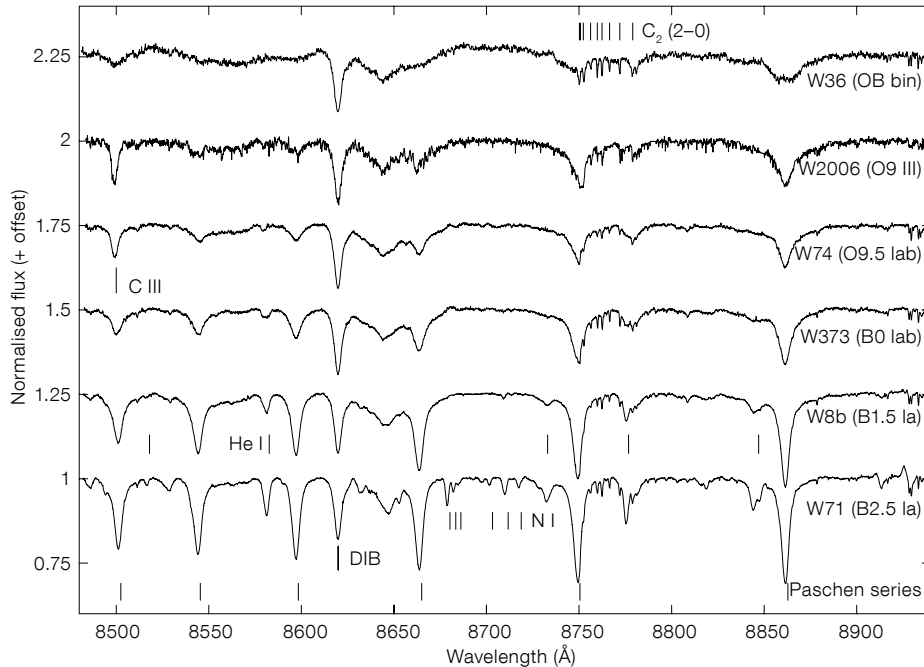


Figure 2. Montage of representative red-end optical spectra of evolved OB stars in Wd1 showing the smooth progression in both spectral type and luminosity class expected for a coeval stellar population (from Clark et al., in prep.).

populations. In order to investigate this issue, follow-up observations of the evolved OB star population were made with the suite of Very Large Telescope (VLT) instrumentation. These revealed a highly uniform population, with the spectral type and luminosity class of stars evolving continuously from O9 III to B2.5 Ia (see Figure 2; Negueruela et al. [2010] and Clark et al. in prep.). This behaviour is exactly that expected for a simple homogeneous and co-eval stellar population at an age of ~ 5 Myr, exactly the time for which one might expect the co-existence of WRs and RSGs. Critically, these observations would have detected a population of either younger or older supergiants if present within Wd1, the absence of such stars implying that it formed in a near instantaneous starburst. Such a conclusion was independently reached via observations at the other extreme of the mass function, with an age spread of < 0.4 Myr suggested for Wd1 via the properties of stars at the MS turn-on (Kudryavtseva et al., 2012).

How did Wd1 form?

The deduction of a nearly instantaneous burst immediately begs the question of how Wd1 formed. Observations of other star-forming regions in the Galaxy, and

beyond, appear to show an additional level of hierarchy, whereby star clusters themselves form in larger complexes embedded within the remains of their natal giant molecular clouds. Exemplars include 30 Doradus, which hosts a number of clusters distributed throughout its confines (Figure 1, bottom), and the G305 complex, comprising a number of apparent proto-clusters embedded on the periphery of a wind-blown bubble driven by the young massive clusters Danks 1 and 2 (Clark & Porter, 2004; Davies et al., 2012). A further, diffuse population of massive stars is distributed across both regions, which taken together are indicative of ongoing star formation activity over several Myr.

However wide-field optical imaging of Wd1 reveals no such ongoing star formation activity, nor satellite clusters (Figure 1, top and middle); a conclusion supported by inspection of near- and mid-infrared data (e.g., the Two Micron All Sky Survey [2MASS] and the Spitzer Galactic Legacy Infrared Mid Plane Survey [GLIMPSE] and Multi Band Imaging Photometer Galactic [MIPSGAL] surveys). Mindful that it might be surrounded by a diffuse halo of isolated massive stars (either OB stars or RSGs; c.f., Negueruela et al., 2011), we obtained AAOmega multi-object spectroscopic observations

of photometrically selected targets, but no such population was identified. Entirely unexpectedly, Wd1 appears to have formed in splendid isolation. Given both its coevality and the absence of additional, contaminating populations it thus serves as a “gold-standard” laboratory for the analysis of massive stellar evolution.

This, however was not the only surprise. Ostensibly designed to search for binary candidates, a multi-epoch radial velocity (RV) survey of the OB star population of Wd1 was undertaken with VLT/FLAMES (Ritchie et al., 2009). However the resultant dataset also permitted a determination of the cluster velocity dispersion, once the intrinsic RV variables, which would artificially inflate this measurement, were removed from the sample. Such an analysis of the pre-2010 dataset returns a velocity dispersion of < 4.6 km s $^{-1}$ (Clark et al., 2014). This implies that Wd1 is sub-virial, which is difficult to explain since, in conjunction with its radial extent, one would instead expect it to be dynamically relaxed and hence in virial equilibrium. One potential solution to this apparent paradox might be that Wd1 formed, or is in the process of forming, via the merger of a number of discrete sub-clumps. However no statistical evidence for such spatially distinct co-moving groups was found within the RV data.

Our new observations appear to raise more questions than answers. Why is Wd1 currently in a sub-virial state? How was so much mass accumulated in such a small volume of space? What was the nature of the physical agent that led to its apparently instantaneous formation in an otherwise unassuming region of the Galaxy before quenching any further activity? The pronounced differences between Wd1 and other massive galactic stellar aggregates demand answers to such questions, even before one considers that it represents the outcome of the dominant mode of star formation in starburst galaxies and, that, given its sub-virial nature, we are witnessing the

formation of a proto-globular cluster in the local Universe.

Binary evolution in action

Despite the uncertainty in the mode of its formation, the highly coeval nature of Wd1 makes it an ideal laboratory to study the effects of binarity on stellar evolution. Binary systems may be identified via a number of methodologies, from the RV survey described above and periodic (eclipsing or ellipsoidal) photometric modulation, to indirect diagnostics such as hard, over-luminous X-ray emission and/or the presence of host dust, both forming in the wind collision zones of massive binaries (Clark et al., 2008). A synthesis of these disparate criteria has to date resulted in the identification of over 70 confirmed and candidate binaries within Wd1 (Ritchie et al., in prep.), with the Monte Carlo simulations required to return an unbiased binary fraction underway.

The central role that binarity plays in stellar evolution is clearly illustrated by

contrasting the homogeneous population of OB giants and supergiants to the remarkably diverse cohort of further-evolved transitional and WR stars within Wd1 (Clark et al., 2005; Crowther et al., 2006). Binary interaction in compact systems has the effect of prematurely removing the outer H-rich mantle of the primary and hence modifying evolution, by both preventing a subsequent transition through a cool hypergiant phase and initiating the extreme mass-loss that characterises WRs earlier than anticipated. Subject to limits imposed by its rapid spin-up, the secondary accretes some of the material lost by the primary, while some is lost to the system. This is well illustrated by Wd1-9, where the central binary appears completely veiled by a dense dusty circumstellar torus, resulting in the rich emission-line spectrum and infrared excess that characterises such supergiant B[e] stars (Figure 3; Clark et al., 2013).

The subset of early (Wd1-5, -13 and -44) and late (Wd1-7, -33 and -42a) BHGs apparently represents the immediate outcome of both pathways. Showing no indi-

cation of binarity, the latter group forms a natural extension of the sequence of B0-2Ia supergiants as predicted by evolutionary theory. Conversely the properties of the former are consistent with binary-driven mass loss; indeed RV data for both Wd1-13 and -44 reveal them to be short-period systems (Ritchie et al., 2010 and in prep.).

The WC9+O star binary Wd1-239 ($P_{orb} \sim 5.05$ days; Clark et al., 2011) is consequently of interest since its properties are consistent with expectations for the pre-SN endpoint of such a pathway. Under this scenario, the early onset of the WR phase leads to significant additional mass loss, a low pre-SN core mass and the production of a neutron star. However the current compact configuration of Wd1-239 accommodates an even more exciting scenario: the rapid rotation induced in massive, tidally locked binaries naturally leads to highly efficient internal mixing and hence chemically homogeneous evolution. This halts the expansion of the primary and, as a consequence, it remains within its Roche lobe, preventing binary-driven mass loss.

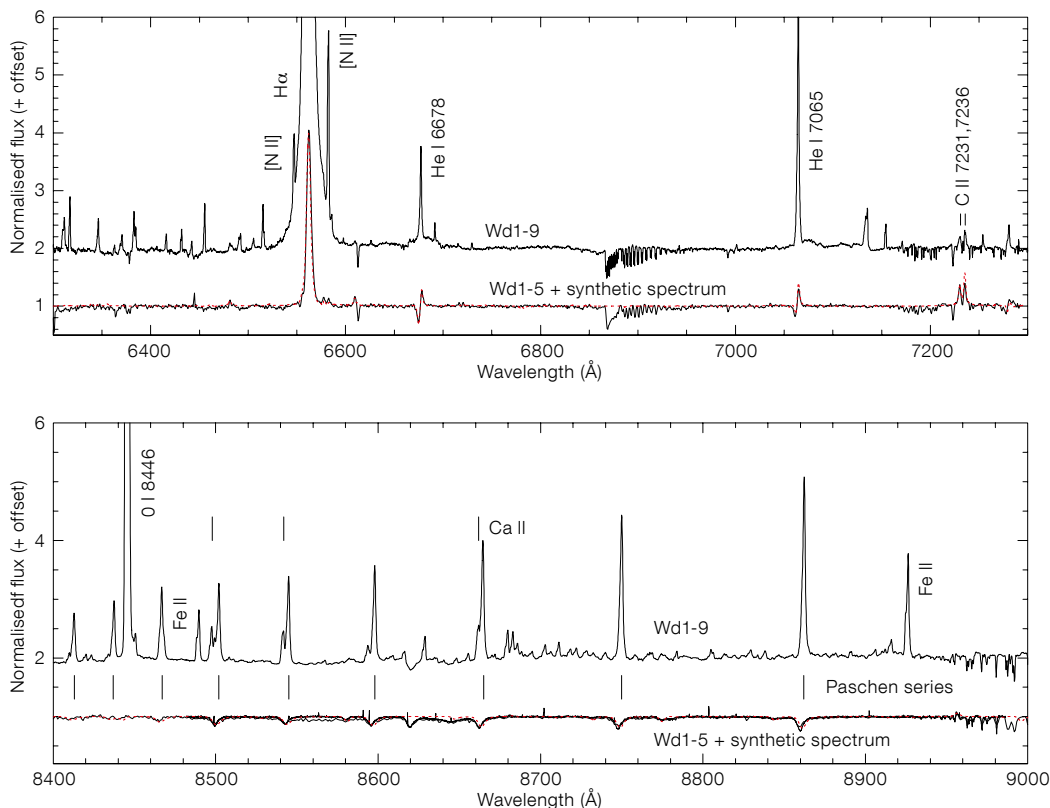


Figure 3. Optical spectra of the supergiant B[e] binary Wd1-9 and the blue hypergiant Wd1-5, a post binary interaction product. A best-fit synthetic spectrum derived from a non-local thermal equilibrium model atmosphere for Wd1-5 is overplotted in red. Major transitions are indicated; weaker emission features in the spectrum of Wd1-9 are from low excitation metals such as Fe II.

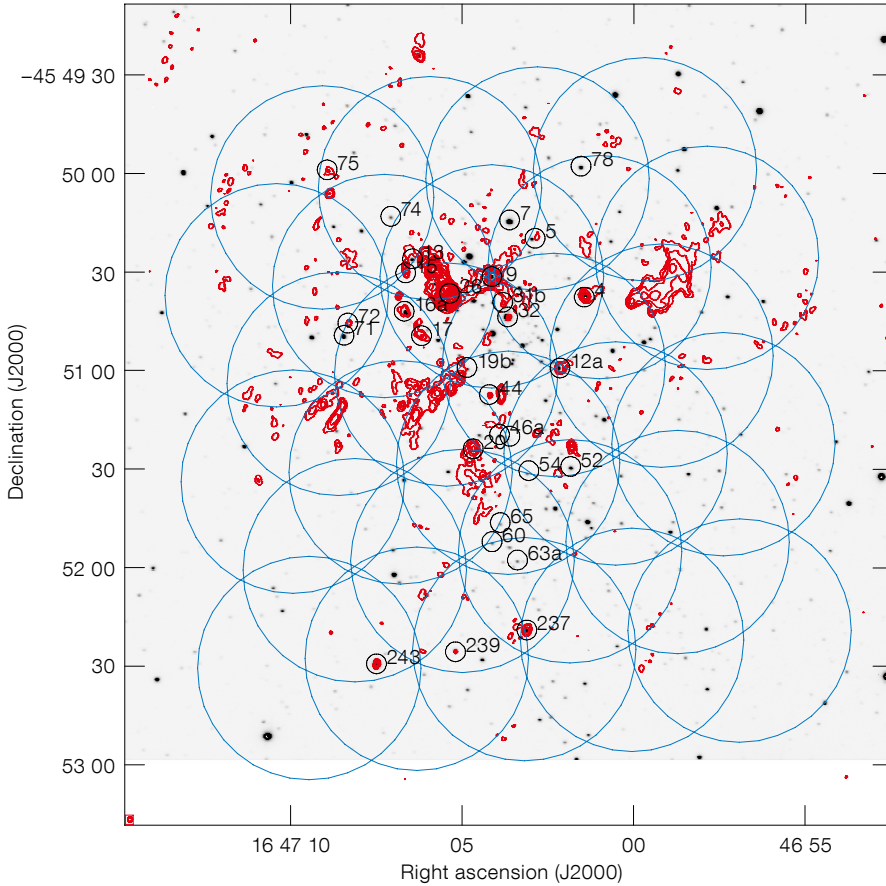


Figure 4. Optical image of Westerlund 1 (greyscale) with both the 3 cm radio map (red contours; Dougherty et al., 2010) and ALMA pointings (blue circles) overlaid.

In contrast to the former scheme this in turn leads to a high pre-SN core mass and resultant black hole (BH) formation.

Clearly then, the evolutionary history of a given star — e.g., single versus binary and chemically homogeneous versus inhomogeneous — plays a critical role in the “choice” of post-SN relativistic remnant. With an initial mass $> 35 M_{\odot}$ (c.f., Ritchie et al., 2010), one would expect that any single star undergoing a SN within Wd1 at this epoch would result in the formation of a BH. Hence, following the arguments above, the discovery of a young, highly magnetised neutron star within Wd1 — a magnetar (Muno et al., 2006) — provides a powerful motivation for validating these scenarios, more so since the birth of such magnetars has been implicated in some of the most energetic explosions in the

Universe (gamma-ray bursts and super-luminous SNe).

It is therefore reassuring that observational support for this paradigm has been provided by the discovery of a candidate for the pre-SN binary companion of the magnetar — the runaway BHG Wd1-5 (Figures 1 and 3; Clark et al., 2014). Tailored spectral analysis reveals a carbon-rich chemistry that can only have arisen via binary evolution, a conclusion buttressed by its over-luminosity for its spectroscopic mass. We employed the current properties of Wd1-5 to infer a pre-SN history for the putative Wd1 magnetar progenitor system whereby the primary in a compact ($P_{orb} < 8$ days) $41 + 35 M_{\odot}$ binary transfers its outer layers to the secondary. As a result it rapidly spins up and becomes so massive that it evolves more rapidly than the primary, initiating a

second interactive phase in which its outer layers are also ejected, revealing the chemically processed core. A final phase of reverse mass transfer from this newborn WR star pollutes the primary, yielding carbon-enhanced chemistry, before the secondary is lost to the type Ibc SN in which the magnetar forms and the primary is unbound, which we observe today as Wd1-5. Encouragingly, such a binary pathway naturally leads to rapid rotation in the magnetar progenitor, as well as physical conditions in which a significant magnetic field may be born, which are both pre-requisites of current theories of magnetar formation.

Future prospects

In the preceding text we have highlighted some recent results from our ongoing efforts to fully exploit the opportunity presented by Wd1, but where do we go from here? In the near future our immediate goals are to fully characterise the binary population in terms of frequency, separation and period. Tailored quantitative analyses of individual systems will run in parallel to this; the first aim of this strand being the determination of the evolutionary status of the cool BHG population — i.e., are they the progenitors or descendants of the RSGs?

Our current and archival data will also permit us to identify massive blue stragglers and other binary products within Wd1 that have been predicted on theoretical grounds (de Mink et al., 2014). This is of importance for both the verification of our putative magnetar formation scenario and also because Schneider et al. (2014) suggest that such a route may produce some of the most massive stars known — essentially suggesting that massive star formation may be a two-stage process, and in the process modifying the primordial cluster initial mass function.

The advent of the K-band Multi Object Spectrograph (KMOS) enables the efficient accumulation of spectra sampling the chemical and rotational diagnostics essential for the model-atmosphere analysis of the lower luminosity, less-evolved stars; hitherto inaccessible due to interstellar extinction. Novel approaches

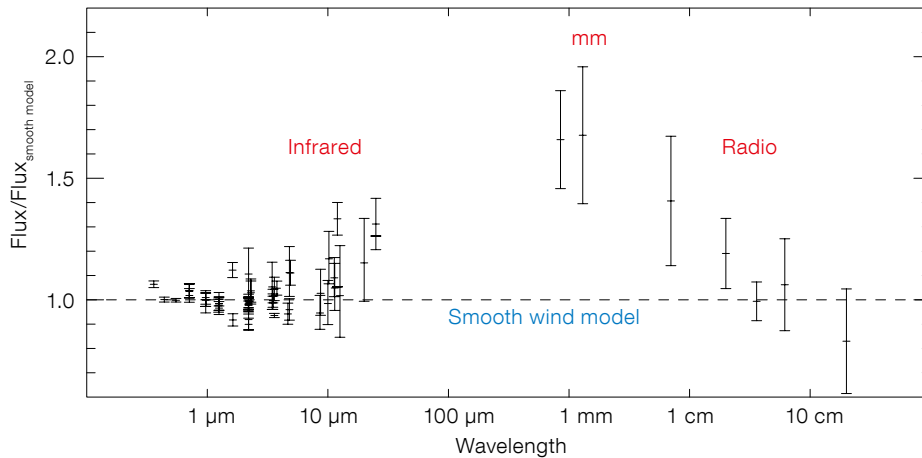


Figure 5. Representative spectral energy distribution for the B0 Ia star ϵ Ori showing the submillimetre excess introduced by wind clumping (from Blomme et al., 2002).

to understand the nature of these stars may also be employed. For instance current observations indicate that pulsational variability is ubiquitous across all stellar populations within Wd1 (Clark et al., 2010); theoretical modelling by Saio et al. (2013) suggests that the periodicities of such pulsations provide important information on the evolutionary state of the pulsators. A synthesis of such data would allow the accurate construction of an enhanced Hertzsprung–Russell diagram for the cluster, potentially allowing us to break temperature/luminosity degeneracies and determine whether, for example, a given BSG or B-/YHG is in a pre- or post-RSG phase.

Moving beyond multi-object spectroscopy, the proximity of Wd1 permits the resolution and detection of individual stars at submillimetre and radio wavelengths, a feat not yet replicable for 30 Dor. Figure 4 shows the coverage of extant radio observations (Dougherty et al., 2010) and approved Atacama Large Millimeter/submillimeter Array (ALMA) observations (PI: Fenech). At long wavelengths, the submillimetre and radio observations will allow the degree of substructure (clumping) present in the winds of the OB star cohort to be quantified, and refinement of the mass-loss estimates, which are currently uncertain by a factor of ~ 5 or more due to their dependence on this parameter. Figure 5 shows as an example the effect of wind clumping compared to the smooth wind model for a nearby B0 supergiant. Similarly, the ALMA observations will permit estimates of mass loss for the YHGs and

RSGs to be made via the dust content of their winds. In combination these approaches will better constrain the rate at which mass is lost throughout the full evolutionary cycle of massive stars — critical input physics for theoretical modelling.

Very Large Telescope (VLT) observations of the hypergiant population permit the direct resolution of their photospheres and circumstellar environments. This is essential in order to quantify the effects of the harsh ultraviolet environment of Wd1 on such distended stars — do they experience surface ablation and/or dust destruction, and are the extended CO and water layers (called MOL-spheres; Arroyo-Torres et al., 2015) that characterise isolated RSGs precluded? Similar observations will also allow constraints to be placed on the geometry and properties of the circumstellar torus of Wd1-9 and hence on the physics of the common-envelope binary evolution.

Binary interactions may also be probed with the ~ 350 ks of archival Chandra and XMM-Newton observations that have accumulated via studies of the magnetar (Bartlett et al., in prep.), a six-fold increase in integration time compared to previous studies (Clark et al., 2008). Determining the origin of the high-energy emission of Wd1 is a particularly exciting prospect, given that it has recently been recognised to be both a GeV and TeV source (Ohm et al., 2013).

To summarise, Wd1 is an enticing target across the whole electromagnetic spec-

trum, with its youth, mass and proximity conspiring to create a unique environment for the study of massive star and star cluster formation and evolution. Complementing ongoing studies in the low-metallicity environment of 30 Dor, it naturally falls along a sequence of Galactic clusters with ages ranging from 1–3 Myr (e.g., the Arches and NGC 3603) through to 15–20 Myr (the RSG-dominated clusters at either end of the Galactic bar) allowing us to address the evolution of stars from ~ 10 to $> 100 M_{\odot}$, while providing fresh insights into the recent star formation history of the Milky Way. Moreover its integrated mass and stellar density allow us to probe the physics of the unresolved super star clusters that characterise external starburst galaxies through cosmological time and, given its apparent sub-virial nature, the birth throes of a future globular cluster.

References

- Arroyo-Torres, B. et al. 2015, A&A, in press, arXiv:1501.01560
- Blomme, R. et al. 2002, A&A, 382, 921
- Clark, J. & Porter, J. 2004, A&A, 427, 839
- Clark, J. et al. 2005, A&A, 545, 949
- Clark, J. et al. 2008, A&A, 477, 147
- Clark, J., Ritchie, B. & Negueruela, I. 2010, A&A, 516, A78
- Clark, J. et al. 2011, A&A, 531, A28
- Clark, J., Ritchie, B. & Negueruela, I. 2013, A&A, 560, A11
- Clark, J. et al. 2014, A&A, 565, A90
- Crowther, P. et al. 2006, MNRAS, 372, 1407
- Davies, B. et al. 2012, MNRAS, 419, 1871
- Dougherty, S. et al. 2010, A&A, 511, A58
- de Mink, S. et al. 2014, ApJ, 782, 7
- Evans, C. et al. 2011, A&A, 530, A108
- Kudryavtseva, N. et al. 2012, ApJ, 750, L44
- Muno, M. et al. 2006, ApJ, 636, L41
- Negueruela, I., Clark, J. & Ritchie, B. 2010, A&A, 516, 78
- Negueruela, I. et al. 2011, A&A, 528, A59
- Ohm, S., Hinton, J. A. & White, R. 2013, MNRAS, 434, 2289
- Ritchie, B. et al. 2009, A&A, 507, 1585
- Saio, H., Georgy, C. & Meynet, G. 2013, MNRAS, 433, 1246
- Sana, H. et al. 2013, A&A, 550, A107
- Schneider, F. et al. 2014, ApJ, 780, 117
- Walborn, N. & Blades, J. 1997, ApJS, 112, 457

The GIRAFFE Inner Bulge Survey (GIBS)

Manuela Zoccali^{1,2}
 Oscar A. Gonzalez³
 Sergio Vasquez^{1,2}
 Vanessa Hill⁴
 Marina Rejkuba^{3,5}
 Elena Valenti³
 Alvio Renzini⁶
 Alvaro Rojas-Arriagada⁴
 Carine Babusiaux⁷
 Tom Brown⁸
 Dante Minniti^{2,9,10}
 Andy McWilliam¹¹

¹ Instituto de Astrofísica, Pontificia Universidad Católica de Chile, Santiago, Chile

² The Millennium Institute of Astrophysics, Chile

³ ESO

⁴ Université de Nice Sophia Antipolis, CNRS, France

⁵ Excellence Cluster Universe, Garching, Germany

⁶ INAF–Osservatorio di Padova, Italy

⁷ GEPI, Observatoire de Paris, France

⁸ Space Telescope Science Institute, Baltimore, USA

⁹ Departamento de Ciencias Físicas, Universidad Andres Bello, Chile

¹⁰ Vatican Observatory, Italy

¹¹ Carnegie Institute of Washington, Pasadena, USA

The GIRAFFE Inner Bulge Survey (GIBS) is a spectroscopic survey of ~ 6500 core helium burning (red clump) stars in the Milky Way Bulge, carried out with the FLAMES GIRAFFE spectrograph at the VLT. The aim of the GIBS survey is to derive the metallicity and radial velocity distributions of Bulge stars, across 31 fields in the region of Galactic longitude range -10° to $+10^\circ$ and latitude range -10° to $+5^\circ$. This is the area also mapped by the VISTA Variables in the *Vía Láctea* (VVV) ESO Public Survey.

With a mass $\sim 10^{10} M_\odot$ in stars, the Galactic Bulge is the only bulge in which we can resolve individual stars down to the bottom of the main sequence. It is also the only bulge for which high-resolution spectra can be obtained for giant stars, providing chemical abundances of several atomic species. Nevertheless,

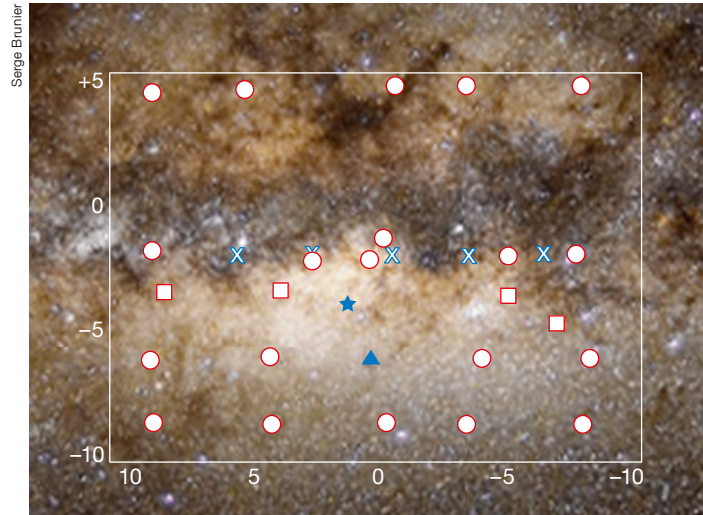


Figure 1. Approximate location of the observed fields, overplotted on an optical image of the Milky Way Bulge. The large white rectangle is the area covered by the VVV survey. Open circles are fields observed at $R \sim 6500$ in the CaT spectral region (LR8), while open squares are fields observed at $R \sim 22\,500$ around ~ 6300 Å (HR13). Crosses are fields observed in LR8 in programme 89.B-0830. The blue star is the field, in Baade's Window, used for the CaT calibration and the blue triangle is the field discussed in Vásquez et al. (2013).

due to the high level of crowding, absolute and differential interstellar extinction, and foreground disc contamination, our knowledge of the Bulge structure, kinematics and stellar population is still relatively poor. The ultimate goal, when studying the Galactic Bulge, is to set constraints on the formation mechanism(s) of the Milky Way and, by extension, of galaxies in general.

The inner region (< 3 kpc) of the Milky Way has been known for a long time to host a bar (Blitz & Spergel, 1991). Only recently, however, have detailed 3D maps been constructed using red clump stars as distance indicators; these maps have revealed that the outer Bulge exhibits a strong boxy/peanut component, sometimes also called X-shaped (e.g., McWilliam & Zoccali, 2010). Dynamical models predict the formation of boxy/peanut structures as the outcome of the secular evolution of a disc, through the formation and subsequent vertical heating of a bar. Observationally, these models are confirmed by the cylindrical rotation of the Bulge (Howard et al., 2009) and by the asymmetries in the radial motions of the near and far edges of the Bar (Vásquez et al., 2013). We might conclude, therefore, that we understand the Bulge structure, kinematics and formation mechanism, except that several other observations indicate the presence of at least another component in the Bulge. The metal-poor component of the Bulge has spheroid-like kinematics and high α -element to iron ratios $[\alpha/\text{Fe}]$, while

the metal-rich component has kinematics more typical of a bar, and relatively low $[\alpha/\text{Fe}]$ (e.g., Hill et al., 2011). Moreover, when tracing the 3D structure of the Bulge using RR Lyrae variables, which are clean tracers of the oldest stellar population, a spheroidal structure is found, with no evidence of either a bar or a boxy/peanut structure (Dékány et al., 2013).

The main goal of GIBS is to couple chemical and kinematical information for 200–400 stars in each of 31 fields across the Bulge area in order to investigate whether we can confirm the presence of two distinct components, and what their properties are. The core of the project is the ESO Large Programme 187.B-0909 (PI: Zoccali), targeting red clump stars in 24 fields. These data complement other archival data acquired using the same GIRAFFE instrument setup, wavelength range and signal to noise (S/N). Specifically, we also analysed another 111 red clump stars in Baade's Window acquired within a pilot programme designed to build a calibration of Calcium II Triplet (CaT) equivalent widths versus $[\text{Fe}/\text{H}]$ (Programme 385.B-0735; Vásquez et al., 2015, in preparation). Another ~ 100 red clump stars in each of five fields at Galactic latitude, $b = -2^\circ$ were added from programme 089.B-0830 (PI: Gonzalez). Finally, we include in all the plots another 454 red clump stars in a field at $(l, b) = (0^\circ, -6^\circ)$ for which the CaT spectral region was measured with the Inamori Magellan Areal Camera and Spectrograph (IMACS)

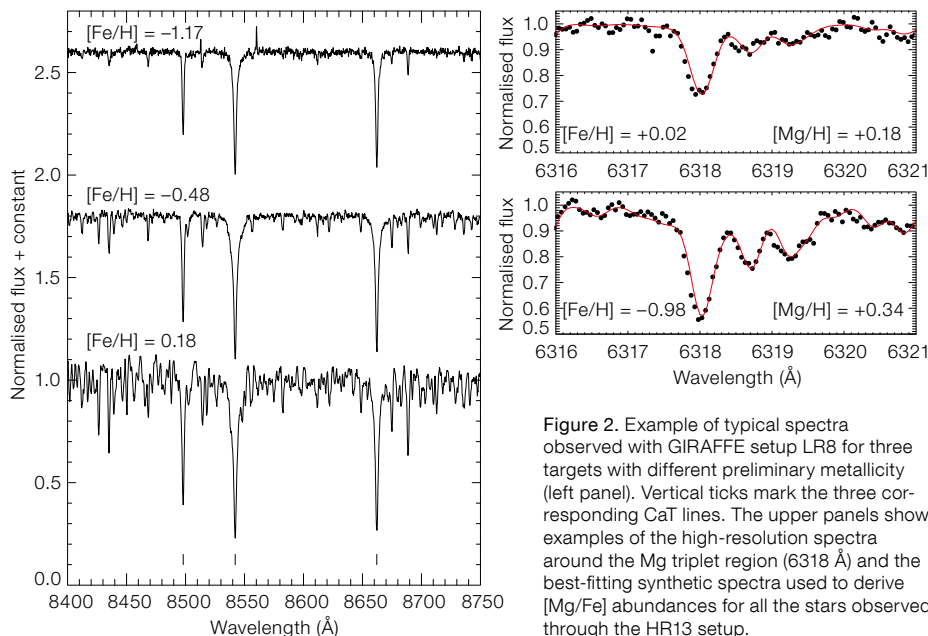


Figure 2. Example of typical spectra observed with GIRAFFE setup LR8 for three targets with different preliminary metallicity (left panel). Vertical ticks mark the three corresponding CaT lines. The upper panels show examples of the high-resolution spectra around the Mg triplet region (6318 Å) and the best-fitting synthetic spectra used to derive $[Mg/Fe]$ abundances for all the stars observed through the HR13 setup.

spectrograph at the Magellan Telescope (Vásquez et al., 2013). Figure 1 shows the location of the 31 observed fields on an image of the Bulge.

All the spectra, with the exception of those in the fields at latitude -4° were obtained with the FLAMES GIRAFFE setup LR8, at a resolution $R = 6500$, centred on the CaT spectral feature at ~ 8500 Å. Their typical S/N, per pixel, is ~ 50 . About 200 stars were targeted in most of the fields, with the only exceptions being the fields along the Bulge minor axis, where spectra for ~ 400 stars were obtained. Stars in the fields at $b \sim -4^\circ$ were observed at a higher spectral resolution ($R = 22\,500$) with setup HR13, centred at ~ 6500 Å, in order to measure the chemical abundance of iron and the light elements, and to investigate the presence of radial gradients in the α -element ratios across different longitudes. The typical S/N per pixel of these high-resolution spectra is ~ 100 . Figure 2 shows sample spectra for stars of different metallicity taken with the two setups.

Radial velocities

Heliocentric radial velocities (RVs) were measured by cross-correlations using the IRAF *fxcor* task. For the low-resolution spectra the adopted template was a synthetic spectrum for stellar surface

parameters $T_{\text{eff}} = 4750$ K, $\log g = 2.5$ and $[Fe/H] = -1.3$. The template metallicity was chosen to be on the low side of the distribution in order to avoid including too many weak, unresolved lines. For the high-resolution, HR13 spectra, the cross correlation was performed with the same IRAF routine, but a template synthetic spectrum with $T_{\text{eff}} = 4500$ K, $\log g = 2.3$ and $[Fe/H] = -0.3$. The typical error on these velocities is ~ 0.6 km s $^{-1}$.

The GIBS survey allows the radial distribution of the inner Bulge regions ($b = -1^\circ$, -2°) to be investigated for the first time; both are inaccessible to the Bulge Radial Velocity Assay survey (BRAVA; Rich et al., 2007) and the Abundances and Radial velocity Galactic Origins Survey (ARGOS; Freeman et al., 2013). Extensive discussion of the RVs is presented in Zoccali et al. (2014), including a comparison with previous works. We show in Figure 3 the observed mean RV and velocity dispersion in each field, together with the rotation profiles predicted by the boxy peanut bulge models by Martínez-Valpuesta et al. (2006). A remarkable agreement is apparent at all latitudes, except for the velocity dispersion profile at $b = -2^\circ$, where the data show a central peak not present in the models. The peak, visible in the third row, right panel of Figure 3, at $l = 0^\circ$, might be due to a high density peak in the inner ~ 250 pc, or perhaps to some anisotropy in the velocity distribution.

The general rotation pattern of the Bulge, together with the central peak in the velocity dispersion can both be appreciated much better in a kinematical map of the inner Galaxy, constructed by interpolating the data points shown in Figure 3. The map, shown in Figure 4, and discussed in Zoccali et al. (2014), can be directly compared with kinematical maps of external bulges of external galaxies from integral field unit (IFU) surveys such as, e.g., ATLAS^{3D} (Emsellem et al., 2004) and the Calar Alto Legacy Integral Field Area Survey (CALIFA; Sánchez et al., 2012). In addition, it provides the expected mean RV and velocity dispersion, σ , at any location within the area mapped by GIBS.

Metallicity distribution function across the inner Galactic Bulge

Iron abundances from GIRAFFE low-resolution spectra are obtained using CaT lines as a metallicity indicator. The correlation between the equivalent widths of CaT lines and global metallicity was first demonstrated in the late 1980s by means of integrated spectra of Galactic globular clusters. Later on this empirical evidence was confirmed in several studies of individual star spectra, and it has been extensively used in the study of Galactic star clusters and Milky Way satellites. Before starting the present programme we made sure that such a correlation would hold for super-solar metallicities, with the $[Ca/Fe]$ profile appropriate for Bulge K giants. About 200 red clump and red giant branch stars were observed at both high resolution (HR13, HR14) and low resolution (LR8). These observations were used to derive a CaT versus $[Fe/H]$ calibration specifically designed for the targets of the GIBS programme (Vásquez et al. 2015, in preparation).

For the stars observed at $R \sim 22\,500$, with the HR13 setup, metallicities and element ratios are derived using the same iterative method described in Zoccali et al. (2008) and Gonzalez et al. (2011). Specifically, equivalent widths of isolated Fe lines are obtained automatically by means of the DAOSPEC automated code. The list of lines is the same as that which was used in Zoccali et al. (2008) and Gonzalez et al. (2011),

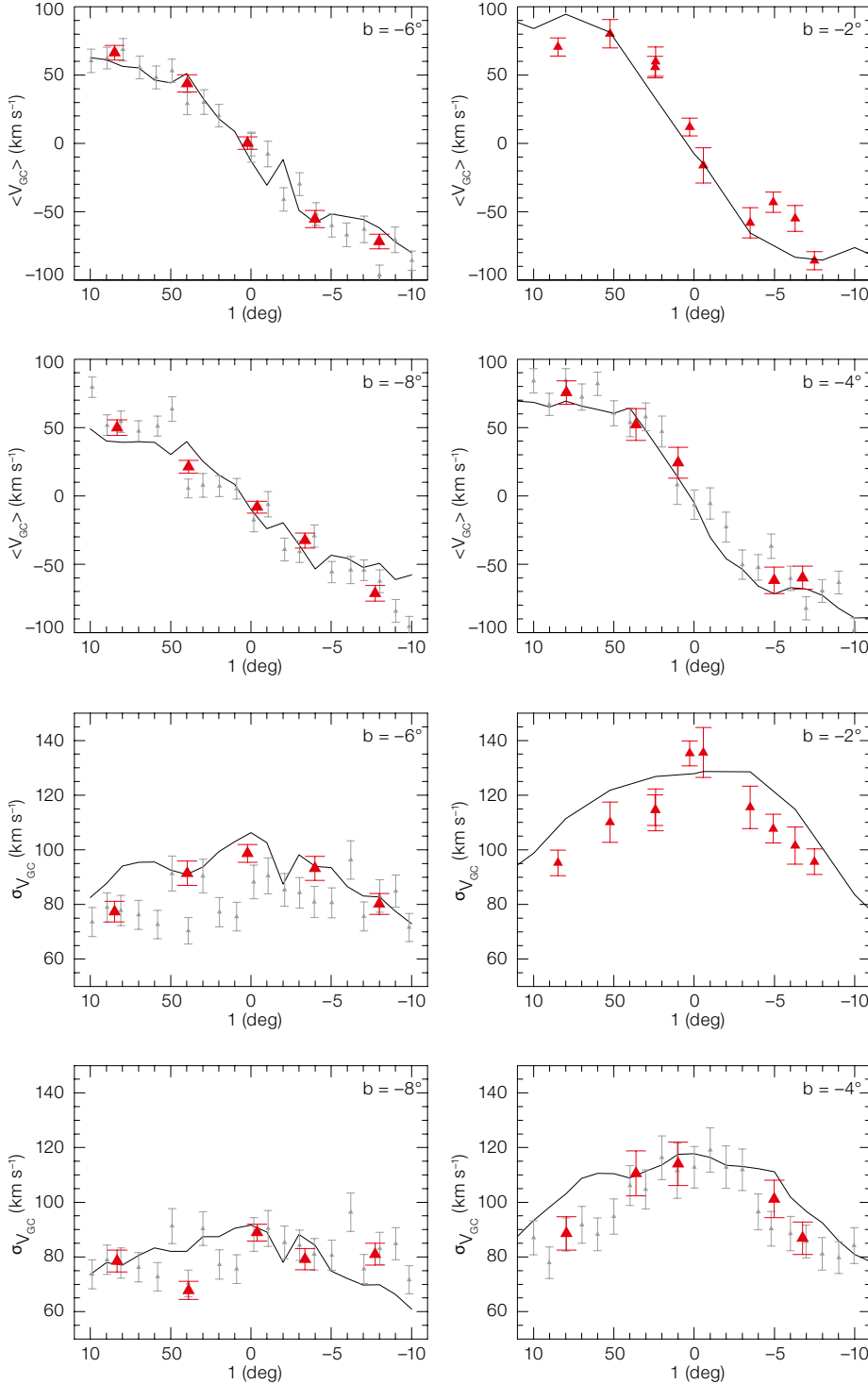


Figure 3. Mean galactocentric RV (upper four panels) and velocity dispersion (lower four panels) as a function of Galactic longitude for GIBS fields at different latitudes (red symbols) compared to the models by Martínez-Valpuesta et al. (2006; solid lines) at the same latitudes. Data for the BRAVA survey, when available, are also plotted in grey.

which was carefully calibrated to template stars μ Leonis, Arcturus and the Sun. First-guess photometric temperatures and gravity were obtained from the Optical Gravitational Lensing Experiment (OGLE-II) optical photometry, after

correcting for interstellar extinction using the map by Gonzalez et al. (2012). Surface gravity was derived photometrically as described in Zoccali et al. (2008). The first-guess parameters were used to create an ATLAS9 model atmosphere (Castelli & Kurucz, 2004). Effective temperature and micro-turbulent velocity were then spectroscopically refined by simultaneously imposing excitation equilibrium on a list of unblended Fe I and Fe II lines and by forcing a zero slope in the relation between equivalent widths and the derived abundance of each line. A new ATLAS9 model atmosphere was then generated using the new set of parameters and the procedure was repeated until the optimal set of parameters was found. The entire procedure was carried automatically for the entire high-resolution sample using the code GALA (Mucciarelli et al., 2013). Final metallicities were used to construct the metallicity distributions that are shown in Figure 5.

The derived metallicities allow us to explore by direct spectroscopic measurements the metallicity gradient along latitude and longitude in the inner Galactic Bulge. Figure 5 shows a subsample of 26 out of 31 fields following a regular grid, for a direct comparison of the metallicity distribution functions along longitude and latitude strips. The data clearly show a vertical gradient at each given longitude, which is consistent with the pattern derived from photometry using VVV data (Gonzalez et al., 2013). The spatial coverage of GIBS allows us to explore this gradient as close to the Galactic Plane as $b = -2^\circ$. Along the minor axis ($l = 0^\circ$) there is an extra field $b = -1^\circ$. The inner fields show a flattening of the vertical gradient close to the Plane, validating and extending the results by Rich et al. (2012) based on infrared spectroscopy of a few dozen stars along $l = 0^\circ$.

Chemical abundances

Using the spectroscopic stellar parameters, Ca and Mg abundances were calculated by means of fitting synthetic spectra to each observed spectrum of our sample. Synthetic spectra were created using the MOOG code fed by the corresponding MARCS model atmosphere and the line list from Gonzalez et al. (2011).

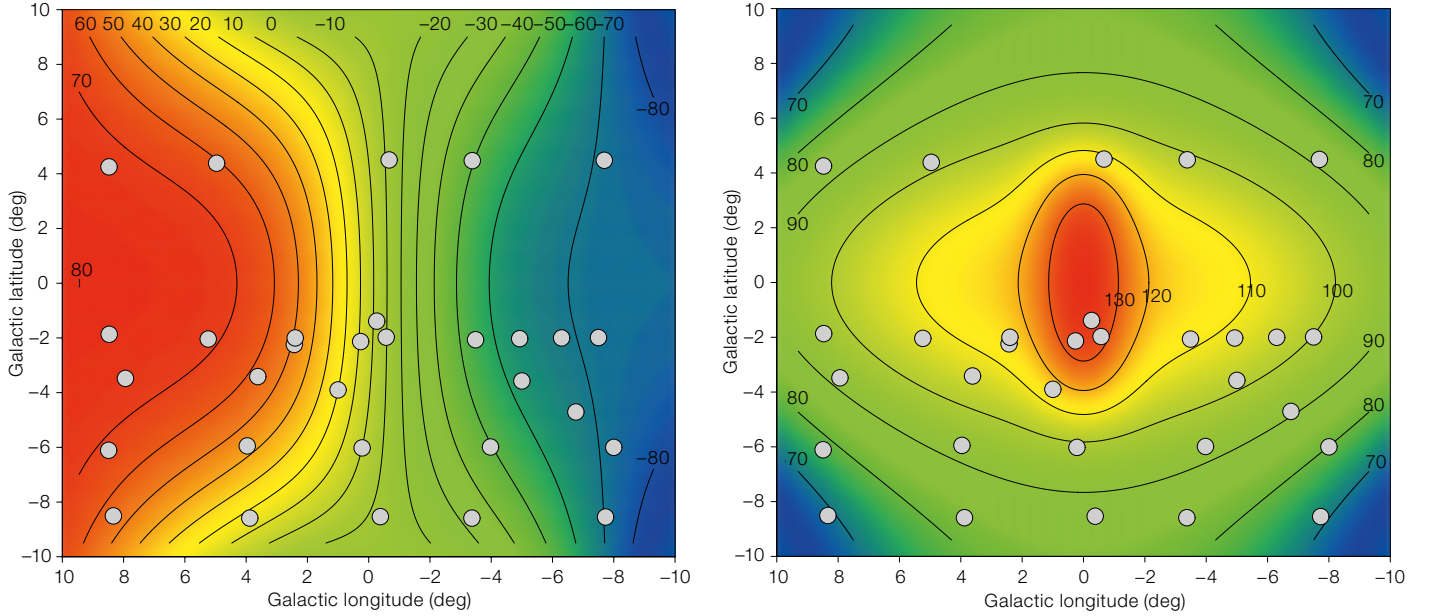


Figure 4. Mean radial velocity (left) and velocity dispersion (right) surfaces in the longitude–latitude plane, constructed from the measured rotation profiles at negative latitudes. Grey points show the positions of the GIBS 31 observed fields, while the black contour lines are labelled with the relevant velocity in km s^{-1} .

Figure 2 showed an example of the Mg region for a metal-poor and a metal-rich star in our sample and, in addition, the best-fit synthetic spectrum is also shown. Mg abundances derived in this way allow us to investigate the $[\text{Mg}/\text{Fe}]$ trend as a function of $[\text{Fe}/\text{H}]$, which is related to the

star formation timescale of a given stellar system. A high $[\text{Mg}/\text{Fe}]$ at a given $[\text{Fe}/\text{H}]$ indicates a rapid star formation. Figure 6 shows the $[\text{Mg}/\text{Fe}]$ trend for the entire GIBS high-resolution sample of Bulge red clump stars, together with the abundances for the sample of Bulge giants presented in Gonzalez et al. (2011). The smaller scatter in the GIBS data indicates the superior quality of the new data compared to previous ones. The higher S/N and a refined procedure to derive accurate stellar parameters have resulted in a fine set of measurements that will allow us to probe the Bulge abundance gradients with unprecedented accuracy. By comparing this relation to that of other Galactic components we are able to investigate the presence of chemical similarities/differences between the Bulge and the thin/thick Disc, and establish the relative star formation timescales (Gonzalez et al. 2015, in preparation).

The observations for the GIBS survey are currently complete. At least three major papers are about to be submitted, on the chemical abundances from the high-resolution spectra (as shown in Figure 6),

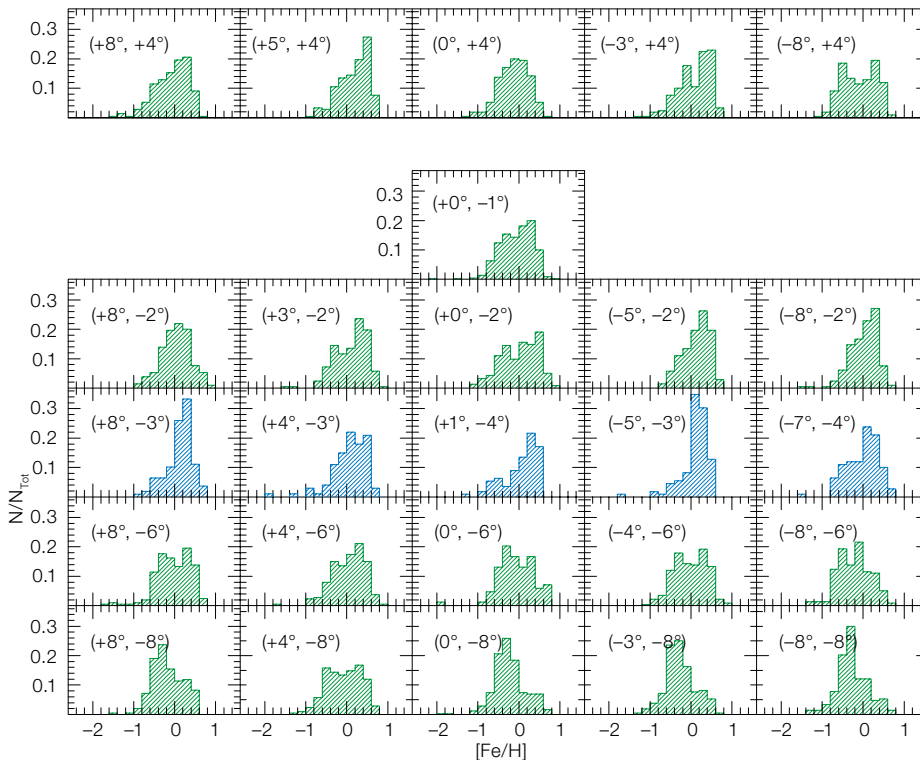


Figure 5. Metallicity distribution functions for a subsample of 26 fields along an approximately regular grid in Galactic coordinates (see labels). Metallicities measured from low- (green) and high- (blue) resolution GIRAFFE spectra are shown as dashed histograms.

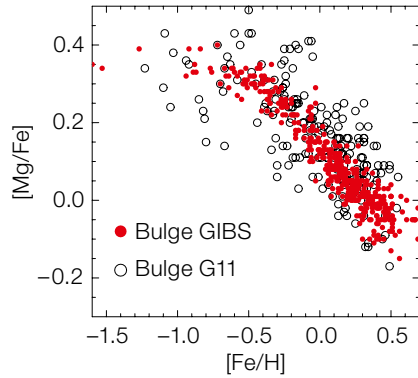


Figure 6. $[Mg/Fe]$ abundance ratios obtained from the HR13 spectra of 468 red clump stars in four GIBS fields (red), compared to those for red giant branch stars from the sample of Gonzalez et al. (2011; black symbols). See text for discussion.

the metallicity distribution function across all the fields (c.f., Figure 5) and a detailed analysis of the kinematics, from RVs and proper motions, coupled with metallicity. A further step includes tracing the oldest Bulge component, by means of RR Lyrae variables. Extensive catalogues of RR Lyrae stars are becoming available from the OGLE-IV survey in the optical (Soszynski et al., 2014) and the VVV survey in the near-infrared. A VIMOS spectroscopic programme aimed at deriving the radial velocity distribution of RR Lyrae stars in some inner Bulge fields has been awarded time for our group in Period 95.

References

- Blitz, L. & Spergel, D. N. 1991, *ApJ*, 379, 631
 Castelli, F. & Kurucz, R. F. 2004, *astro-ph/0405087*
 Dékány, I. et al. 2013, *ApJ*, 776, L19
 Emsellem, E. et al. 2004, *MNRAS*, 352, 721
 Freeman, K. et al. 2013, *MNRAS*, 428, 3660
 Gonzalez, O. A. et al. 2011, *A&A*, 530, A54
 Gonzalez, O. A. et al. 2012, *A&A*, 543, A13
 Gonzalez, O. A. et al. 2013, *A&A*, 552, A110
 Hill, V. et al. 2011, *A&A*, 534, A80
 Howard, C. D. et al. 2009, *ApJ*, 702, L153
 Martinez-Valpuesta, I. et al. 2006, *ApJ*, 637, 214
 Minniti, D. et al. 2010, *New Astronomy*, 15, 433
 Mucciarelli, A. et al. 2013, *ApJ*, 766, 78
 Rich, R. M. et al. 2007, *ApJ*, 658, L29
 Rich, R. M. et al. 2012, *ApJ*, 746, 59
 Sánchez, S. F. et al. 2012, *A&A*, 538, 8
 Soszynski, I. 2014, *Acta Astronomica*, 64, 177
 Vásquez, S. et al. 2013, *A&A*, 555, A91
 Zoccali, M. et al. 2014, *A&A*, 562, A6

ESO/VVV Team/A. Guzmán



The Galactic Plane star-forming region associated with IRAS 16562-3959 is shown in a VISTA *JHKs* colour image. The central source of this embedded and molecular region contains the high-mass ($\sim 15 M_{\odot}$) young stellar object G345.4938+01.4677. This luminous source is situated in a molecular rotating disc and has an outflow with an ionised jet. See Picture of the Week potw1448 for details.

Variable and Polarised Near-infrared Emission from the Galactic Centre

Banafsheh Shahzamanian^{1,2}Andreas Eckart^{1,2}Monica Valencia-S.¹Gunther Witzel³Mohammad Zamaninasab²Michal Zajaček^{1,2,4}Nadeen Sabha¹Macarena García-Marín¹Vladimir Karas⁴Florian Peissker¹Grischa D. Karssen¹Marzieh Parsa¹Nicolas Grosso⁵Enmanuelle Mossoux⁵Delphine Porquet⁵Behrang Jalali¹Matthew Horrobin¹Rainer Buchholz¹Michal Dovčiak⁴Devaky Kunneriath⁴Michal Bursa⁴Anton Zensus^{2,1}Rainer Schödel⁶Jihane Moultaqa⁷Christian Straubmeier¹

¹ I. Physikalisches Institut der Universität zu Köln, Germany

² Max-Planck-Institut für Radioastronomie, Bonn, Germany

³ Department of Physics and Astronomy, University of California, Los Angeles, USA

⁴ Astronomical Institute of the Academy of Sciences, Prague, Czech Republic

⁵ Observatoire Astronomique de Strasbourg, Université de Strasbourg, CNRS, UMR 7550, Strasbourg, France

⁶ Instituto de Astrofísica de Andalucía (CSIC), Granada, Spain

⁷ Université de Toulouse III – CNRS – IRAP, Observatoire Midi-Pyrénées, France

Infrared observations of the Galactic Centre (GC) provide a unique opportunity to study stellar and bow-shock polarisation effects in a dusty environment. For the infrared counterpart of the supermassive black hole Sgr A* these observations reveal new insights into the physical processes at work. The observations were carried out with NACO in the Ks-band (2.2 μm) from 2004 to 2012 and several linearly polarised flares were observed during these years. We find that the distribution of

polarised flux density is closely related to the single-state power-law distribution of the total flux densities. A typical polarisation degree of the order of 10–20 % and a preferred polarisation angle of $13^\circ \pm 15^\circ$ are derived, likely linked to the intrinsic orientation of the Sgr A* system. We discuss different scenarios for the accretion process for the Sgr A* system based on our findings.

Introduction

Sagittarius A* (Sgr A*) is a compact radio source associated with the supermassive black hole of four million solar masses located at the centre of the Galaxy. It is the galactic nucleus nearest to us. Sgr A* is time variable in the near-infrared (NIR) and X-ray regimes, and also in the radio to submillimetre domain but with a lower degree of variability.

Studying the polarisation of the electromagnetic radiation helps us to understand the underlying physics governing the emission mechanism of Sgr A*. The polarised NIR flux density excursions often exhibit X-ray counterparts, which suggests synchrotron-self-Compton (SSC) or inverse Compton emission as the mechanisms responsible for the radiation (Eckart et al., 2012). Several relativistic models that match the observations assume the variability of Sgr A* to be related to the accretion process and, in particular, to emission from matter close to the last stable orbit around the

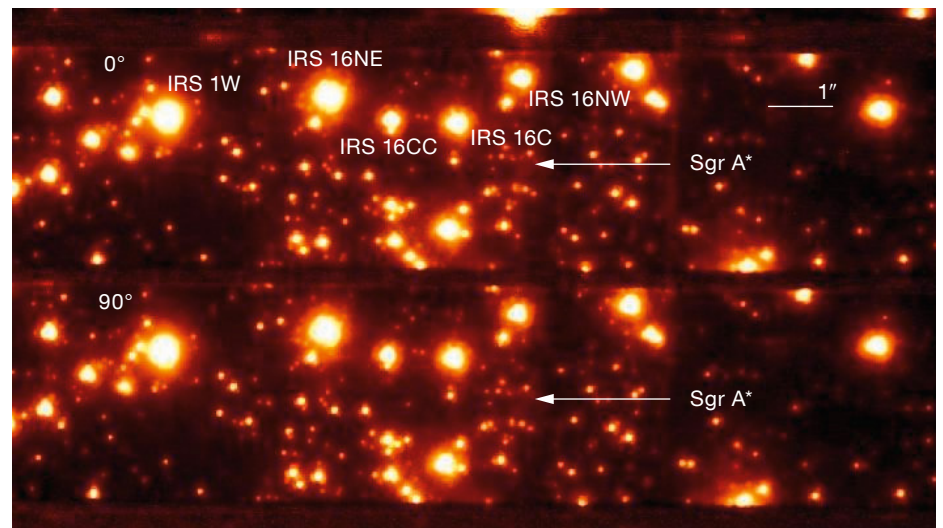
black hole. Correlations between the modulations of the observed flux density light curves and changes in polarisation degree and angle are expected from models where matter is orbiting the supermassive black hole Sgr A* at relativistic speed (e.g., Zamaninasab et al., 2010).

The time-variable NIR emission from Sgr A* can be understood as a result of a single continuous power-law process (Witzel et al., 2012). This continuous process shows a break timescale around a few hundred minutes at which the Fourier power in the flux variability drops. Extreme flux density excursions typically last for about 100 minutes and these excursions are referred to as flares. Here we report on the most comprehensive sample of NIR polarimetric data for Sgr A*.

Polarimetry with NACO

All observations have been carried out with the adaptive optics (AO) module NAOS and NIR camera CONICA (together NACO) at Unit Telescope 4 (Yepun) at the Very Large Telescope (VLT). We collected all Ks-band (2.2 μm) data of the central cluster at the Galactic Centre in 13 milli-arcsecond (mas) pixel-scale polarimetric

Figure 1. The arrangement of the Wollaston prism images on the NACO detector. The two central strips show the images in orthogonally polarised light. Another exposure with the retarder rotated by 45° provides a complementary pair of orthogonal measurements from which the full linear polarisation information can be derived.



imaging from mid-2004 to mid-2012 that exhibits flaring activities. The infrared wavefront sensor of NAOS was used for locking the AO loop on the NIR super-giant IRS7 with $K_s \sim 6.5\text{--}7.0$ mag, located ~ 5.5 arcseconds north of Sgr A*. NACO is equipped with a Wollaston prism combined with a half-wave retarder plate that allows simultaneous measurements of two orthogonal directions of the electric field vector and a rapid change between different angles of the electric field vector. A typical pointing towards the Galactic Centre is shown in Figure 1.

The non-normalised analogue-to-digital converter (ADC) values from the detector were directly used to obtain the normalised Stokes parameters, Q and U , and to derive the linear polarisation degree p and angle ϕ (see Equations 1–5 in Shahzamanian et al., 2014). The polarised flux density was computed as a product of the degree of polarisation and the total flux density. Uncertainties for Q , U and the obtained p and ϕ were determined from the flux density uncertainties. The model derived by Witzel et al. (2011) was employed to reduce the systematic uncertainties of polarisation angles and degrees caused by instrumental polarisation to about $\sim 1\%$ and $\sim 5^\circ$ respectively.

Polarised flux in the central stellar cluster

Using AO-assisted K_s - ($2.2\ \mu\text{m}$) and L' -band ($3.8\ \mu\text{m}$) observations with NACO (Buchholz et al., 2011; 2013), high-precision photometry and the new polarimetric calibration method, the polarisation of the Galactic Centre stellar cluster including Sgr A* was mapped (Witzel et al., 2011; Shahzamanian et al., 2014). In the L' -band these are the first polarimetric observations of the GC for 30 years. The vastly improved spatial resolution allows resolved polarimetry on bright bow-shock sources in this area for the first time at this wavelength. The foreground polarisation is largely parallel to the Galactic Plane (K_s -band: 6.1% at 20° ; L' -band: 4.5% at 20°). The bow-shock sources like IRS 1W and 21 clearly show contributions from intrinsic K_s - and L' -band polarisation. The data provided support for the presumed bow-shock nature of several of these sources (IRS 1W, 5, 5NE, 10W and 21) and for the model of bow-shock polarisa-

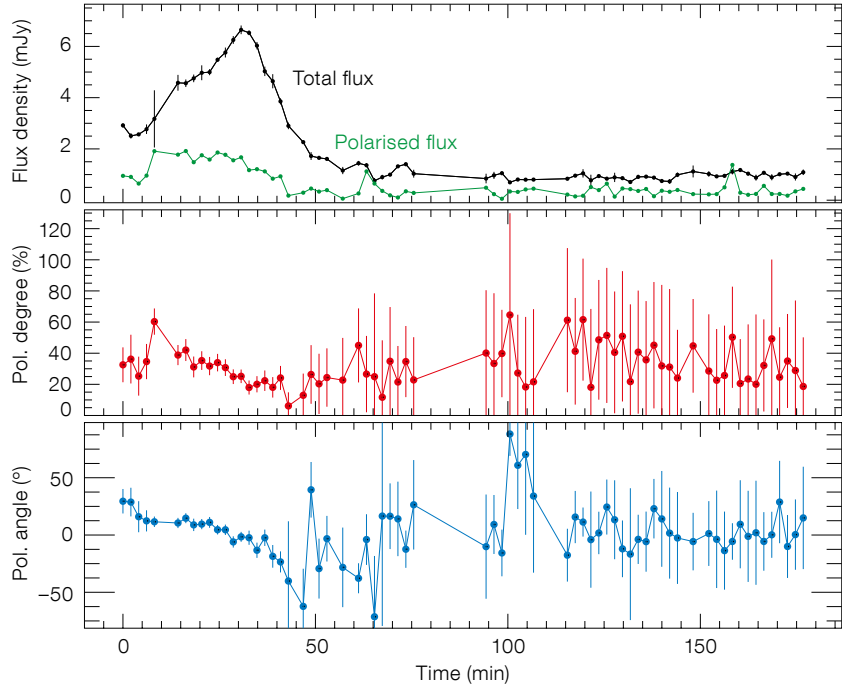


Figure 2. Flare observed in NIR K_s -band polarimetry mode of Sgr A* on 17 May 2012. Top: Total flux density (black) and polarised flux density (green) measured in mJy; Middle: Linear polarisation degree (orange); Bottom: Linear polarisation angle (blue).

tion. For the stellar sources, the origin of the polarised emission arises from a combination of scattering and selective dichroic absorption and emission of dust. In the case of Sgr A*, strongly time-variable polarisation is a clear indication for intrinsic emission mechanisms (such as synchrotron emission) at work, which provide strongly polarised radiation. Figure 2 shows a light curve resulting from typical Sgr A* measurements with NACO in polarisation mode. For high flare flux, the polarisation degree and angle are very well defined.

Sgr A*: Analysis of polarisation degree and angle

We analysed polarised NIR light curves of Sgr A* covering the years 2004 to 2012. A detailed description is given by Shahzamanian et al. (2014). In order to interpret the data it is important to take into account the statistical behaviour of the polarisation measurements. Polarisation degree p is a positive quantity that takes values between zero and one (or, equivalently, 0–100%). The uncertainties

in Q and U , which in our case are the result of observational noise in the polarisation channels, bias the value of p . This leads to an overestimate of p at low signal-to-noise (S/N) measurements. Moreover, polarimetric observations require a higher S/N compared to photometric measurements. Monte Carlo simulations of the measured intensities and their uncertainties in the polarisation channels were performed to derive the expected uncertainties in p and ϕ for different S/N ratios.

Simulations show that for intrinsic flux lower than ~ 2 mJy the recovered polarisation degree is not Gaussian distributed, and especially for low intrinsic polarisation degrees the intrinsic value is not recovered with satisfactory confidence and the uncertainties are very large. On the other hand, for weak flares that are intrinsically strongly polarised, the intrinsic polarisation degrees are statistically recovered, but the asymmetric uncertainties remain large. Therefore, the total statistical behaviour of the observed polarisation data is composed of the properties of subsamples of different polarisation degrees and flare flux.

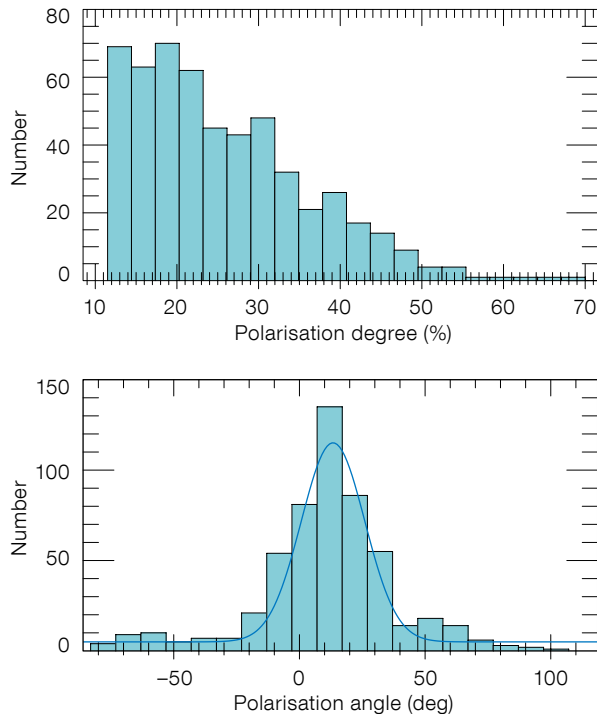


Figure 3. Histogram of the result from all light curves of Sgr A* observed in polarised Ks-band obtained in 2004–2012. Upper: Distribution of polarisation degree; Lower: Distribution of polarisation angle. The dark blue line shows the fit with a Gaussian distribution.

In Figure 3 (upper plot) the distribution of the Ks-band polarisation degree of Sgr A* is shown. Only the significant measurements are plotted, i.e., successful retrievals of the intrinsic p and ϕ . The distribution of p does not have a Gaussian shape: it is flat until $\sim 20\%$ and then starts dropping towards smaller values and is also strongly influenced by systematic effects with uncertainties of several tens of percent. Figure 3 (lower) shows the distribution of significant Ks-band polarisation angles for Sgr A*. The distribution of ϕ shows a peak at 13° and has a width of the order of 30° , therefore, the preferred polarisation angle that can be derived from the distribution is $13^\circ \pm 15^\circ$ (see Figure 4). The distribution of ϕ can be described by a Gaussian function that peaks at the preferred value whose width then corresponds to the combined effect of the intrinsic polarisation angle variability and the measurement uncertainties.

In general, the linear polarisation is linked in degree and angle to the magnetic field structure and the source geometry.

In the case of Sgr A*, neither is it clear whether it has a permanent accretion disc nor whether it has a permanent jet. All of these structures may occur as transient phenomena and then affect the properties of the expected polarisation degree and angle due to the corresponding emission mechanisms. It is very likely that the NIR flare emission originates from optically thin synchrotron radiation (Eckart et al., 2012). Hence one may expect a link between the preferred NIR polarisation angle and the NIR/radio structure of Sgr A*. At millimetre wavelengths the interstellar scattering is small and allows insight into the intrinsic source structure of Sgr A*. Bower et al. (2014) find an intrinsic major axis position angle of the structure of $95^\circ \pm 10^\circ$ (3σ). This angle of the radio structure is, within the uncertainties, orthogonal to the preferred infrared polarisation angle (see Figure 4).

In a range of position angles between 120° and 130° one finds a few elongated NIR features and an elongated X-ray feature (see Figure 4, and Figure 9 in Eckart et al. [2006]). These features may

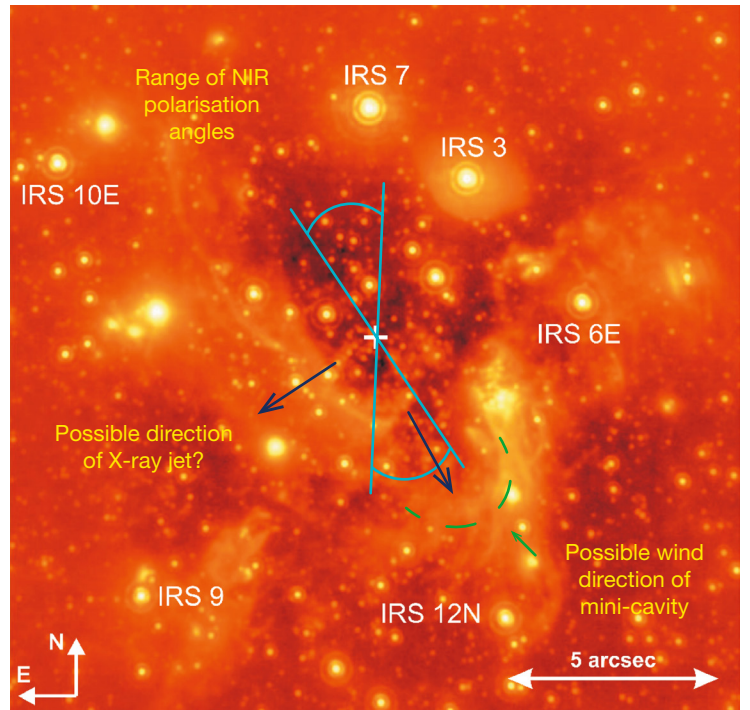


Figure 4. Direction of intrinsic polarisation angle of Sgr A* in the Galactic Centre. The cyan lines include the range over which the NIR polarisation angle varies. The dark blue arrows summarise results from imaging and spectroscopy observation from the radio to X-ray domain: a) the direction of a possible wind responsible for the formation of the mini-cavity; and b) a jet almost perpendicular to it. The green dashed line indicates the wind front of the mini-cavity. Several of the key infrared sources in the region are also indicated.

be associated with a jet phenomenon. In this case the preferred NIR polarisation angle may be associated with the jet components close to or at the foot point of the jet; the polarisation of these components may be along or perpendicular to the jet direction.

It is also possible that the NIR emission originates in hot spots on an accretion disc in a sunspot-like geometry, in which the electric vector is mainly perpendicular to the equatorial plane. The mini-cavity (wind front shown as a dashed line in Figure 4), which may be caused by a collimated outflow from Sgr A*, is located at a position angle of about 193° (i.e. $13^\circ + 180^\circ$; see also Li et al. [2013]). The cometary tails of sources X3 and X7 (Múzic et al., 2010) present additional observational support for the fast wind from Sgr A* at that

position angle. It is unclear how the wind may be related to the possible jet: either there is an additional outflow to the jet, the X-ray feature is not related to the jet, or the mini-cavity was created when the outflow geometry was different.

The distribution of polarisation angles of Sgr A* is not dependent on the strength of the flare and the position of this source in the sky or the instrumental orientation. Instead, the preferred polarisation angle of 13° is a source-intrinsic property. For strong flares, disturbing measuring effects are small and the polarisation degree during these flares is much stronger than that of the background. From these flares we have a direct insight into the source-intrinsic polarised variable infrared emission.

The polarised flux density distribution

The histogram of the polarised flux density distribution of Sgr A* for the fraction of data which is significant is shown in Figure 5. In this histogram the distribution is normalised by the total number of points and the bin size. The distribution of measured polarised flux densities is found to be much broader in comparison to the corresponding distribution of total flux density measurements as presented by Witzel et al. (2012), which were found to be consistent with a single-state emission process. The broader distribution can be explained by the convolution of an intrinsic relative frequency total flux density histogram applied to a range of individual polarisation states; see Shahzamanian et al. (2014) for more details.

Our simulations have shown that the polarisation degree can be recovered with a small uncertainty only for the bright flare flux. Therefore, the properties of the polarised flux density distribution — i.e., the product of the polarisation degree and the total flux density (Figure 5) — can be investigated best for high levels of polarised flare flux. A power-law fit to the data at high flux densities is shown as a dot-dashed red line. For high flare flux, the fit results in a slope, $\alpha = 4.00 \pm 0.15$, which is very close to the value of 4.21 ± 0.05 obtained for the total flux density distribution by Witzel et al. (2012).

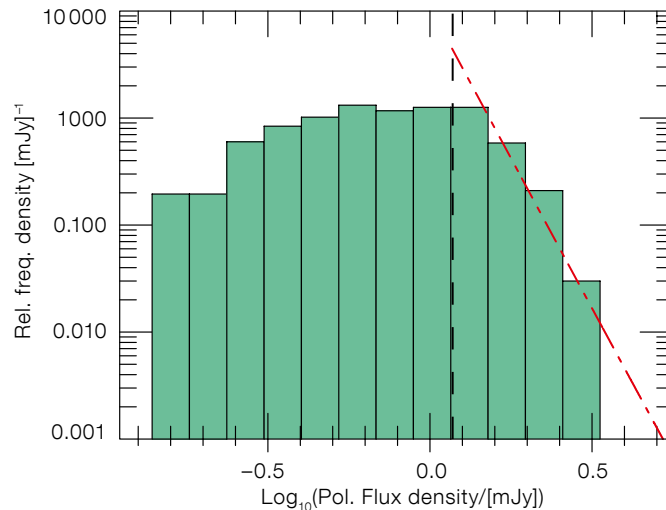


Figure 5. Histogram of polarised flux density (total flux density times polarisation degree) for all significant data is shown with a logarithmic scale, after correction for stellar contamination. The slope at the high flux end compares very well with the slope found for the total flux density.

Recovering this exponent for the polarised flare flux density distribution indicates that the intrinsic polarisation degree is centred around a fixed expectation value and has not varied strongly over the time interval from 2004 to 2012.

The dusty S-cluster object

Gillessen et al. (2012) reported a fast-moving infrared excess source which they interpret as a core-less gas and dust cloud (G2) approaching Sgr A* on an elliptical orbit. Eckart et al. (2014a) present Ks-band identifications and proper motions of the dusty S-cluster object (DSO) derived from VLT and Keck continuum imaging data. In Valencia-S. et al. (2015) new near-infrared (1.45–2.45 μm) observations of the DSO during its approach to the black hole at the centre of the Galaxy are reported; they were carried out with SINFONI at the VLT from February to September 2014. With SINFONI, spatially compact Brackett- γ line emission was detected from DSO/G2 at all epochs before and after its peribothron passage and are in agreement with the detection reported by Witzel et al. (2014) from L-band observations in March 2014.

Combining these observational facts indicates that the DSO is possibly associated with a young accreting stellar object (e.g., a young star; see references given in Valencia-S. et al., 2015) on an elliptical orbit around Sgr A* formed through a process outlined by Jalali et al.

(2014). The observational data were also used to derive the orbit of this object and to predict its periastron transition. With the ellipticity $e = 0.976$ and the half-axis length of 33 mpc, a peribothron distance of about 163 ± 16 au is obtained, which is comparable to previous estimates (e.g., Meyer et al., 2014) and indicates that even if the DSO is an embedded star, its outer shell may very well be subject to tidal disruption (Eckart et al., 2013; Witzel et al., 2014; Zajaček et al. 2014).

Our polarisation statistics show that Sgr A* must be a very stable system, both in terms of geometrical orientation of a jet/wind or an accretion disc and in terms of the variability spectrum that must be linked to the accretion process. The close fly-by of the DSO or similar dusty sources (e.g., Eckart et al., 2014a) might have an effect on the accretion flow onto Sgr A* that depends on the nature of these objects (Zajaček et al., 2014; Jalali et al., 2014). Hence, polarisation and variability measurements of Sgr A* need to be continued as they are the ideal tool to probe any change in the apparently very stable system as a function of the DSO fly-by.

Summary and prospects

We have analysed the near-infrared light curves obtained with NACO at the VLT for Sgr A* at the centre of the Milky Way. Both the steep spectral index (Bremer et al. [2011] and references therein) and the strong variability in the NIR demon-

strate that we are most likely dealing with optically thin synchrotron radiation. Therefore, all properties based on the observation of variable polarised NIR radiation can be directly interpreted as source-intrinsic properties. Some of the main results are depicted in Figure 4 and can be summarised in the following points:

- For flare flux above 5 mJy a range of polarisation degrees of 10–30% is found. If the variable polarised flux from Sgr A* is due to optically thin synchrotron radiation this may indicate depolarisation due to a spatially unresolved complex source structure. For low flare flux the polarisation degree and angle are dominated by measuring uncertainties.
- There is a preferred variable polarisation angle of $13^\circ \pm 15^\circ$. Corrected for the measuring uncertainties, the intrinsic variability of Sgr A* is of the order of 10%. The angle may be linked to jet/wind directions of the corresponding orientation of a temporary accretion disc.
- For the number density distribution of the polarised flux densities, a power-law slope of ~ 4 is found, which is very close to the slope in number density distribution of the total flux densities.
- The well-defined preferred ranges in polarisation degree and angle as

well as the number density power-law slope of four suggest that over the past eight years the geometry and accretion process for the Sgr A* system have been rather stable.

Further progress in investigating the faint polarisation states of Sgr A* in the NIR will require a higher angular resolution in order to better discriminate Sgr A* against background contamination. It is also of interest to use the well-defined NIR polarisation properties of Sgr A* to better determine the apparent stability of the geometrical structure of the system and potentially use variations in this stability to trace interactions of the super-massive black hole at the centre of the Milky Way with its immediate environment.

The known properties of the NACO camera as well as the known polarisation properties of Sgr A* and (most importantly) the many stars in the central cluster that serve as secondary calibrators will allow us to perform a sensitive test of the polarisation characteristics of the new UT1/NACO combination after the move from UT4-Yepun.

Acknowledgements

We acknowledge support through the International Max Planck Research School (IMPRS) for Astronomy

and Astrophysics and the Bonn–Cologne Graduate School (BCGS) for Physics and Astronomy and the University of Cologne. We received funding and support through the FP7/2007-2013 agreement No.312789, the DFG grant SFB 956, the DAAD Czech MSMT grant (Effects of Albert Einstein's General Relativity Revealed), and the EU COST Actions MP0905 and MP1104.

References

- Bower, G. C. et al. 2014, *ApJ*, 790, 1
 Bremer, M. et al. 2011, *A&A*, 532, A26
 Buchholz, R. M. et al. 2013, *A&A*, 557, A82
 Buchholz, R. M. et al. 2011, *A&A*, 534, A117
 Eckart, A. et al. 2012, *Journal of Physics Conference Series*, 372, 012022
 Eckart, A. et al. 2014a, in *IAU Symposium*, Vol. 303, ed. Sjouwerman, L. O., Lang, C. C. & Ott, J., 269
 Eckart, A. et al. 2013, *A&A*, 551, A18
 Eckart, A. et al. 2006, *A&A*, 455, 1
 Eckart, A. et al. 2014b, *The Astronomer's Telegram*, 6285, 1
 Gillessen, S. et al. 2012, *Nature*, 481, 51
 Jalali, B. et al. 2014, *MNRAS*, 444, 1205
 Li, Z., Morris, M. R. & Baganoff, F. K. 2013, *ApJ*, 779, 154
 Meyer, L. et al. 2014, in *IAU Symposium*, Vol. 303, ed. Sjouwerman, L. O., Lang, C. C. & Ott, J., 264
 Muzic, K. et al. 2010, *A&A*, 521, A13
 Shahzamanian, B. et al. 2014, *A&A*, in press, arXiv:1411.0006
 Valencia-S., M. et al. 2015, *ApJ*, 800, 125
 Witzel, G. et al. 2012, *ApJS*, 203, 18
 Witzel, G. et al. 2011, *A&A*, 525, A130
 Witzel, G. et al. 2014, *ApJ*, 796, L8
 Zajaček, M., Karas, V. & Eckart, A. 2014, *A&A*, 565, A17
 Zamaninasab, M. et al. 2010, *A&A*, 510, A3



Observing the Galactic Centre with the VLT's Unit Telescope 4 with the aid of a laser guide star. See potw1045 for more information.

VEGAS-SSS: A VST Programme to Study the Satellite Stellar Systems around Bright Early-type Galaxies

Michele Cantiello¹
 Massimo Capaccioli^{2,3}
 Nicola Napolitano³
 Aniello Grado³
 Luca Limatola³
 Maurizio Paolillo^{2,4}
 Enrica Iodice³
 Aaron J. Romanowsky^{5,6}
 Duncan A. Forbes⁷
 Gabriella Raimondo¹
 Marilena Spavone³
 Francesco La Barbera³
 Thomas H. Puzia^{8,9}
 Pietro Schipani³

¹ INAF–Osservatorio Astronomico di Teramo, Italy

² Dipartimento di Fisica, Università di Napoli Federico II, Italy

³ INAF–Osservatorio Astronomico di Capodimonte Napoli, Italy

⁴ Agenzia Spaziale Italiana — Science Data Center, Roma, Italy

⁵ University of California Observatories, Santa Cruz, USA

⁶ Department of Physics and Astronomy, San José State University, USA

⁷ Centre for Astrophysics & Supercomputing, Swinburne University, Hawthorn, Australia

⁸ Institute of Astrophysics, Pontificia Universidad Católica de Chile, Santiago, Chile

⁹ National Research Council Canada, Herzberg Institute of Astrophysics, Victoria, Canada

The VEGAS-SSS programme is devoted to studying the properties of small stellar systems (SSSs) in and around bright galaxies, built on the VLT Survey Telescope early-type galaxy survey (VEGAS), an ongoing guaranteed time imaging survey distributed over many semesters (Principal Investigator: Capaccioli). On completion, the VEGAS survey will have collected detailed photometric information of ~ 100 bright early-type galaxies to study the properties of diffuse light (surface brightness, colours, surface brightness fluctuations, etc.) and the distribution of clustered light (compact “small” stellar systems) out to previously unreachable projected galactocentric radii. VEGAS-SSS will define an accurate and homogeneous dataset that will have an important legacy value

for studies of the evolution and transformation processes taking place in galaxies through the fossil information provided by SSSs.

Satellites of massive ellipticals

The surroundings of massive galaxies are populated by a zoo of dynamically hot satellite stellar systems: globular clusters (GCs), extended clusters (ECs), ultra-compact dwarfs (UCDs), dwarf spheroidals (dSphs), dwarf ellipticals (dEs), compact ellipticals (cE), etc; see, for example, Forbes et al. (2013) and references therein.

Characterising the properties of SSSs in the potential well of their host galaxy is fundamental, not only because they play a key role in understanding the basic processes of formation and evolution of the structures in the Universe from star clusters to galaxies, but also for a variety of other reasons. These include: i) the stellar populations of SSSs are less complex than those of massive galaxies, which allows a more accurate comparison of their ages and metallicities with stellar population models; ii) SSSs are relatively easy to detect out to large distances, which offers the unique opportunity to scrutinise various environments beyond the Local Group, and thus to study how the properties of SSSs vary across space and time. SSSs are thus ideal tracers of the host galaxy’s gravitational potential as well as of the assembly history of the galaxy’s stellar populations. Therefore, increasing the sample of SSSs with accurate estimates of their physical properties is of paramount interest to scrutinise the scaling relations of SSSs over a complete and unbiased range of parameters.

The characteristic magnitude, colours, half-light radii R_h , etc., of objects in different SSS classes can change significantly. Nevertheless, the distinction between different SSS types is sometimes not trivial because of the lack of a clear-cut distinction between the classes of SSSs. A natural explanation for this lack is that there is none. Indeed, the transformation processes occurring in dense environments may disrupt or transform massive SSSs, littering the galaxy field with the remains of disrupted systems, such as

low-mass SSSs, stellar streams, etc. (e.g., West et al., 1995).

Small stellar systems, especially GC systems, have been studied for decades, and progress has been limited not so much by telescope collecting area, but by the field of view and the image quality (both to reduce contamination and to reduce the exposure times). Thus, the use of telescopes with large collecting areas (4-metre or even 8-metre-class) is not compelling, at least for the photometry, and original achievements are possible from smaller telescopes.

Through the VEGAS-SSS programme, and taking advantage of the large field of view of the 2.6-metre VLT Survey Telescope (VST), we intend to dig into the zoo of SSSs hosted by bright galaxies in different environments, observed as part of the VEGAS survey, and comprehensively study their properties out to very large galactic radii on a homogeneous and self-consistent basis. Here, we present an overview of the project and some first results for the galaxy NGC 3115.

VEGAS: Observational strategy, aims of the survey and SSSs

VEGAS is a deep multiband *gri* imaging survey of early-type galaxies (ETGs) carried out with the VST. The large field of view of OmegaCAM, mounted at the VST (Capaccioli & Schipani, 2011), together with its high efficiency and spatial resolution will allow us to map, with a reasonable integration time, the galaxy surface brightness from the core out to isophotes encircling about 95 % of the total light. Observations started in October 2011 (ESO Period 88), and data for about 20 galaxies for a total of 80 hours have been acquired up to Period 93. The survey plan is to analyse the photometry of about 100 galaxies with radial velocity ≤ 4000 km s⁻¹ in different environments and covering the range of parameter space. The observational plan is designed to reach a depth of 27.3, 26.8 and 26 mag arcsecond⁻² with signal-to-noise > 3 in the *gri*-bands.

The data reduction, including dither combination, exposure correction, CCD gain harmonisation, illumination correction,

astrometric solution and photometric calibration was performed with the VST-Tube pipeline (Grado et al., 2012). VST-Tube is a very versatile software package for astronomical data analysis, tested against imaging data taken with different telescopes/detectors and adaptable to existing or future multi-CCD cameras (e.g., Cantiello et al., 2013). Further details about the survey and the overall data quality can be found in Capaccioli et al. (2015, in preparation).

The main science goals of the VEGAS survey are: 1) to study the 2D light distribution out to at least ~ 10 effective radii, R_e , focusing on the galaxy structural parameters and the diffuse light component, highlighting the presence of inner substructures as a signature of recent cannibalism events and/or inner discs and bars fuelling the active nucleus that is present in almost all objects of our sample; 2) to map the surface brightness profile and isophote geometry out to $10R_e$ or more; 3) to analyse the colour gradients and their connection with galaxy formation theories, also taking advantage of stellar population synthesis techniques; 4) to study the external low surface brightness structures of the galaxies and the connection with the environment; 5) to measure the surface brightness fluctuations (SBF), and SBF gradients for the chemical characterisation of the stellar population within $2R_e$, or more.

The survey depth will allow the light distribution, colour gradients and SBF magnitudes to the largest galactocentric distances to be characterised on a homogeneous and self-consistent basis. At large radii, from $\sim 10R_e$ and beyond, the dynamical times are of the order of 10^9 yr, and the signatures of the secondary merging events due to the interaction with the environment last longer. VEGAS will look for the expected signatures of processes occurring at various scales of the galaxy environment by the study of surface brightness, colours and SBF analysis.

In addition to the diffuse light, the wealth of SSSs in the potential well of the host galaxy is the other fossil tracer of the past formation events in ETGs. Hence, one further science goal of VEGAS is to

derive the census of SSSs out to several tens of R_e , allowing the study of the properties of dynamically hot stellar systems in the outermost galaxy regions. This latter part of the survey is also called VEGAS-SSS.

VEGAS-SSS

We started the VEGAS-SSS project with the study of g - and i -band data of NGC 3115, an isolated, relatively nearby lenticular galaxy, at a distance ~ 10 Mpc, mostly focused on the properties of the GC system in the galaxy. The choice of NGC 3115 was also motivated by the many photometric and spectroscopic studies available in the literature (both from 8–10-metre class ground-based telescopes, and from the Hubble Space Telescope [HST]), which were particularly useful for testing the procedures and the methods that will be used for the

future targets of the survey. A VST colour-composite image of the galaxy is shown in Figure 1.

To improve the detection and the analysis of the spatial extent of the sources in the frame, we did not use the full sample of images available for the study of diffuse light, and restricted our analysis to the data with average seeing better than ~ 0.8 arcseconds. With this choice, the total exposure time available is ~ 2700 s in g -band and ~ 1250 s in i -band.

In order to obtain accurate photometry over the entire VST frame, including the brightest inner regions of NGC 3115, we modelled and subtracted the galaxy. Then using our own procedure, based on various common astronomical tools

Figure 1. The lenticular galaxy NGC 3115 is shown in a VST colour-composite (u , g and i filter) image; the size is about 52 arcminutes square.



(Pyraf, SExtractor, SuperMongo, etc.), we obtained accurate photometry of the compact sources, derived and applied the proper extinction and aperture corrections, matched the g and i photometric catalogues and analysed source colour, obtaining a separation between compact objects in the galaxy and foreground contaminants (Milky Way stars, background galaxies along the line of sight, etc.).

Our photometry was verified against the various catalogues existing in the literature, and provided in all cases satisfactory agreement. As an example, we took as reference the recent study of the Advanced Camera for Surveys (ACS) on the HST, based on a mosaic of six pointings covering the central $\sim 6 \times 9$ arc-minute region of NGC 3115 ($\sim 1.5\%$ of the total VST field of view). By comparing our g -band photometry with the ACS results from Jennings et al. (2014), a median ~ 0.01 mag difference is found over a sample of ~ 200 matching GCs.

In addition to photometry, a further physical parameter that can be estimated using imaging data is the physical extent of the source. Size measurements can be very challenging, especially with ground-based imaging data. Moreover, only angular sizes can be measured, which require the knowledge of the object distance to be transformed to linear scale. Nevertheless, angular sizes and shapes have been estimated for a large sample of SSSs using both space- and ground-based telescopes (e.g., Larsen et al., 1999; Jordan et al., 2004). To estimate object sizes we used the software Ishape (Larsen et al., 1999), a commonly used tool for the purpose, which, in our case, proved very efficient.

We inspected the properties of SSSs out to ~ 23 arcminutes, which is more than twenty times the R_e of NGC 3115, and the largest distance ever used to inspect SSSs in this galaxy. Thanks to the large field of view of the images, we applied a statistical approach to study the properties of the GC population versus galactocentric radius R_{gal} . The basic idea is simple: foreground objects are evenly distributed in the field around the galaxy, while SSSs “trapped” in the potential well of the galaxy have a power-

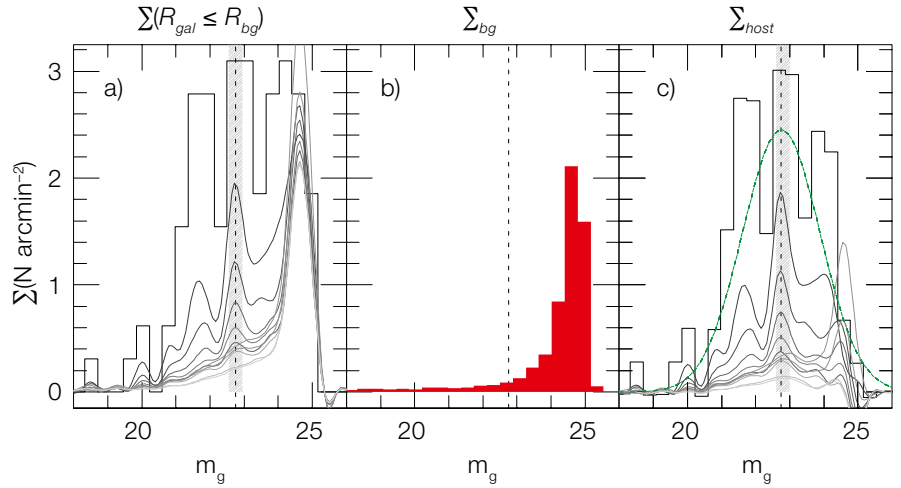


Figure 2. Surface density histograms versus magnitude. Panel (a): Surface density Σ for sources within $R_{gal} \leq R_{bg}$. Darker colours refer to areas with smaller galactocentric radii. Panel (b): Same as left, but for background sources at $R_{gal} \geq R_{bg}$. Panel (c): residual surface density $\Sigma_{host} = \Sigma(R_{gal} \leq R_{bg}) - \Sigma_{bg}$.

law radial density profile. Thus, we estimated the surface density of objects satisfying some well-defined criteria (colour, magnitude, size, etc.) at different R_{gal} , and analysed the properties of the residual over-density, Σ , of the central galaxy regions with respect to the background regions.

To describe how the method works, in Figure 2 we show the diagrams related to the GC luminosity function (GCLF) analysis. Panel (a) shows the GCLF at various projected R_{gal} , starting from the innermost regions with the largest surface densities Σ . In the plot, different colours show the surface density histograms at different radii, starting from 2 arcminutes out to $R_{bg} = 23$ arcminutes. Panel (b) shows the surface density Σ_{bg} of objects beyond $R_{bg} = 23$ arcminutes. The difference between the surface density $\Sigma - \Sigma_{bg}$ inside and outside of the galaxy is clearly visible in the two panels, as shown in panel (c).

The effectiveness of the method adopted is demonstrated by the extremely good agreement with other existing studies covering smaller areas. In the following, we describe the first VEGAS-SSS results and show the potential of the project in providing original results on SSS-related science. More details can be found in Cantiello et al. (2014b).

First results of VEGAS-SSS

GC luminosity functions

We analysed the luminosity function of sources in the field of NGC 3115, with the specific purpose of inspecting the GCLF to estimate the galaxy distance modulus μ_0 using the GCLF turn-over magnitude (TOM; Harris et al. [2014] and references therein), and to further study how, and whether, the TOM in g -band, m_g^{TOM} , changes as a function of galactocentric distance.

As shown in Figure 2, panel (c), the density distribution of sources in the host galaxy has a peak at $m_g^{TOM} \sim 22.8$ mag. Using the calibration of the absolute TOM from the ACS Virgo Cluster Survey, we estimated a distance modulus $\mu_0 = 29.9 \pm 0.3$ mag, or 9.8 ± 1.4 Mpc, in good agreement with the literature distance of the galaxy.

The approach adopted allowed us to investigate how the GCLF might change with R_{gal} . To date, the scarce literature on the topic shows galaxies both with (Harris et al., 2014) and without (Jordan et al., 2007) a radial dependence of the TOM. Our result is that for this galaxy there is no obvious variation of m_g^{TOM} with the projected galactocentric distance. The peak of luminosity of the GCLF is influenced by various physical factors. However, to a

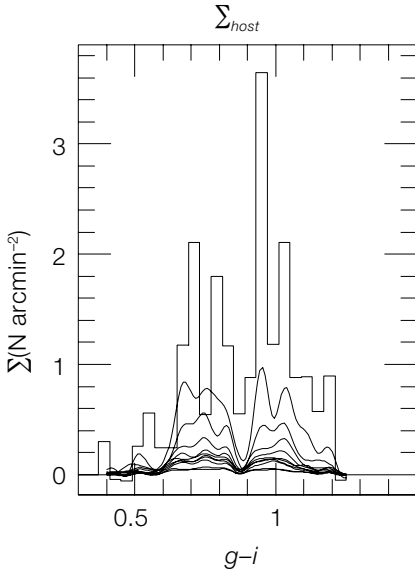


Figure 3. Residual surface density, as the right panel of Figure 2, but shown versus colour.

first approximation, the simplest interpretation of the gradient (or lack of it) in the peak luminosity of the GCLF is a trend (or lack of it) in the mean GC mass with R_{gal} .

We further inspected how the TOM differs between the red and blue GCs, after dividing the blue/red GCs by adopting a sharp colour separation at $g - i = 0.9$ mag (see below). Our analysis showed that the GCLF of the blue and of the red GCs has a peak consistent with the TOM of the total GC selection. The interesting point here is that a ≈ 0.2 mag offset exists between the red and blue GCLF, with the red system being fainter. Indeed, from a stellar population viewpoint, such behaviour is expected if the GC mass function is universal across metallicity (Jordan et al., 2007).

With the future VEGAS-SSS studies, we will further explore the dependence of m_g^{TOM} with the projected radii and the possible systematic differences between the blue and red GCLFs, for galaxies in different environments and with different masses.

GC colour distribution

The choice of NGC 3115 as the first VEGAS-SSS target was also motivated by the fact that the galaxy is the first one beyond the Local Group with a confirmed bimodal metallicity distribution

(see Brodie et al., 2012; Cantiello et al., 2014a; and references therein for more details). In the last decade, the nearly universal presence of two well-separated peaks in the optical colour distribution of GCs in ETGs, has inspired a vigorous and prolific debate. Historically, the bimodal colour of GCs in optical bands has been equated to metallicity ([Fe/H]) bimodality, implying a fundamental constraint on GCs and galaxy formation scenarios. Metallicity bimodality requires two distinct epochs or mechanisms of formation, or both, for the blue/metal-poor and red/metal-rich GC subpopulations. However, this assumption became the subject of debate when various authors independently, using observations and stellar population models, pointed out non-negligible nonlinearities in the colour-metallicity relations of GCs, and demonstrated that the presence of such nonlinearities naturally produces bimodal colour histograms from non-bimodal [Fe/H] distributions. This interpretation provided a simple, alternative explanation for the ubiquity of bimodal GC colour distributions, based on stellar evolution.

Using the same approach adopted for the GCLF, we analysed the colour distribution of GC candidates in NGC 3115. The results are shown in Figure 3. The figure shows the “total - background” density distribution, similar to panel (c) in

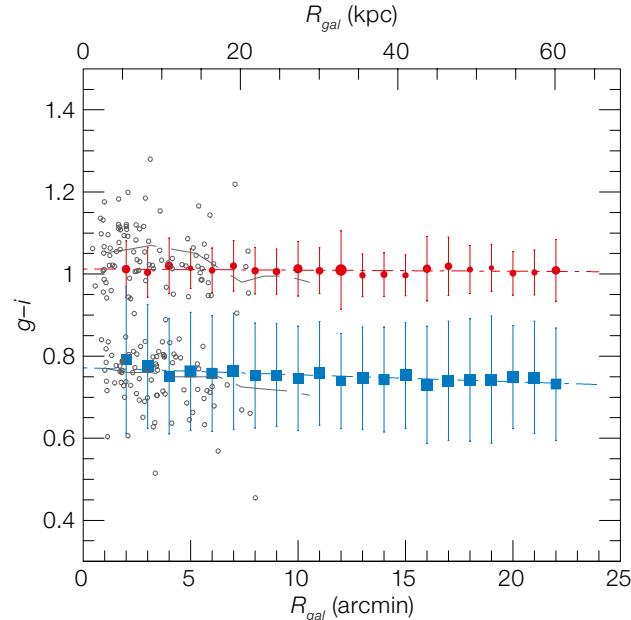


Figure 4. Position and width of the blue and red GCs (blue squares and red circles respectively) plotted at different R_{gal} . Symbol size is proportional to the fraction of objects associated with each peak. A fit to the data is shown with dot-dashed lines. Grey dots show spectroscopically confirmed GCs; grey long-dashed lines mark the rolling fits of the blue and red GC peaks as derived by Arnold et al. (2011) obtained from a combination of spectroscopically and photometrically selected GCs.

Figure 2, versus colour. The plot shows two obvious features: i) the presence of a dip at $g - i \sim 0.9$ mag with two well-defined peaks at ~ 0.75 and 1.00 mag; and ii) the dip and the peaks are seen at all inspected radii.

By analysing the position of the blue and red peaks as a function of R_{gal} (Figure 4), various features appear:

- A clear colour- R_{gal} correlation for the blue GC component, and no correlation, or only a very weak one, for the red GCs;
- The fraction of red GCs has a slight but significant decrease with respect to the blue GCs at large radii;
- The width of the two sequences is relatively stable with radius, with the blue distribution being broader at all radii.

In Figure 4 we also added data from Arnold et al. (2011) from the SAGES Legacy Unifying Globulars and GalaxyS (SLUGGS) survey. The grey symbols show spectroscopically confirmed GCs (dots), and the rolling fits for the blue and red GC peaks as derived by combining the spectroscopic and photometric samples (grey dashed lines). There is a good match between the VEGAS-SSS and SLUGGS results. In particular, we highlight the very good match with the colours of spectroscopically confirmed GCs. The agreement appears even more

striking if one takes into account that the SLUGGS data were obtained by coupling *gri*-band imaging data from Suprime-Cam at the 8.2-metre Subaru Telescope and spectroscopy from the 10-metre Keck-II telescope with DEIMOS.

Finally, we analysed the radial profiles of the projected surface density of GC candidates, inspecting the full GC sample, and the red and blue subsystems separately. The results are shown in Figure 5. Our analysis reveals that the total, red and blue GCs follow very closely an $R^{1/4}$ de Vaucouleurs profile, and that the profile of red GCs appears steeper than that for the blue GCs while both are shallower than the galaxy light profile. Moreover, the red GCs and the galaxy light profile match at $R_{gal} \geq 7.5$ arcminutes, while the density of GCs is lower at smaller radii. Such a depletion, already observed in other galaxies brighter than NGC 3115, has been interpreted as a higher efficiency for GC-disruption mechanisms in the inner galaxy regions by dynamical friction, two-body relaxation and GC tidal shocking (see Goudfrooij et al. [2007] and references therein).

Overall, the properties observed support a scenario where blue GCs are associated with the galaxy halo, while red ones are more centrally concentrated and associated with the bulge stellar component in the galaxy, and suggest that the galaxy has undergone a relatively quiescent evolution, without major star-forming events.

SSS sizes

The selection of SSSs based on one single colour is inherently uncertain and results in a catalogue with large fractions of contaminating sources. An additional optical colour certainly reduces the fraction of contaminants, especially if *u*-band photometry is available. To partly overcome the problem of using one optical colour alone, we also estimated the physical extent of SSSs using the aforementioned tools. We finally obtained a catalogue containing $\sim 30\,000$ sources with both photometry and R_h estimates; the latter have been compared with literature studies, with encouraging results.

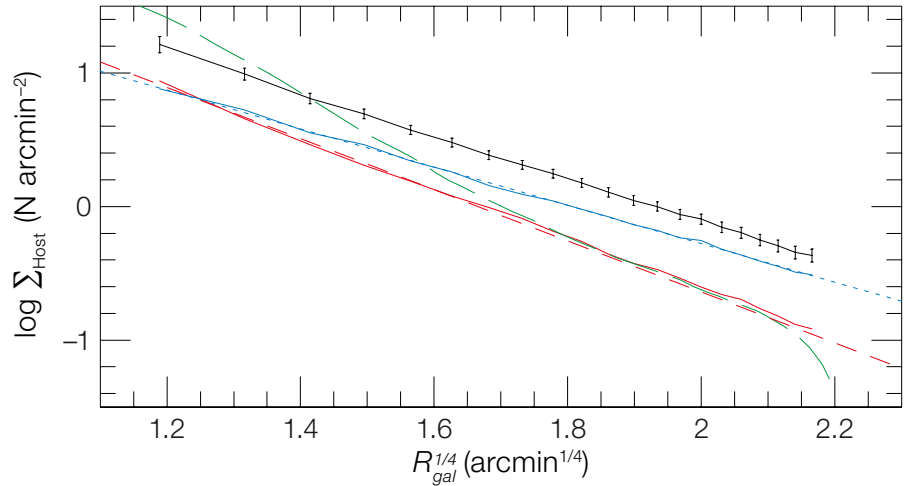


Figure 5. Surface density profiles of blue, red and total GC population (blue, red and black lines respectively). The galaxy surface brightness profile in *g*-band from Capaccioli et al. (2015, in prep.) is also shown by a green long-dashed line. The linear fit to the surface density is shown by a dotted line. The scale of the galaxy profile is arbitrary.

Object sizes provided another attribute to discriminate between real SSSs hosted in the field of NGC 3115, and fore/background sources. Future studies with new deep VEGAS-SSS *gri*- and *u*-band data will be used to further study the issue, and — for targets at larger distances, where GC sizes cannot be reliably estimated — constrain even more tightly the properties of other, less populated classes of SSSs, such as UCDs and cEs.

Future perspectives

The final catalogues from VEGAS-SSS will contain accurate photometry, positions and sizes for thousands of SSS candidates in the field of bright ETGs. The programme will have a twofold legacy value. First, for preparing future observational studies. The coupling of optical data with just one near-infrared band is very effective in reducing the fraction of SSS contaminants to $\approx 5\%$ or less. The VEGAS-SSS catalogues will then be perfectly suited to be complemented by single-band near-infrared imaging (e.g., with a large-format near-infrared imager like VISTA). Moreover, having complete and clean SSS catalogues is essential for the preparation of spectroscopic follow-up campaigns.

Second, the results obtained for the GC population in NGC 3115, based on *g*- and *i*-band data, suggest that a similar analysis carried out on the final VEGAS-SSS target list, and extended to other SSS classes, will have great value in studies of the evolution and transformation processes taking place in galaxies in a range of environments.

Acknowledgements

Michele Cantiello acknowledges support by FIRB-MIUR 2008 (P.I. G. Imbriani) and the PO-FSE Abruzzo Sistema Sapere e Crescita.

References

- Arnold, J. A. et al. 2011, *ApJ*, 736, L26
- Brodie, J. et al. 2012, *ApJ*, 759, L33
- Cantiello, M. et al. 2013, *A&A*, 552, 106
- Cantiello, M. et al. 2014a, *A&A*, 564, L3
- Cantiello, M. et al. 2014b, *A&A*, in press, DOI: 10.1051/0004-6361/201425165
- Capaccioli, M. & Schipani, P. 2011, *The Messenger*, 146, 2
- Forbes, D. A. et al. 2013, *MNRAS*, 435, L6
- Goudfrooij, P. et al. 2007, *AJ*, 133, 2737
- Grado, A. et al. 2012, *Mem. S. A. It. S.*, 19, 362
- Harris, W. et al. 2014, *ApJ*, 797, 128
- Jennings, Z. G. et al. 2014, *AJ*, 148, 32
- Jordan, A. 2004, *ApJ*, 613, L117
- Jordan, A. et al. 2007, *ApJS*, 171, 101
- Larsen, S. S. 1999, *A&AS*, 139, 393
- West, M. J. et al. 1995, *ApJ*, 453, L77



Architekten Bernhardt + Partner

Astronomical News

The groundbreaking ceremony to mark the beginning of the main construction phase for the ESO Supernova Planetarium & Visitor Centre (artist's impression above) took place on 24 February 2015 at ESO Headquarters in Garching. See Announcement ann15011 for details.



Astronomy at High Angular Resolution

held at ESO Headquarters, Garching, Germany, 24–28 November 2014

Henri Boffin¹
Linda Schmidtbreich¹
Gaitee Hussain¹
Jean-Philippe Berger¹

¹ ESO

A workshop took place in Brussels in 2000 on astrotomography, a generic term for indirect mapping techniques that can be applied to a huge variety of astrophysical systems, ranging from planets, single stars and binaries to active galactic nuclei. It appeared to be timely to revisit the topic given the many past, recent and forthcoming improvements in telescopes and instrumentation. We therefore decided to repeat the astrotomography workshop, but to put it into the much broader context of high angular resolution astronomy. Many techniques, from lucky and speckle imaging, adaptive optics to interferometry, are now widely employed to achieve high angular resolution and they have led to an amazing number of new discoveries. A summary of the workshop themes is presented.

The workshop brought together people from different communities (see the conference photograph, Figure 1), who use various techniques to construct images at very high angular resolution, with the aim of reviewing these methods, the progress in the field, the new harvest of results that have been collected, as well as to prepare the next generation of astronomers to use these tools and techniques. The various techniques used to beat the seeing and the telescope diffraction limit can be roughly distributed as follows:

- single-dish imaging methods have been developed to beat the seeing at the focus of telescopes (e.g., adaptive optics, lucky/speckle/holographic imaging, sparse aperture masking) aiming at sub-arcsecond spatial resolution up to the diffraction limit of single telescopes;
- techniques that allow the diffraction limit to be beaten in order to achieve milliarcsecond angular resolution using direct (optical interferometry) and indirect (e.g., spectro-astrometry) techniques; and



Figure 1. Photograph of the participants at the workshop in the entrance hall at ESO Headquarters.

- single-dish tomographic reconstruction methods (astrotomography), with microarcsecond resolution, but applicable only to certain classes of objects.

The workshop was structured to present the various techniques, with extensive reviews, and then to consider the various scientific fields that have profited from these techniques: exoplanets and brown dwarfs, stars, binaries, and large-scale phenomena. We give a very short summary of the material presented; the programme of the workshop is available¹ and the presentations can be downloaded².

Beating the seeing: Reaching the diffraction limit

Atmospheric turbulence creates inhomogeneities in the refractive index of air that affects the image quality — the infamous “seeing”. To counter this, astronomers have devised a series of techniques, such as lucky imaging, speckle imaging and adaptive optics.

Adaptive optics (AO), which has a long history at ESO, aims at neutralising the atmospheric turbulence by a closed-loop system. As Julien Milli reminded us in his presentation, the first astronomical system ever online was Come-On at the Observatoire de Haute-Provence, which later became operational at the 3.6-metre

telescope in La Silla (Merkle et al., 1989). AO is now part of many systems at the Paranal Observatory, as well as in all major observatories, and has led to many of the most important ESO discoveries: the supermassive black hole at the centre of the Milky Way, the first image of an exoplanet and imaging of the young discs around stars. AO comes in many different flavours and can be defined by the total corrected field of view versus the Strehl ratio which the system achieves. These flavours include ground-layer AO (GLAO), multi-conjugated AO (MCAO) and eXtreme AO (XAO). All major telescopes have second generation AO instruments currently in operation, which can reach typically 15–50 milliarcsecond (mas) resolution with high Strehl ratios and have ten times more actuators than the first generation AO systems.

At the Very Large Telescope (VLT), the second generation AO system is SPHERE (an XAO system), which is beginning regular operations (see article on Science Verification by Leibundgut et al., p. 2) and is based on a system with 1600 actuators (see the result in Figure 2, right). A GLAO system (part of the VLT Adaptive Optics Facility [AOF]) is under development at ESO to assist instruments such as MUSE and Hawk-I, combining diffraction-limit imaging and relatively wide-field imaging spectroscopy. Not least, the whole concept of the European Extremely Large

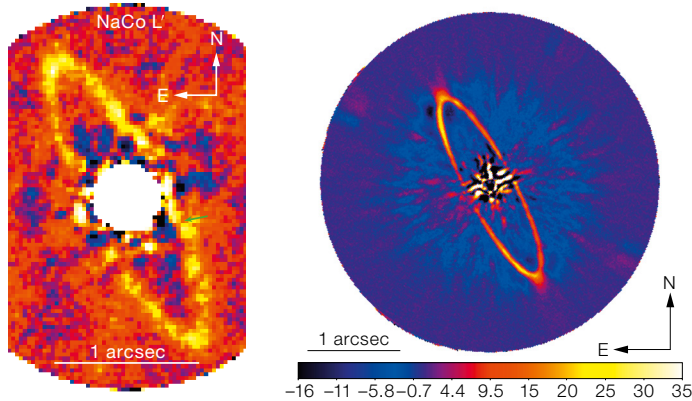


Figure 2. Showing the progress achieved in AO: a comparative study of the disc around HR 4796 A by NACO (left; from Milli et al., 2014) and, more recently, with SPHERE (right; from Milli et al. [2015] in prep.).

Telescope (E-ELT) requires the use of AO. The future lies also in the development of wide-field AO systems (WFAO), as shown by Benoît Neichel in his talk. By using multiple laser guide stars (LGS), WFAO significantly increases the field of view of AO-corrected images. The first such system in routine operation is GeMS, the Gemini Multi-Conjugate AO System, which uses five LGS and provides 87 by 87 arcsecond AO-corrected images in the *H*-band with a resolution of 80 mas. Such wide-field images with uniform point-spread functions over the full field of view are particularly useful for astrometric studies, for example in clusters or at the Centre of the Milky Way. Moreover, such developments are critical, as all the ELTs rely on multi-LGS WFAO systems.

Wolfgang Brandner reviewed lucky imaging, which is often presented as a poor man's adaptive optics. It exploits moments of good seeing, that is, it takes many short exposures and then retains only those images that have the best quality (typically 10 % of the whole). The technique is still quite popular and new projects are being devised, especially since the availability of noise-free detectors such as L3 (Low Light Level, LLL) and extended multiplication (EM) charge coupled devices (CCDs), and the fact that these systems are quite affordable. For example, the AstroLux Sur on the ESO New Technology Telescope (NTT) had a total hardware cost of only 50 000 euros. Lucky imaging is also quite useful as it generally has fainter limiting magnitudes than most AO systems, and it can work in the visible where AO is not so developed. As pioneer and expert, in his presentation, Craig Mackay mentioned

that, at the 5-metre Palomar telescope, AO and lucky imaging are combined, leading to the highest resolution image ever taken in the visible on faint targets, with a resolution of 35 mas in the *I*-band and a Strehl ratio of 17 %. Gergely Csépany combined lucky imaging and AO to study a sample of 38 T Tauri multiple systems over a 20-year period, and was able to cover the orbits in several of them. In addition, Mackay presented a proposal for a mosaic of lucky imagers for the NTT. This project, called GravityCam, will consist of no less than 100 CCDs with 70 mas pixels and will mainly be used for exoplanet microlensing surveys, down to below an Earth mass.

Speckle imaging was introduced by Sridharan Rengaswamy, who showed the advantages of the method and its significant contribution to the imaging of binary stars. More details about this technique is given in Rengaswamy et al. (2014). This technique was further developed, as speckle holography, by Rainer Schödel, which he calls "lucky imaging on steroids" to reconstruct images of crowded and "wide" fields of view of several tens of arcseconds, while keeping the instrument sensitivity.

In sparse aperture masking (SAM; or non-redundant masking [NRM] depending on which side of the Atlantic you work), a mask with a few holes is placed in front of the AO system. This transforms the primary mirror into a separate element, multiple-aperture interferometer and allows diffraction-limited imaging of (bright) astrophysical targets to be reconstructed, such as dust-enshrouded evolved stars. The technique was pre-

sented in detail by Mike Ireland. In particular, he pointed out that there are some moderate to high Strehl regimes, where working in the Fourier plane using a non-redundant mask offers improved performance over standard pupil-plane analysis; the example of a putative forming planet in a young disc in LkCa 15 was discussed. As a complement, Makoto Uemura showed how sparse aperture modelling can be applied, in a cross-disciplinary approach, to Very Long Baseline Imaging (VLBI) images, Doppler tomography and gamma-ray Compton imaging. In another vein, Jaeho Choi presented a non-interferometric phase-differential imaging method that uses Foucault knife-edge filtering.

Beating the diffraction limit: The milliarcsecond horizon

In order to reach higher spatial resolutions, different techniques, such as long-baseline interferometry where two or more telescopes are combined to obtain fringes, are required. The technique was reviewed by Jean-Baptiste LeBouquin. The contrast ("visibility") and phase information ("closure" or "differential phases") of the interference fringe packets can be used to retrieve direct information on the observed object brightness distribution. While the technique has been in widespread use in the radio domain for several decades, it is now also becoming a routine technique in the optical domain, in particular at the VLT Interferometer (VLTI) where the angular resolution in the near-infrared is of the order of a few milli-arcseconds.

Two regimes of data analysis were presented. In the first, the measurements are fitted with a parametric model of the object. This is particularly well suited when the number of measurements is limited, the object structure is well understood or the object is only marginally resolved. This was, and still is, the bread and butter of interferometry and is applied to the measurement of precise diameters, binary parameters or simple morphological parameters; it is well illustrated by the spectacular case of the expansion of a nova shell (Schaeffer et al., 2014) or the mass-loss in stars across the Hertzsprung–Russell diagram (e.g.,

Boffin et al. 2014). In the second case, the object complexity precludes simple modelling. If an object is well resolved (e.g., about 10 mas or more) it is then possible to acquire many measurements in the (u,v) -plane in order to carry out image reconstruction. Fabien Baron introduced the art of aperture synthesis and presented some magic tips and tricks for imaging stellar surfaces with interferometry, introducing the SQUEEZE and SIMTOI software. Clearly still an active area of research, it was shown that a large range of priors and model selection methods can be used. It is critical to test the methods and in this respect, the blind interferometric beauty contest plays an important role (Baron et al., 2012; see Figure 3). In the same vein, Christian Hummel presented a novel imaging algorithm that allows the combination of multi-channel interferometric data in a single image.

Interferometry is now coming of age and the VLTI has become a major piece of infrastructure with which it is possible to carry out surveys of hundreds of objects, such as for young stellar objects as part of the Exozodi survey, presented by Steve Ertel (see Ertel et al., p. 24). Gains in sensitivity now allow several dozens of active galactic nuclei (AGN) to be observed and their nuclei to be probed at unprecedented angular resolution. Sebastian Hoenig explained how the VLTI observations challenge the popular dusty torus model and reveal the true complexity of the inner kiloparsecs of AGN, such as its clumpiness and the inflow–outflow connection. This idea was supported by various other talks on interferometric observations that all agreed that there is more structure present in the mass around the black hole than previously assumed (Daniel Asmus, Leonhard Bartscher & Noel Lopez Gonzaga).

Pierre Cruzalèbes showed how to use interferometry to relate deviations from centro-symmetry of evolved stars to the K giant–red supergiant–asymptotic giant branch (AGB) star sequence. Zooming in on one object, Claudia Paladini showed nice results from an imaging project of the carbon-rich Mira R Fornicis, taking data with PIONIER for six half-nights over two weeks with three different quadruplets, leading to 294 visibility points and

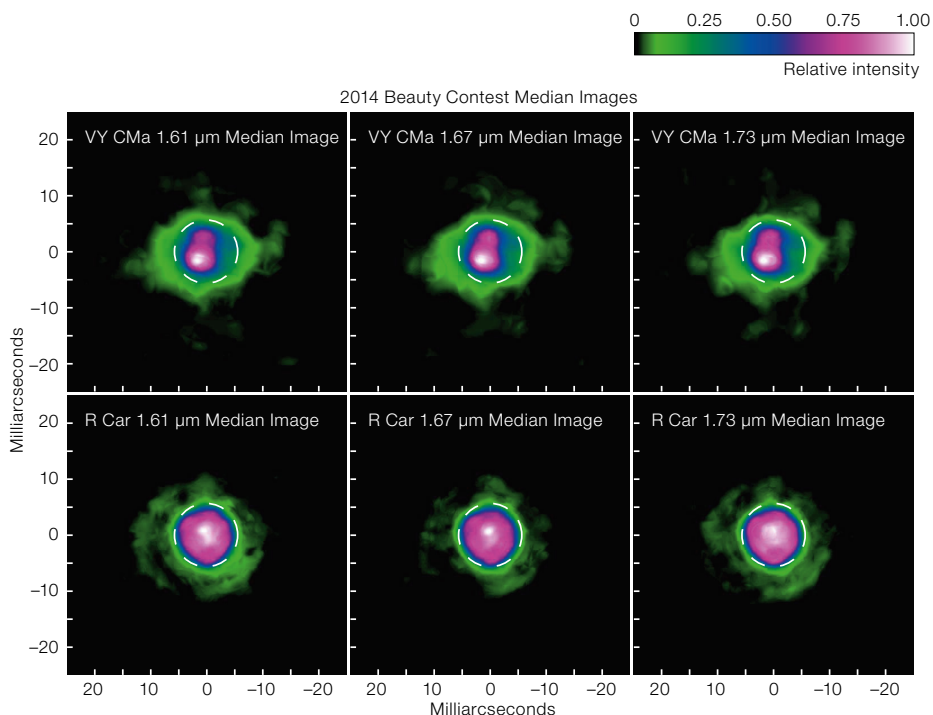


Figure 3. Results from the 2014 image reconstruction contest (see Monnier et al., 2014) based on data recorded with VLTI PIONIER. Upper: The VY CMa supergiant. Lower: The Mira star R Car.

201 closure phases. The resulting image is clearly aspherical, and shows that the surface is partially obscured by a mixture of dust and molecular opacity, similarly to R Coronae Borealis. The case was made that the combination of image reconstruction and spectral resolution should, in the future, become a major development at the VLTI, since it should allow astronomers to peer through the molecular layers in the complex stellar atmosphere. Michel Hillen looked at even more evolved stars using interferometry to study the discs around post-AGB stars and to constrain their vertical structure and dust distribution.

New instruments will soon be available, such as GRAVITY (Eisenhauer et al., 2011) and MATISSE (Lopez et al., 2014) at the VLTI. Jean-Philippe Berger showed in particular how GRAVITY will be useful for exoplanet detection. The increase in sensitivity through the use of efficient fringe tracking was discussed by Jorg-Uwe Pott, while Romain Petrov provided a detailed analysis of the possibility of more sensitivity gains.

Often, it is necessary to use many complementary techniques to gain the necessary knowledge. This was most evident in Stephan Gillesen's review on the already legendary observations of the Galactic Centre: many years of AO observations have resolved the stars of the central cluster and revealed the orbits of the inner stars around the Galactic Centre. These observations have proved the central object to be a supermassive black hole. Gillesen reported on follow-up observations that were taken to address more details and a campaign to follow the periastron passage of the star S2 in 2017 with several AO instruments. Future observations with GRAVITY in the Galactic Centre will be able to test whether Einstein's theory of general relativity holds in the vicinity of a black hole.

Stefan Kraus discussed the long-term plans to build a planet formation imager with the goal of studying the formation process and early dynamical evolution of exoplanetary systems on spatial scales corresponding to the Hill sphere of the forming planets. This requires angular

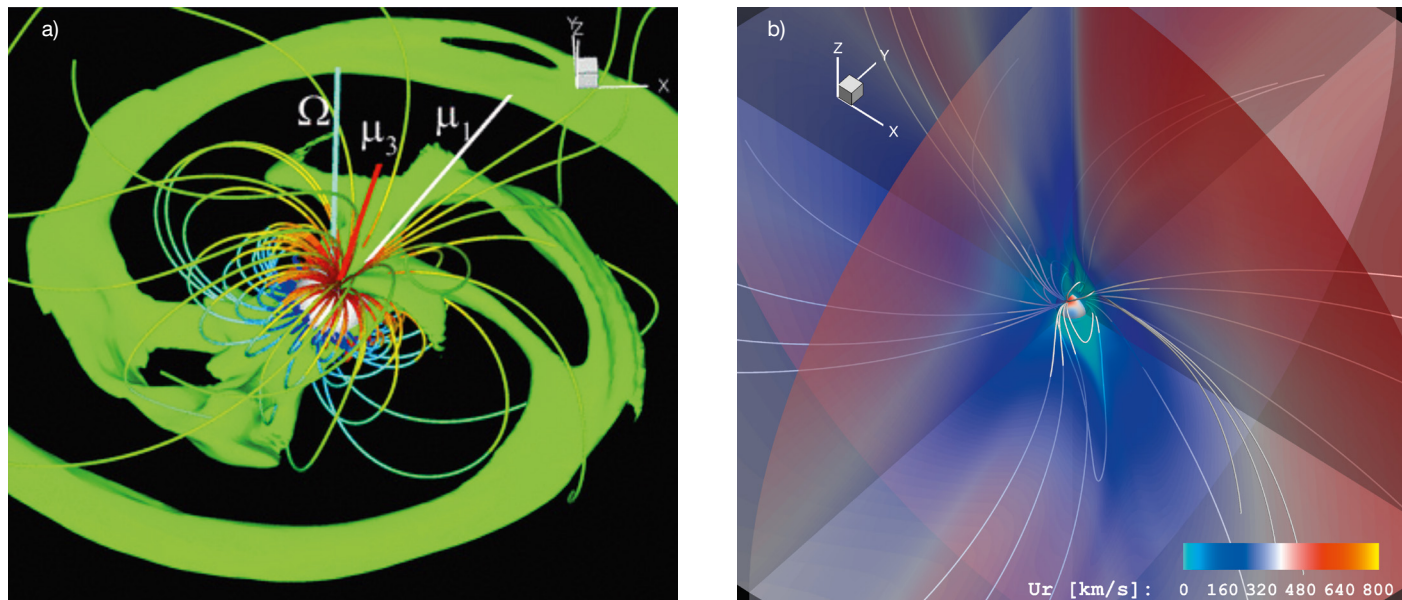


Figure 4. Large-scale magnetic field maps obtained using Zeeman Doppler imaging are key inputs for numerical simulations of their coronae and extended environments. a) In pre-main sequence stars that are still accreting from their circumstellar discs, magnetic

field maps have been used to test magnetospheric accretion scenarios (Romanova et al., 2011). b) In main sequence stars they can be used to model stellar winds, and the conditions in interplanetary environments (from Alvarado-Gomez et al., in prep.).

resolution of 0.03 AU, or 0.2 mas, which clearly points to a whole new facility.

While interferometry provides direct information with milliarcsecond resolution, Klaus Pontoppidan presented spectro-astrometry, an inexpensive method for measuring spatial properties of line-emitting gas far beyond the diffraction limit, and particularly powerful in determining the position angles and sizes of rotating and jet-like compact objects on scales as small as 0.1 mas. The rather simple idea is to measure the centroid on a spectrum as a function of wavelength, giving two-dimensional information. The technique has been applied to a wide range of astronomical objects, from protoplanetary discs, binary stars, discs around massive stars to AGN. Although it can be carried out with most spectrographs, AO-fed high dispersion echelle spectrographs allow much higher spatial resolution to be reached and this is why instruments such as the CRYogenic high-resolution InfraRed Echelle Spectrograph (CRIRES) or NIRSPEC with AO are ideal for this technique. Miwa Goto described spectro-astrometry with CRIRES at the VLT to study the anomalies in discs around stars, Mónica Blanco Cárdenas

looked at the cores of planetary nebulae, while on another scale, Jonathan Stern used the same technique to spatially resolve the kinematics of 0.1 mas wide quasar broad-line regions.

Luca Pasquini presented a new method, tachoastrometry, which aims at doing astrometry with radial velocities, and is particularly adapted for double-lined spectroscopic binaries, leading to a precision of better than two mas.

Microarcsecond resolution

The last set of techniques, allowing astronomers to reach microarcsecond spatial resolutions, are known together as astrotomography, and consist of indirect imaging techniques from observations of projections, that are obtained through eclipses, Doppler shifts, and/or time delays (Boffin et al., 2001). These techniques have been used to probe the orbits of exoplanets, map the surfaces of a variety of stars and the structure of accretion discs in binary systems.

Andrew Cameron showed how the distinctive signature from transiting exoplan-

ets in time series of high-resolution spectra could be used to recover details of the system's spin-orbit alignment through the Rossiter-McLaughlin effect. Measuring these spin-orbit alignments is important for understanding the origins of the system. In rapidly rotating stars, similar studies are important for exoplanet validation and for breaking degeneracy between $v \sin i$ and spin-orbit misalignment for low impact parameters. Tilted and retrograde orbits have been recovered for a number of systems, pointing to a number of different migration pathways. Studies of time series of near-infrared spectra have been employed to detect the transmission spectra of exoplanets themselves, enabling the masses of both the planet and star to be computed. The recent detection of the dayside spectrum of the hot Jupiters, τ Boo b, 51 Peg b and HD 189733b show that non-transiting planetary atmospheres can be detected; with β Pic b found to spin significantly faster than any planet in the Solar System. These are key pathfinder studies for the ELT.

Stellar surface-imaging techniques, Doppler imaging, Zeeman Doppler imaging and Roche tomography exploit the

information in time series of intensity and polarised spectra to reconstruct detailed maps of stellar photospheres. In the brightest, most rapidly rotating systems, these maps can achieve a latitudinal spatial resolution close to two degrees. Oleg Kochukhov, Julien Morin and Chris Watson reviewed the application of inversion techniques to reconstruct surface brightness maps, inhomogeneities in chemical elements and the large-scale magnetic fields on stars in systems including: brown dwarfs; G–M-type main sequence and pre-main sequence stars; Ap and Bp stars; B-type HgMn stars; and late-type stars in cataclysmic variable binaries (CVs) and X-ray binaries (examples in Figure 4). These maps probe fundamental processes including surface differential rotation, timescales of flux emergence and diffusion processes, and in CVs may explain the properties and timescales of accretion outbursts.

Julian Alvarado Gomez presented a robust criterion to prevent over/under-fitting in maps obtained with Doppler imaging techniques. He demonstrated how the large-scale magnetic fields reconstructed for cool stars can be used to model the extended environments and mass loss properties using three-dimensional magnetohydrodynamic models that have been developed for the Sun. Colin Hill reported the first measurement of differential rotation at the surface of the K4-type secondary of the CV, AE Aqr in contrast to predictions of tidal locking causing solid-body rotation. The timescales of the variability of activity implied by the measured differential rotation rates may contribute to the observed mass-transfer variations in the CV.

Tom Marsh introduced the technique of Doppler tomography, reviewing how structure within accretion discs and flows can be recovered from well-sampled spectroscopic time series. Results were shown for a range of accreting systems, showing how different diagnostics can allow more detail to be reconstructed. Axel Schwabe showed how Doppler tomography can be applied to polars (cataclysmic binary stars) to map the detail of magnetic accretion spots on white dwarfs. Petr Hadrava showed how Fourier disentangling of the spectra of binaries can be used to study various

phenomena, including pulsations, and can be applied to CVs. Jan Cechura described how hydrodynamic simulations can be used to construct synthetic Doppler tomograms of the high-mass X-ray binary, Cyg X-2, in both hard and soft states. These can be directly compared with observations and aid the conversion of tomograms, which are in velocity space, into spatial coordinates.

Raymundo Baptista reviewed how the detailed structure in accretion discs can be probed using eclipse mapping techniques including the white dwarf, mass donor, disc and outflowing gas. He also demonstrated how the time evolution of discs can be used to follow changes during outburst events and changes in disc viscosity during flickering (using light curves of HT Cas spanning two years). Stephen Potter showed how photopolarisation light curves could be inverted to create images of accretion shocks and detail in the structure near the white dwarf photosphere in magnetic CVs. Genetic optimisation is found to be effective in finding robust fits to the Stokes parameters. The models used for these reconstructions employ realistic stratifications of the accretion column structure based on radiation hydrodynamic simulations. The latest results of tomographic studies of polars, covering consecutive half-orbits for two systems and revealing the variability in the structure of the magnetic accretion flow in V834 Cen and HU Aqr, were presented by Enrico Kotze.

Misty Bentz introduced the technique of AGN reverberation mapping (or echo mapping), where time delays between signals in the continuum and in various broad lines are transformed into spatial information on the broad-line region (BLR). This allows the measurement of the mass of the black hole and, together with velocity delays of the lines, also gives a detailed picture of the BLR itself. As shown by Suvendu Rakshit, combining the angular sizes of the interferometric measurements with the reverberation maps yields geometric distances to the AGNs, which is necessary for the calibration of black-hole masses as well as for general cosmology.

As is most fitting for an ESO workshop, the final session was devoted to current

and future instrumentation. Suzanne Ramsay presented the current and future ESO instruments that may be used for high angular resolution, and the list is quite long: MATISSE, GRAVITY, the future AO Facility, ERIS, as well as many instruments to come with the E-ELT. Ulli Kaeufl presented the recent VISIR upgrade (see Kaeufl et al., p. 15).

The workshop was purposely limited to the optical and infrared domain, but of course high angular resolution astronomy can also be done in other wavelength ranges, and the recent, amazing images coming from ALMA (Atacama Large Millimeter/submillimeter Array) are a perfect demonstration. If the workshop has shown how much progress is evident on many fronts, it has also highlighted how very bright the future is!

Acknowledgements

It is a pleasure to thank the other members of the Scientific Organising Committee who helped to set up a very nice scientific programme for a very stimulating meeting: Keith Horne, Danny Steeghs, Klaus Strassmeier and Claus Tappert. Thanks go as well to the members of the Local Organising Committee who made for a very smooth and enjoyable workshop: Julian Alvarado Gómez, Stella Chasiotis-Klingner, Gergely Csépany and Jason Grunhut. Special thanks should also go to Keith Horne for presenting the summary talk of the workshop and to Stella Chasiotis-Klingner for her efficient help in all the practical aspects of the organisation.

References

- Baron, F. et al. 2012, SPIE, 8445, 84451E
- Boffin, H. M. J., Steeghs, D. & Cuypers, J. 2001, *Astromotography, Indirect Imaging Methods in Observational Astronomy*, LNP Series 573, Springer
- Boffin, H. M. J. et al. 2014, *The Messenger*, 156, 35
- Eisenhauer, F. et al. 2011, *The Messenger*, 143, 16
- Lopez, B. et al. 2014, *The Messenger*, 157, 5
- Merkle, F. et al. 1989, *The Messenger*, 58, 1
- Milli, J. et al. 2014, arXiv:1407.2539
- Monnier, J. D. et al. 2014, *Proc. SPIE*, 9146, 91461Q
- Rengaswamy, S. et al. 2014, *The Messenger*, 155, 12
- Romanova, M. M. et al. 2011, *MNRAS*, 411, 915
- Schaefer, G. H. et al. 2014, *Nature*, 515, 234

Links

- ¹ Workshop programme: <http://www.eso.org/sci/meetings/2014/hires2014/program.html>
- ² Workshop presentations available: <http://bit.ly/1y4WR4W>

New President of Council

Patrick Roche¹

¹ Department of Physics, University of Oxford, United Kingdom

Last year, the delegates to ESO Council elected me as Council President for 2015, following the completion of Xavier Barcon's three-year term of office. This is both a great honour and a daunting challenge for me, made all the greater by Xavier's exemplary performance in the role of President. Xavier showed enormous commitment, investing large fractions of his time and energy, together with cheerful and wise leadership. I am particularly pleased that at his final meeting as President in December 2014, Council approved the start of construction of the European Extremely Large Telescope (E-ELT), bringing the long years of studies, refinements, proposals and diplomacy to the point where ESO now embarks on the challenging task of building the next astronomical and technological jewel. This is a very fitting conclusion to Xavier's presidency.

Brief biography

I am a Professor of Physics at the University of Oxford and a Fellow of Hertford College, one of the constituent colleges of the University. Like most university faculty, my main roles include teaching undergraduate and graduate students, and conducting research in astrophysics, but in Oxford nothing is quite as simple as it seems. I only found out when I joined the College that I would inherit the position of senior member of the Hertford College Boat Club. I also oversee the College investments, which has provided a useful background for the periodic council discussions on the state of the CERN Pension Fund. In the Physics Department, I chair the Workshop Committee and am part of the Astrophysics Sub-department of Physics.

Before I started university, I worked for a year as an engineering technician in transistor production at Texas Instruments. This experience was valuable in providing me with hands-on contact with industrial manufacturing processes



and semiconductor fabrication. It also enabled me to save enough money to buy a motorbike! I have had one ever since, although do not get to use it very often these days. My current bike is 22 years old, and owning old machinery certainly prompts one's appreciation of the need for regular mechanical repairs and maintenance, and the ever-present possibilities of obsolescence.

My PhD thesis project at University College London was to develop and exploit a mid-infrared spectrometer, under the supervision of Dave Aitken. The instrument was deployed at telescopes in Australia, Hawaii, California and Tenerife, and even on the original Isaac Newton Telescope in the marshes of Herstmonceux before it was moved to La Palma. For more than a decade, it was the most sensitive instrument of its kind in the world and it characterised the mid-infrared spectra of a wide range of astronomical objects from planets in the Solar System to star-forming galaxies and active galactic nuclei. A polarimetric upgrade allowed the first detailed investigations of the 10 and 20 μm polarisation properties. The requirements for the assembly and dismantling of this instrument for the campaigns at different telescopes emphasised the virtues of reliability and good engineering. I have retained an abiding interest in astronomical instrumentation and the development

of observational techniques throughout my career, and have been involved with several infrared instruments, and led the construction of William Herschel Infra-Red Camera (WHIRCAM) for the William Herschel Telescope (WHT) and United Kingdom Infra-Red Telescope (UKIRT) Fast-Track Imager (UFTI).

I have been privileged to chair several telescope boards and advisory committees, including the Anglo Australian Telescope (AAT) and UKIRT Boards, and the NOVA (Nederlandse Onderzoekschool voor de Astronomie) Instrument Steering Committee, and was UK Gemini project scientist for the last six years of the construction project. I have had close associations with ESO since the UK accession process started, serving on the Scientific Technical Committee (STC) and Council, and chairing the STC and the Very Large Telescope Interferometer (VLTI) subcommittee. I have also served on the Atacama Large Millimeter/submillimeter Array (ALMA) Board. I am hugely grateful for the opportunities that have been given to me to work closely with the dedicated staff at these observatories. Many of the remarkable discoveries and developments in astronomy over the last few decades have arisen through the deployment of innovative instruments, supported by close interactions between the astronomical community and observatory staff.

To the future

ESO is an outstanding example of what can be achieved through collaboration and shared vision. I list a few examples: the second generation VLT instruments are the most ambitious and powerful capabilities available anywhere on optical/infrared telescopes and will doubtless provide a stream of high-profile results in the coming years; the results from ALMA over the last few months have demonstrated its enormous potential, and there is more to come as the number of antennas in use increases and the observatory moves towards full operations; and the first instruments for the E-ELT are moving towards approval for construction. At the same time, further

VLT and VLTI instruments are in the pipeline and upgrades to current capabilities will maintain their power.

ESO is a remarkably powerful and capable organisation, with very strong support from its Council delegates and the community. ESO is seen as a model for other communities to follow and I am both proud of this and eager to contribute to future developments. At a time when many funding agencies have had to make very difficult decisions about funding priorities within their national programmes, they have provided a ringing endorsement of ESO's programme by not only maintaining their investments, but ramping up their contributions to ensure that the E-ELT can be built and operated

at the level needed to sustain the programme.

The last couple of years have seen some very important anniversaries marking ESO's early years, and reflecting on those gives a very real sense of the way that it has developed from initial ideas to the world-leading organisation that we see today. There will doubtless be substantial challenges in the next few years as the current facilities are consolidated and the E-ELT construction programme pushes ahead, but these will come at a time when the capabilities and productivity of ESO's facilities have established us at the forefront of astronomy.

I look forward to the exciting times ahead!

Fellows at ESO

Bernd Husemann

I was born 1981 in the small village of Amelunxen, located almost at the centre of Germany between Paderborn and Göttingen, or Kassel and Hannover. When I was about nine years old *Star Trek — The Next Generation* started on German TV and became my obsession. I admired the enthusiasm with which the *Enterprise* crew explored the huge and vastly unknown Universe, and their curiosity for new civilisations. I dreamt of being a part of their Universe and exploring it when I grew up. Thus, I read a lot of children's books about the Solar System, the Galaxy and the history of the Universe. Given my never-ending desire to understand how the world around me really works, it was a natural choice for me to become a scientist.

Although I had not yet seen a telescope, I had already decided two years before finishing school that I wanted to study astronomy. Checking the available universities in Germany left me with just a few

options. I chose the University of Potsdam for two basic reasons: it is a small university with good contacts among the students and lecturers; and, the Leibniz-Institute for Astrophysics (AIP) is nearby and I was already thinking about doing a PhD there. Indeed it was the best choice I could have made and the best time of my life. We were a group of only 20 young and motivated physics students locked together in a room each day solving maths exercises, hunting down the lecturers for questions and complaining about our exams being far too difficult.

An important milestone for my personal development, education and career was to study for one year abroad in Southampton (UK) in 2003. It was a coincidence that the University of Southampton offers one week of training at the Teide Observatory (Tenerife, Spain) each year for their astronomy students. Although I was only a short-term visiting student, Phil Charles and Christian Knigge decided that I could attend the training course without additional cost. Visiting a



Bernd Husemann

remote observatory for the first time allowed me to see the night sky in its full beauty. The star sign Scorpio became my favorite and I realised that looking deep into the Universe with big telescopes at amazing locations is a true privilege. This was the job I really wanted to do!

The astronomy department at Southampton was focused on high-energy phenomena and I became interested in accreting supermassive black holes at the centres of galaxies (active galactic nuclei; AGN). Back in Potsdam a year later, I continued my studies and contacted Lutz Wisotzki as a local expert on AGN. He gave me the opportunity to work for my diploma thesis in his group for one year starting in autumn 2006. My task was to reduce and analyse optical integral field spectroscopy (IFS) data for a large sample of luminous AGN in order to understand their interplay with the interstellar medium. Since IFS was a rather new optical observing technique at that time, I had to tackle many technical issues. Python became my best friend during that period. Apparently, I did not perform too badly and I continued towards a PhD in 2007 supervised by Lutz Wisotzki and Sebastian F. Sanchez to expand the work I had started during the diploma.

During my PhD I enjoyed many observing trips to the Calar Alto Observatory (Spain) together with my fellow students Andreas Schulze, Sebastian Kamann and Christian Herenz. I developed into an experienced astronomer and an expert in IFS by working with data from many different instruments, like VIMOS at the VLT and the Potsdam Multi-Aperture Spectrophotometer (PMAS) at Calar Alto. Although it is unusual to stay at one place so long, I spent another two years as a postdoc at AIP after graduating in 2011. My expertise in IFS was strongly required to support the Calar Alto Large Integral Field Area (CALIFA) survey that was initiated by Sebastian F. Sanchez, in collaboration with many international institutes. As part of such a large collaboration, I experienced working with many scientists around the world and established a network that is of great value to me.

It was time for a change, and I luckily became an ESO Fellow in Garching in the autumn of 2013. As an optical astronomer, ESO always appeared like heaven on earth to me. I am grateful for the opportunity to develop my profile as an independent researcher at ESO. The diversity of research at ESO and the neighbouring institutes on the Garching campus provide a unique environment that often leads to new projects and col-

laborations. On the other hand, I am also happy to contribute with my experience and I became part of the ESO team supporting the commissioning of the MUSE instrument at the VLT. MUSE is a next generation integral field spectrograph and I am happy to be one of the few researchers who has already received data from the first period of observations.

Currently, I am building up an international collaboration called the Close AGN Reference Survey (CARS) to exploit MUSE data and enhance its value by acquiring multi-wavelength observations from X-rays to radio. This is an exciting new challenge for me, which certainly sets the next stage in my career. I will never lose the energy and enthusiasm for astronomy, but having a family with a 20-month-old daughter often sets constraints incompatible with an optimal career path. To make both things work is probably an even greater challenge for me right now than being just a successful astronomer.

Tayyaba Zafar

I grew up in Lahore, Pakistan and from a young age I wanted to do a PhD in physics, but couldn't make up my mind in which particular subject. Originally my interest in science was from a very mathematical viewpoint, but as I progressed in my studies, I found myself becoming more and more fascinated with its applications, in particular in physics. Therefore, I decided to take an MSc in physics. I was in particular interested more in particle physics, or the standard model to be exact. During my time as a "particle apprentice", I acquired a strong background in particle physics, quantum field theory and the theory of general relativity. I scored the highest marks in MSc Physics from amongst 438 students who took the exam in the whole of the Punjab province. I was immediately hired as a lecturer by the University of the Punjab, Lahore, after the MSc result and worked there for one and a half years. During that time, for teaching other courses I chose cosmology, since my interest in cosmology and astrophysics had developed through reading books in the library.

I started applying for PhD positions in the field of astrophysics in the United States



Tayyaba Zafar

and Germany. In early 2008, I coincidentally met with the Danish Ambassador at a seminar and he suggested that I should apply to Denmark as well. So I applied for a PhD vacancy at the Dark Cosmology Centre (DARK), University of Copenhagen. I was finally short-listed and after a written test and an interview, I was selected. So I stepped into wonderful Copenhagen, which was my first exposure to the wide world, and started my PhD in late 2008. Copenhagen has been my favourite city ever since. During the first year of my PhD I worked on acquiring more astrophysics knowledge, especially as I was hired for hunting high-redshift Ly α emitters using X-shooter. However, near the end of my first year, we realised that X-shooter was delayed and to obtain my degree I would need another project. Life shrinks and expands in proportion!

Out of the various projects my supervisor, Darach Watson, and I considered, we found that dust extinction in gamma-ray burst (GRB) afterglows was the most feasible. The absorption of the stellar light at optical and ultraviolet bands by the intervening condensed matter phase of stellar dust particles provides insights into hidden star formation. While stars are being born and dying everywhere, the fascinating aspect is that we come from that stardust. Ever since I have been attracted to the obscured Universe. I worked in particular on GRB afterglows, energetic serendipitous objects, offering a relatively unexplored view of the darkest and furthest side of the Universe. Later

on I expanded the dust studies to quasars and their intervening absorbers. At DARK, I not only moved from physics to astrophysics, but also learned enormously from my colleagues in various fields.

Even during my PhD, I did not limit myself to a narrow range of topics. I also worked on Damped Ly α Absorbers (DLAs), seen along the sightlines towards luminous quasars, to study their chemical and physical properties. DLAs, classified on the basis of their neutral hydrogen, are distant foreground galaxies usually faint and small (on the sky). I defended my thesis in April 2011 and continued working as a visitor at DARK for six months. I started my first postdoc at the Laboratoire d'Astrophysique de Marseille, France, working with Céline Péroux. There I ex-

panded my studies of intervening absorbers to a larger sample of DLAs and sub-DLAs, obtained from the UVES archive. I also started combining samples of GRBs and quasar absorbers to infer dust properties in distant diverse environments.

I left sunny Marseille, to commence my current ESO fellowship in Garching during late 2013. The fellowship not only gives us independence scientifically, but also provides the opportunity to perform functional duties at amazing ESO sites. Since I have mostly used VLT data during my career path, I therefore picked my duties to be at the driest place on Earth, Paranal Observatory. During my PhD, I went to the Nordic Optical Telescope, La Palma, Spain, for two weeks for a summer observing school. Now ESO has given me opportunities to observe with its powerful

facilities. During my first year I provided both day- and night-time support mainly for Unit Telescope 3 (UT3), and now I have switched to UT2. I adore the environment at Paranal, and every visit there is a great experience, where I not only perform service mode observations, but also learn to deal with specific technical issues.

The beauty of astronomy is that we are billions beneath the starry sky but when we peer out, we see one single player, the Universe. I love doing research in astrophysics, starting from general chemical and physical properties and putting them in context of a global picture. I am looking forward to the powerful European Extremely Large Telescope, which will target many more hidden mysteries of the obscured Universe.

Staff at ESO

Konrad Tristram

To be honest right from the start: it was never my childhood dream to become an astrophysicist. I had totally different ideas of what I would like to become as a small boy: medical doctor, shopkeeper, bank clerk, tram driver. At some point, I even wanted to become a waste collector because they wore such nice orange suits. Rather, the path towards becoming an astrophysicist just laid itself out in front of me with time, especially during my studies at university.

My first notable contact with astronomy was during my last year at school when I picked astronomy as an optional course. I excelled at the astrophysical part. Learning the names of stars and constellations, on the other hand, was not my calling. Fortunately it turned out that this was not an important part of the course and I nevertheless got full marks. In fact, I remember standing out in the fields not

far from my parents' house identifying constellations and trying to learn by heart the names of their most important stars. Even today my orientation on the night sky is limited. For example, it took me about a year to find out that one of the galaxies I was working on for my PhD, the Circinus galaxy, was in fact called like that because it was the galaxy in the small southern constellation of Circinus, the Compass.

I started studying physics in the north German town of Rostock on the Baltic Sea. There I enjoyed the friendly atmosphere of the physics department, the good ratio of professors to students and above all the possibility to learn for exams on the beach. However, the choice of courses for specialisation was limited and upon receiving my Vordiplom I moved to Heidelberg, in order to have a larger field of options for research. At that time I was still dreaming of saving the world by contributing to physics with a practical



Konrad Tristram

use, for example by working on fusion power. However the group doing that at Heidelberg closed. "Fortunately" I must say from my current point of view.

When discussing options for a diploma thesis with professors, one of them suggested trying an internship at the Max Planck Institute for Astronomy (MPIA) up on the Königstuhl mountain. He assured me that astronomy was a promising field of research, in contrast to particle physics where the soon-to-be-expected discovery of the Higgs particle would lead to the conclusion that everything is more or less understood. I had already taken courses and practicals for astronomy as part of my curriculum with great interest and I was well prepared for a deeper experience in astrophysics. So I ended up at the MPIA for an internship, which then later turned into a diploma thesis under the supervision of Almudena Prieto and Hans-Walter Rix.

During my work for the diploma thesis, I started using the 70-centimetre KING telescope at the MPIA with great joy, in that sense my first observing experience. “Old school” as one would say now, sitting in the dark directly next to the telescope, counting the seconds until the exposure finished. With freezing hands and shivering in the winter. My interest in observing must have also come to the attention of my supervisors, because it did not take long before the first opportu-

nity arrived to get some “real” observing experience. Towards the second half of my diploma thesis, Hans-Walter Rix came into my office asking, on a normal Tuesday: “Do you want to go observing in Chile on Friday?” I was so astonished that it probably took me several minutes to speak a coherent sentence. An observing run had been changed from Service to Visitor Mode at short notice and, because everyone was busy, they were looking for an observer. It didn’t take too long for me to decide: on that Friday I was on my way to Chile for observations with SOFI at the NTT, my first contact with ESO and with Chile.

I still clearly remember Emanuela Pompei being my first support astronomer. I wouldn’t have imagined at that time that we would become colleagues now. Interestingly, this first trip remains my only observing trip to La Silla. From my second observing trip on, during my PhD thesis, I became a regular visitor to Paranal. It was the second observing run that sparked my interest not only in observations with the Very Large Telescope, but also in the country of Chile itself. I went observing together with Almudena Prieto and she strongly suggested that I should stay a few days longer to visit San Pedro de

Atacama. This first non-astronomical activity, as well as many subsequent ones, led me to get in contact with Chileans and to appreciate this country very much.

During my PhD, I specialised in studying the warm dust distributions around active galactic nuclei at the highest spatial resolution, mainly by infrared interferometry. After obtaining my degree from the University of Heidelberg I moved to the infrared interferometry group of Gerd Weigelt in Bonn, where I could continue and expand my research. Visits to Paranal deepened my connection with this observatory and I got to know my future colleagues more closely. My desire to work at this unique observatory grew over several years, but was brought to the point by the conclusion that observing was always the most fun part of my work as an astronomer. Also I grew more and more fond of Chile, the more I got to know it.

Now my wish has finally come true and I have started with an assignment as support astronomer at the VLT Interferometer. Exciting times are ahead of us with the arrival of the second-generation interferometric instruments and I am eagerly looking forward to the new possibilities these instruments will offer.



A busy night scene in January 2015 at La Silla taken from the 3.6-metre dome looking west to the Panamericana Highway (the source of all the light pollution). Comet Lovejoy is visible in the centre of the image, and the Pleiades open cluster (M45) and the California Nebula (NGC 1499) to the north (right). See Picture of the Week potw1504 for more details.

In Memoriam Luis Wendegass

Fernando Comerón¹

¹ ESO

Luis Wendegass passed away on 22 January 2015 at the age of 59 after a sudden heart attack. Luis joined ESO in September 1977 working at the La Silla Observatory, initially as Air Conditioning and Refrigeration Technician and lately in General Maintenance Support.

Luis devoted more than 37 years of his life to working at ESO, joining ESO when he was very young and also when ESO itself was quite young. During those four decades, ESO has grown and developed to become what it is today, setting a world-class standard in astronomy. This achievement owes much to the people

who, like Luis, tirelessly devoted the best of their professional lives to it, carrying out excellent work day after day and being an example to others.

The La Silla Observatory was an important part of Luis's life, and Luis will always be remembered as an important part of the life of the observatory. Luis was a cheerful and intelligent presence, and his help and wise advice could be counted on in all circumstances.

During those 37 years of professional service, Luis's colleagues became friends and a second family. Despite his long dedication, his unexpected departure still seems painfully premature. He will be deeply missed by his family and the many colleagues, current and past, who had the privilege of getting to know him and sharing with him the many tasks of the observatory.



Personnel Movements

Arrivals (1 January–31 March 2015)

Europe	
Cabrera Ziri Castro, Ivan (VE)	Student
Conlon, Pauline (UK)	HR Advisor
Egner, Sebastian Elias (DE)	Instrumentation Physicist
Jamialahmadi, Narges (IR)	Student
Rosenquist, Calle (SE)	Software Engineer

Chile	
Aguilera, Gregorio (CL)	Mechanical Technician
Arancibia, Jimmy (CL)	Technical Officer
Arrau, Maria Adriana (CL)	Secretary
Díaz Catalá, Eva Montserrat (ES)	Instrumentation Group Leader
Garafulich, Alicia (CL)	Administrative Assistant
Guerra, Juan Carlos (ES)	Instrumentation Engineer
Herrera, Cristian (CL)	Software Engineer
Pérez, Manuel Angel (ES)	Operation Staff Astronomer
Sani, Eleonora (IT)	Operation Staff Astronomer
Toledo, Pedro (CL)	Software Engineer
Torstensson, Karl (SE)	User Support astronomer

Departures (1 January–31 March 2015)

Europe	
Aniyan, Suryashree (IN)	Student
De Pascale, Marco (IT)	Student
Duchateau, Michel (FR)	Electronics Engineer

Chile	
Barkats, Denis (FR)	System Astronomer
Blanchard, Guillaume (FR)	Coating Expert/Optical Engineer
Esparza, Cristian (CL)	Telescope Instruments Operator
Mawet, Dimitri (BE)	Operation Staff Astronomer
Monaco, Lorenzo (IT)	Operation Staff Astronomer
Parraguez, Andres (CL)	Telescope Instruments Operator
Wiklind, Gert Tommy (SE)	Operation Staff Astronomer



ESO

European Organisation
for Astronomical
Research in the
Southern Hemisphere



ESO Studentship Programme 2015

The research studentship programme of the European Southern Observatory provides an outstanding opportunity for PhD students to experience the exciting scientific environment at one of the world's leading observatories for a period of up to two years.

ESO is the foremost intergovernmental astronomy organisation in Europe. Its approximately 110 staff astronomers, 40 Fellows and 50 PhD students conduct front-line research in fields ranging from exoplanets to cosmology, offering one of the most vibrant and stimulating scientific settings anywhere in the world.

ESO's studentship positions are open to students enrolled in a PhD programme in astronomy or related fields. Students accepted into the programme work on their doctoral project under the formal supervision of their home university, but they come to ESO to work and study under the co-supervision of an ESO staff astronomer, normally for a period of between one and two years. Studentships may be hosted either at ESO's Headquarters in Garching (Germany) or at ESO's offices in Santiago (Chile), where up to two positions per year are provided for students enrolled in South American universities.

Applicants and their home institute supervisors should agree upon and coordinate their research project jointly with their prospective ESO supervisor. For this purpose the ESO supervisor should be contacted well in advance of the application deadline (1 May 2015). A list of potential ESO supervisors and their research interests can be found at <http://www.eso.org/sci/activities/personnel.html>. A list of PhD projects currently being offered by ESO staff is available at <http://www.eso.org/sci/activities/thesis-topics.html>.

ESO Chile students have the opportunity to visit the observatories and to get involved in small technical projects aimed at giving insights into the observatory operations and instrumentation. Such involvement is also strongly encouraged for Garching students. In addition, students in Garching may attend and benefit from the series of lectures delivered in the framework of the International Max Planck Research School on Astrophysics. ESO students have also the possibility to join in many outreach activities.

Students who are already enrolled in a PhD programme in the Munich area (e.g., at the International Max Planck Research School on Astrophysics or a Munich University) and who wish to apply for an ESO studentship in Garching, should provide a compelling justification for their application.

If you are interested in enhancing your PhD experience through an extended stay at ESO, then please apply by completing the web application form available at <http://jobs.eso.org/>.

Please include the following documents in your application:

- a cover letter;
- a Curriculum Vitae, including a list of publications, if any;
- copies of your university transcript and certificate(s) or diploma(s);
- a summary of your master's thesis project (if applicable) and ongoing projects, indicating the title and the supervisor (maximum half a page);
- an outline of the proposed PhD project highlighting the advantages of coming to ESO (recommended one page, maximum two);

- the names and contact details of your home institute supervisor and the ESO local supervisor. They will be automatically invited to submit a recommendation letter, however, applicants are strongly advised to trigger these invitations (using the web application form) well in advance of the application deadline;
- a letter from the home institute that: i) guarantees financial support for the remaining PhD period after the termination of the ESO studentship; ii) indicates whether the prerequisites to obtain the PhD degree at the home institute have already been met.

All documents should be typed in English (but no translation is required for the certificates and diplomas).

The closing date for applications is 1 May 2015. Review of the application documents, including the recommendation letters, will begin immediately. Incomplete or late applications will not be considered.

Candidates will be notified of the results of the selection process during June–July 2015. Studentships will normally begin between August 2015 and March 2016.

Further information

For more information about the studentship programme please see: <http://www.eso.org/studentship>.

For a list of current ESO staff and fellows, and their research interests, please see: <http://www.eso.org/sci/activities/personnel.html>.

A list of PhD projects currently being offered by ESO staff can be found at: <http://www.eso.org/sci/activities/thesis-topics.html>.

Details on the employment conditions and benefits are available at: <http://www.eso.org/public/employment/student.html>.

For any additional questions, please contact:
For Garching: Eric Emsellem, Tel. +49 89 32006914, email: eric.emsellem@eso.org.
For Chile: Claudio De Figueiredo Melo, Tel. +56 2 4633032, email: cmelo@eso.org.

Although recruitment preference will be given to nationals of ESO Member States (Austria, Belgium, Brazil, the Czech Republic, Denmark, Finland, France, Germany, Italy, the Netherlands, Poland, Portugal, Spain, Sweden, Switzerland and United Kingdom), and, for Chile, to students enrolled in a South American university, no nationality is in principle excluded.

The post is equally open to suitably qualified female and male applicants.



Annual Index 2014 (Nos. 155–158)

Subject Index

Astronomical News

Celebrating Fifty Years of ESO in Chile; Comerón, F.; de Zeeuw, T.; 155, 48

Report on the Workshop Deconstructing Galaxies: Structure and Morphology in the Era of Large Surveys; Gadotti, D. A.; Sánchez-Janssen, R.; 155, 51

Report on the Workshop 400 Years of Stellar Rotation; de Medeiros, J. R.; Melo, C.; Pasquini, L.; 155, 55

Report on the ALMA Community Days: Preparing for Cycle 2; Randall, S.; Biggs, A.; Davis, T.; Lagos, C.; Stanke, T.; Testi, L.; Zwaan, M.; 155, 57

Fellows at ESO; Jones, D.; Muzic, K.; 155, 60

Personnel Movements; ESO; 155, 61

ESO Studentship Programme 2014; ESO; 155, 62

Report on the Workshop "Metal Production and Distribution in a Hierarchical Universe"; Saviane, I.; Bonifacio, P.; Spite, M.; Monaco, L.; 156, 47

Report on the Workshop "Exoplanet Observations with the E-ELT"; Spyromilio, J.; Liske, J.; 156, 51

Report on the ESO/RadioNet Workshop "3D2014: Gas and Stars in Galaxies: A Multi-wavelength 3D Perspective"; Lehnert, M.; De Breuck, C.; Kuntschner, H.; Zwaan, M. A.; 156, 53

Report on the Workshop "Seven Years in Chile: The Accomplishments and Goals of Czech Astronomers at ESO"; Kabáth, P.; Kawka, A.; Paunzen, E.; Vennes, S.; 156, 58

In Memoriam Stanislav Štefl; Baade, D.; 156, 60

Fellows at ESO; Gibson, N.; Lagos, C.; 156, 60

Personnel Movements; ESO; 156, 62

ESO Fellowship Programme 2014/2015; ESO; 156, 63

Report on the Workshop Herbig Ae/Be Stars: The Missing Link in Star Formation; de Wit, W.-J.; Oudmaijer, R. D.; van den Ancker, M. E.; Calvet, N.; 157, 50

Hans-Emil Schuster Celebrates his 80th Birthday; ESO; 157, 54

Fellows at ESO; Grunhut, J.; Geier, S.; 157, 54

External Fellows at ESO; Jiménez-Serra, I.; 157, 56

Announcement of the ESO Workshop ESO in the 2020s; ESO; 157, 57

Personnel Movements; ESO; 157, 58

Confirmation of the Messenger Subscription; ESO; 157, 58

Report on the Workshop Resolved and Unresolved Stellar Populations (RASPUTIN); Bono, G.; Valenti, E.; 158, 55

Jorge Melnick Retires from ESO; Madsen, C.; 158, 59

Fellows at ESO; Galametz, M.; Müller, A.; 158, 60

External Fellows at ESO; Maguire, K.; 158, 61

Personnel Movements; ESO; 158, 63

Confirmation of The Messenger Subscription; ESO; 158, 63

Astronomical Science

VISTA Variables in the Via Láctea (VVV): Halfway Status and Results; Hempel, M.; Minniti, D.; Dékány, I.; Saito, R. K.; Lucas, P. W.; Emerson, J. P.; Ahumada, A. V.; Aigrain, S.; Alonso, M. V.; Alonso-García, J.; Amôres, E. B.; Angeloni, R.; Arias, J.; Bandyopadhyay, R.; Barbá, R. H.; Barbuy, B.; Baume, G.; Beamin, J. C.; Bedin, L.; Bica, E.; Borissova, J.; Bronfman, L.; Carraro, G.; Catelan, M.; Clariá, J. J.; Contreras, C.; Cross, N.; Davis, C.; de Grijs, R.; Drew, J. E.; Fariña, C.; Feinstein, C.; Lajús, E. F.; Folkes, S.; Gamen, R. C.; Geisler, D.; Gieren, W.; Goldman, B.; González, O.; Gosling, A.; Gunthardt, G.; Gurovich, S.; Hambly, N. C.; Hanson, M.; Hoare, M.; Irwin, M. J.; Ivanov, V. D.; Jordán, A.; Kerins, E.; Kinemuchi, K.; Kurtsev, R.; Longmore, A.; López-Corredoira, M.; Maccarone, T.; Martín, E.; Masetti, N.; Mennickent, R. E.; Merlo, D.; Messineo, M.; Mirabel, I. F.; Monaco, L.; Moni-Bidin, C.; Morelli, L.; Padilla, N.; Palma, T.; Parisi, M. C.; Parker, Q.; Pavani, D.; Pietrukowicz, P.; Pietrzynski, G.; Pig-nata, G.; Rejkuba, M.; Rojas, A.; Roman-Lopes, A.; Ruiz, M. T.; Sale, S. E.; Saviane, I.; Schreiber, M. R.; Schröder, A. C.; Sharma, S.; Smith, M.; Sodr  Jr., L.; Soto, M.; Stephens, A. W.; Tamura, M.; Tappert, C.; Thompson, M. A.; Toledo, I.; Valenti, E.; Vanz, L.; Weidmann, W.; Zoccali, M.; 155, 24

Search for Supernovae in Starburst Galaxies with HAWK-I; Miluzio, M.; 155, 30

The VIMOS VLT Deep Survey: Final Public Release of ~ 35 000 Galaxies and Active Galactic Nuclei Covering 13 Billion Years of Evolution; Le Fèvre O.; Adami C.; Arnouts, S.; Bardelli, S.; Bolzonella, M.; Bondi, M.; Bongiorno, A.; Bottini, D.; Cappi, A.; Cassata, P.; Charlot, S.; Cillegi, P.; Contini, T.; Cucciati, O.; de la Torre, S.; Foucaud, S.; Franzetti, P.; Garilli, B.; Gavignaud, I.; Guzzo, L.; Ilbert, O.; Iovino, A.; Le Brun, V.; Lemaux, B.; López-Sanjuan, C.; Maccagni, D.; McCracken, H. J.; Marano, B.; Marinoni, C.; Mazure, A.; Mellier, Y.; Merighi, R.; Merluzzi, P.; Moreau, C.; Paltani, S.; Pell , R.; Pollo, A.; Pozzetti, L.; Scaramella, R.; Scoddeggio, M.; Tasca, L.; Tresse, L.; Vergani, D.; Vettolani, G.; Zamorani, G.; Zanichelli, A.; Zucca, E.; 155, 33

The VIMOS Ultra Deep Survey: 10 000 Galaxies to Study the Early Phases of Galaxy Assembly at $2 < z < 6+$; Le Fèvre O.; Amorin, R.; Bardelli, S.; Capak, P.; Cassara, L.; Cassata, P.; Castellano, M.; Charlot, S.; Cimatti, A.; Contini, T.; Cuby, J.; Cucciati, O.; Durkalec, A.; de la Torre, S.; Fontana, A.; Fotopoulou, S.; Garilli, B.; Gialvalisco, M.; Grazian, A.; Hathi, N.; Ilbert, O.; Le Brun, V.; Lemaux, B.; Lopez-Sanjuan, C.; Maccagni, D.; Mellier, Y.; Moreau, C.; Paltani, S.; Pentericci, L.; Ribeiro, B.; Salvato, M.; Schaerer, D.; Scoddeggio, M.; Scoville, N.; Sommariva, V.; Talia, M.; Taniguchi, Y.; Tasca, L.; Thomas, R.; Tresse, L.; Vanzella, E.; Vergani, D.; Wang, P.; Zamorani, G.; Zucca, E.; 155, 38

When VLT Meets HST: The HUGS Survey; Fontana, A.; Dunlop, J. S.; Paris, D.; Targett, T.; Boutsia, K.; Castellano, M.; Galametz, A.; Grazian, A.; McLure, R.; Merlin, E.; Pentericci, L.; Wuyts, S.; Almaini, O.; Caputi, K.; Chary, R.-R.; Cirasuolo, M.; Conselice, C.; Cooray, A.; Daddi, E.; Dickinson, M.; Faber, S. M.; Fazio, G.; Ferguson, H.; Giallongo, E.; Gialvalisco, M.; Grogin, N.; Hathi, N.; Koekemoer, A.; Koo, D. C.; Lucas, R.; Nonino, M.; Rix, H.-W.; Renzini, A.; Rosario, D.; Santini, P.; Scarlata, C.; Sommariva, V.; Stark, D. P.; van der Wel, A.; Vanzella, E.; Wild, V.; Yan, H.; Zibetti, S.; 155, 42

An Advanced Scattered Moonlight Model; Jones, A.; Noll, S.; Kausch, W.; Szyzska, C.; Kimeswenger, S.; 156, 31

A PIONIER View on Mass-transferring Red Giants; Boffin, M. M. J.; Blind, N.; Hillen, M.; Berger, J.-P.; Jorissen, A.; Le Bouquin, J.-B.; 156, 35

ALMA Resolves Turbulent, Rotating [C II] Emission in a Young Starburst Galaxy at $z = 48$; De Breuck, C.; Williams, R. J.; Swinbank, M.; Caselli, P.; Coppin, K.; Davis, T. A.; Maiolino, R.; Nagao, T.; Smail, I.; Walter, F.; Weiß, A.; Zwaan, M. A.; 156, 38

Combining ALMA with HST and VLT to Find the Counterparts of Submillimetre Galaxies; Wiklund, T.; Conselice, C. J.; Dahlen, T.; Dickinson, M. E.; Ferguson, H. C.; Grogin, N. A.; Guo, Y.; Koekemoer, A. M.; Mobasher, B.; Mortlock, A.; Fontana, A.; Dav , R.; Yan, H.; Acquaviva, V.; Ashby, M. L. N.; Barro, G.; Caputi, K. I.; Castellano, M.; Dekel, A.; Donley, J. L.; Fazio, G. G.; Gialvalisco, M.; Grazian, A.; Hathi, N. P.; Kurczynski, P.; Lu, Y.; McGrath, E. J.; de Mello, D. F.; Peth, M.; Safarzadeh, M.; Stefanon, M.; Targett, T.; 156, 40

The B Fields in OB Stars (BOB) Survey; Morel, T.; Castro, N.; Fossati, L.; Hubrig, S.; Langer, N.; Przybilla, N.; Sch ller, M.; Carroll, T.; Ilyin, I.; Irrgang, A.; Oskanova, L.; Schneider, F. R. N.; D az, S. S.; Briquet, M.; Gonz lez, J. F.; Kharchenko, N.; Nieva, M.-F.; Scholz, R.-D.; de Koter, A.; Hamann, W.-R.; Herrero, A.; Apell niz, J. M.; Sana, H.; Arlt, R.; Barb , R.; Dufton, P.; Kholtygin, A.; Mathys, G.; Piskunov, A.; Reisenegger, A.; Spruit, H.; Yoon, S.-C.; 157, 27

STEP: The VST Survey of the SMC and the Magellanic Bridge; Ripepi, V.; Cignoni, M.; Tosi, M.; Marconi, M.; Musella, I.; Grado, A.; Limatola, L.; Clementini, G.; Brocato, E.; Cantello, M.; Capaccioli, M.; Cappellaro, E.; Cioni, M.-R. L.; Cusano, F.; Dall'Ora, M.; Gallagher, J. S.; Grebel, E. K.; Nota, A.; Palla, F.; Romano, D.; Raimondo, G.; Sabbi, E.; Getman, F.; Napolitano, N. R.; Schipani, P.; Zaggia, S.; 157, 32

The KMOS Redshift One Spectroscopic Survey (KROSS); Bower, R.; Bureau, M.; 157, 38

ALESS: An ALMA Survey of Submillimetre Galaxies in the Extended Chandra Deep Field South; Smail, I.; Walter, F.; 157, 41

The Deepest VLT/FORS2 Spectrum of a $z \sim 7$ Galaxy: An Easy Target for the E-ELT; Vanzella, E.; Fontana, A.; Pentericci, L.; Castellano, M.; Grazian, A.; Gialvalisco, M.; Nonino, M.; Cristiani, S.; Zamorani, G.; Vignali, C.; 157, 46

The Eta Carinae Homunculus in Full 3D with X-shooter and Shape; Steffen, W.; Teodoro, M.; Madura, T. I.; Groh, J. H.; Gull, T. R.; Mehner, A.; Corcoran, M. F.; Damineli, A.; Hamaguchi, K.; 158, 26

The X-shooter Spectral Library (XSL) and its First Data Release; Chen, Y.-P.; Trager, S. C.; Peletier, R. F.; Lançon, A.; Vazdekis, A.; Prugniel, P.; Silva, D.; Gonneau, A.; Lyubenova, M.; Koleva, M.; Barroso, J. F.; Blázquez, P. S.; Walcher, C. J.; Choudhury, O. S.; Meneses-Goytia, S.; 158, 30

Catching Stellar Mergers at Work with the Very Large Telescope Interferometer; Millour, F.; Lagarde, E.; Marco, O. d.; Banerjee, D. P. K.; Mékarnia, D.; Spang, A.; Chesneau, O.; 158, 35

STREGA: STRucture and Evolution of the GALaxy with the VST; Marconi, M.; Musella, I.; Di Criscienzo, M.; Cignoni, M.; Dall'Or, M.; Bono, G.; Ripepi, V.; Brocato, E.; Raimondo, G.; Grado, A.; Limatola, L.; Coppola, G.; Moretti, M. I.; Stetson, P. B.; Calamida, A.; Cantello, M.; Capaccioli, M.; Cappellaro, E.; Cioni, M.-R. L.; Degl'Innocenti, S.; De Martino, D.; Di Cecco, A.; Ferraro, L.; Iannicola, G.; Moroni, P. G. P.; Silvotti, R.; Buonanno, R.; Getman, F.; Napolitano, N. R.; Pulone, L.; Schipani, P.; 158, 39

The Abundance of Lithium Measured for the First Time Beyond Our Galaxy; Mucciarelli, A.; Salaris, M.; Bonifacio, P.; Monaco, L.; Villanova, S.; 158, 45

CLASH-VLT: A VIMOS Large Programme to Map the Dark Matter Mass Distribution in Galaxy Clusters and Probe Distant Lensed Galaxies; Rosati, P.; Balestra, I.; Grillo, C.; Mercurio, A.; Nonino, M.; Biviano, A.; Girardi, M.; Vanzella, E.; CLASH-VLT Team; 158, 48

Telescopes and Instrumentation

ISAAC An Appreciation; Spyromilio, J.; Cuby, J.; Lidman, C.; Johnson R.; Jaunsen, A. O.; Mason, E.; Ivanov, V. D.; Schmidtbreick, L.; 155, 2

Laser Guide Star Facility Upgrade; Lewis, S.; Calia, D. B.; Buzzoni, B.; Duhoux, P.; Fischer, G.; Guidolin, I.; Haimel, A.; Hackenberg, W.; Hinterschuster, R.; Holzlohner, R.; Jolley, P.; Pfrommer, T.; Popovic, D.; Alvarez, J.-L.; Beltran, J.; Girard, J.; Pallanca, L.; Riquelme, M.; Gonté, F.; 155, 6

Speckle Imaging with VLT/NACO No-AO Mode; Rengaswamy, S.; Girard, J.; de Wit, W.-J.; Boffin, H.; 155, 12

Antarctic Air Visits Paranal — Opening New Science Windows; Kerber, F.; Kuntschner, H.; Querel, R. R.; van den Ancker, M.; 155, 17

The Calibration of ALMA using Radio Sources; Fomalont, E.; van Kempen, T.; Kneissl, R.; Marcelino, N.; Barkats, D.; Corder, S.; Cortes, P.; Hills, R.; Lucas, R.; Manning, A.; Peck, A.; 155, 19

The Adaptive Optics Facility Module GRAAL on its Way to Final Validation; Arsenault, R.; Paufigue, J.; Kolb, J.; Madec, P.-Y.; Kiekebusch, M.; Argomedo, J.; Jost, A.; Tordo, S.; Donaldson, R.; Suarez, M.; Conzelmann, R.; Kuntschner, H.; Siebenmorgen, R.; Kirchbauer, J.-P.; Rissmann, A.-G.; Schimpelsberger, J.; 156, 2

CRIRES+: Exploring the Cold Universe at High Spectral Resolution; Dorn, R. J.; Anglada-Escude, G.; Baade, D.; Bristow, P.; Follert, R.; Gojak, D.; Grunhut, J.; Hatzes, A.; Heiter, U.; Hilker, M.; Ives, D. J.; Jung, Y.; Käufel, H.-U.; Kerber, F.; Klein, B.; Lizon, J.-L.; Lockhart, M.; Löwinger, T.; Marquart, T.; Oliva, E.; Origlia, L.; Pasquini, L.; Paufigue, J.; Piskunov, N.; Pozna, E.; Reinert, A.; Smette, A.; Smoker, J.; Seemann, U.; Stempels, E.; Valenti, E.; 156, 7

NAOMI — A New Adaptive Optics Module for Interferometry; Dorn, R. J.; Aller-Carpentier, E.; Andolfato, L.; Berger, J.-P.; Delplancke-Ströbele, F.; Dupuy, C.; Fedrigo, E.; Gitton, P.; Hubin, N.; Le Louarn, M.; Lilley, P.; Jolley, P.; Marchetti, E.; Mclay, S.; Paufigue, J.; Pasquini, L.; Quentin, J.; Rakich, A.; Ridings, R.; Reyes, J.; Schmid, C.; Suarez, M.; Phan, D. T.; Woillez, J.; 156, 12

Mathematical Algorithms and Software for ELT Adaptive Optics — The Austrian In-kind Contributions for Adaptive Optics; Obereder, A.; Ramlau, R.; Fedrigo, E.; 156, 16

The X-shooter Imaging Mode; Martayan, C.; Mehner, A.; Beccari, G.; Peña, E.; Hummel, W.; Smette, A.; Modigliani, A.; Vernet, J.; Dekker, H.; Neumayer, N.; Mainieri, V.; Moehler, S.; Castillo, R.; Riquelme, M.; 156, 21

Phase 3 Status and Access to Science Data Products from ESO Public Surveys; Arnaboldi, M.; Delmotte, N.; Geier, S.; Mascetti, L.; Micol, A.; Retzlaff, J.; Romaniello, M.; 156, 24

An Overview of the MATISSE Instrument — Science, Concept and Current Status; Lopez, B.; Lagarde, S.; Jaffe, W.; Petrov, R.; Schöller, M.; Antonelli, P.; Beckmann, U.; Berio, P.; Bettonvil, F.; Glindemann, A.; Gonzalez, J.-C.; Graser, U.; Hofmann, K.-H.; Millour, F.; Robbe-Dubois, S.; Venema, L.; Wolf, S.; Henning, T.; Lanz, T.; Weigelt, G.; Agocs, T.; Baitel, C.; Bresson, Y.; Bristow, P.; Dugué, M.; Heininger, M.; Kroes, G.; Laun, W.; Lehmitz, M.; Neumann, U.; Augereau, J.-C.; Avila, G.; Behrend, J.; van Belle, G.; Berger, J.-P.; van Boekel, R.; Bonhomme, S.; Bourget, P.; Brast, R.; Clausse, J.-M.; Connot, C.; Conzelmann, R.; Cruzalèbes, P.; Csepman, G.; Danchi, W.; Delbo, M.; Delplancke, F.; Dominik, C.; van Duin, A.; Elswijk, E.; Fantei, Y.; Finger, G.; Gabasch, A.; Gay, J.; Girard, P.; Girault, V.; Gitton, P.; Glazenborg, A.; Gonté, F.; Guittou, F.; Guniat, S.; De Haan, M.; Haguenaer, P.; Hanenburg, H.; Hogerheijde, M.; ter Horst, R.; Hron, J.; Hugues, Y.; Hummel, C.; Idserda, J.; Ives, D.; Jakob, G.; Jasko, A.; Jolley, P.; Kiraly, S.; Köhler, R.; Kragt, J.; Kroener, T.; Kuindersma, S.; Labadie, L.; Leinert, C.; Le Poole, R.; Lizon, J.-L.; Lucuix, C.; Marcotto, A.; Martinache, F.; Martinot-Lagarde, G.; Mathar, R.; Matter, R.; Mauclert, N.; Mehrgan, L.; Meilland, A.; Meisenheimer, K.; Meisner, J.; Mellein, M.; Menardi, S.; Menut, J.-L.; Merand, A.; Morel, S.; Mosoni, L.; Navarro, R.; Nussbaum, E.; Ottogalli, S.; Palsa, R.; Panduro, J.; Pantin, E.; Parra, T.; Percheron, I.; Duc, T. P.; Pott, J.-U.; Pozna, E.; Przygodda, F.; Rabbia, Y.; Richichi, A.; Rigal, F.; Roelfsema, R.; Rupprecht, G.; Schertl, D.; Schmidt, C.; Schuhler, N.; Schuil, M.; Spang, A.; Stegmeier, J.; Thiam, L.; Tromp, N.; Vakili, F.; Vannier, M.; Wagner, K.; Woillez, J.; 157, 5

MUSE Commissioning; Bacon, R.; Vernet, J.; Borisiva, E.; Bouché, N.; Brinchmann, J.; Carollo, M.; Carton, D.; Caruana, J.; Cerda, S.; Contini, T.; Franx, M.; Girard, M.; Guerou, A.; Haddad, N.; Hau, G.; Herenz, C.; Herrera, J. C.; Husemann, B.; Husser, T.-O.; Jarno, A.; Kamann, S.; Krajnovic, D.; Lilly, S.; Mainieri, V.; Martinsson, T.; Palsa, R.; Patricio, V.; Pécontal, A.; Pello, R.; Piqueras, L.; Richard, J.; Sandin, C.; Schroetter, I.; Selman, F.; Shirazi, M.; Smette, A.; Soto, K.; Streicher, O.; Urrutia, T.; Weilbacher, P.; Wisotzki, L.; Zins, G.; 157, 13

Ensuring the Reliability and Performance of Instrumentation at the Paranal Observatory; Gonté, F.; Smette, A.; Abadie, S.; Alvarez, J. L.; Baksai, P.; Beltran, J.; Boffin, H.; Bourget, P.; Carraro, G.; Castillo, R.; de Wit, W.-J.; Diaz, A.; Gadotti, D.; Girard, J.; Haddad, N.; Hau, G.; Ivanov, V.; Lizon, J.-L.; Mardones, P.; Mérand, A.; Mieske, S.; Monaco, L.; O'Neal, J.; Pallanca, L.; Pompei, E.; Ramirez, A.; Riquelme, M.; Rojas, C.; Schmitobreick, L.; Schmutzer, R.; Smoker, J.; Valenzuela, J. J.; Zins, G.; 157, 17

Fifteen Years of Service Mode Operations: Closing the Loop with the Community; Primas, F.; Tacconi-Garman, L.; Marteau, S.; Mainieri, V.; Rejkuba, M.; Mysore, S.; Dumas, C.; Kaufer, A.; Patat, F.; Sterzik, M.; 158, 8

Flux Calibration of Medium Resolution Spectra from 300 nm to 2500 nm — Model Reference Spectra and Telluric Correction; Moehler, S.; Modigliani, A.; Freudling, W.; Giammichele, N.; Gianninas, A.; Gonneau, A.; Kausch, W.; Lançon, A.; Noll, S.; Rauch, T.; Vinther, J.; 158, 16

The GIRAFFE Archive: Reduced Spectra and Datacubes from the VLT FLAMES GIRAFFE Spectrograph; Royer, F.; Jégouzo, I.; Haigron, R.; Tajahmady, F.; Plassard, F.; 158, 21

The Organisation

Groundbreaking for the European Extremely Large Telescope (E-ELT); ESO; 157, 2

Signing of ESO-Poland Accession Agreement; ESO; 158, 2

Constructing the E-ELT; de Zeeuw, T.; Tamai, R.; Liske, J.; 158, 3

Author Index

A

- Arnaboldi, M.; Delmotte, N.; Geier, S.; Mascetti, L.; Micol, A.; Retzlaff, J.; Romaniello, M.; Phase 3 Status and Access to Science Data Products from ESO Public Surveys; 156, 24
- Arsenault, R.; Paufigue, J.; Kolb, J.; Madec, P.-Y.; Kiekebusch, M.; Argomedo, J.; Jost, A.; Tordo, S.; Donaldson, R.; Suarez, M.; Conzelmann, R.; Kuntschner, H.; Siebenmorgen, R.; Kirchbauer, J.-P.; Rissmann, A.-G.; Schimpelsberger, J.; The Adaptive Optics Facility Module GRAAL on its Way to Final Validation; 156, 2

B

- Baade, D.; In Memoriam Stanislav Štefl; 156, 60
- Bacon, R.; Vernet, J.; Borisiva, E.; Bouché, N.; Brinchmann, J.; Carollo, M.; Carton, D.; Caruana, J.; Cerda, S.; Contini, T.; Franx, M.; Girard, M.; Guerou, A.; Haddad, N.; Hau, G.; Herenz, C.; Herrera, J. C.; Husemann, B.; Husser, T.-O.; Jarno, A.; Kamann, S.; Krajnovic, D.; Lilly, S.; Mainieri, V.; Martinsson, T.; Palsa, R.; Patricio, V.; Pécontal, A.; Pello, R.; Piqueras, L.; Richard, J.; Sandin, C.; Schroetter, I.; Selman, F.; Shirazi, M.; Smette, A.; Soto, K.; Streicher, O.; Urrutia, T.; Weilbacher, P.; Wisotzki, L.; Zins, G.; MUSE Commissioning; 157, 13
- Boffin, H. M. J.; Blind, N.; Hillen, M.; Berger, J.-P.; Jorissen, A.; Le Bouquin, J.-B.; A PIONIER View on Mass-transferring Red Giants; 156, 35
- Bono, G.; Valenti, E.; Report on the Workshop Resolved and Unresolved Stellar PopUlaTioNs (RASPUTIN); 158, 55
- Bower, R.; Bureau, M.; The KMOS Redshift One Spectroscopic Survey (KROSS); 157, 38

C

- Chen, Y.-P.; Trager, S. C.; Peletier, R. F.; Lançon, A.; Vazdekis, A.; Prugniel, P.; Silva, D.; Gonneau, A.; Lyubenova, M.; Koleva, M.; Barroso, J. F.; Blázquez, P. S.; Walcher, C. J.; Choudhury, O. S.; Meneses-Goytia, S.; The X-shooter Spectral Library (XSL) and its First Data Release; 158, 30
- Comerón, F.; de Zeeuw, T.; Celebrating Fifty Years of ESO in Chile; 155, 48

D

- De Brueck, C.; Williams, R. J.; Swinbank, M.; Caselli, P.; Coppin, K.; Davis, T. A.; Maiolino, R.; Nagao, T.; Smail, I.; Walter, F.; Weiß, A.; Zwaan, M. A.; ALMA Resolves Turbulent, Rotating [C II] Emission in a Young Starburst Galaxy at $z = 48$; 156, 38
- de Medeiros, J. R.; Melo, C.; Pasquini, L.; Report on the Workshop 400 Years of Stellar Rotation; 155, 55
- de Wit, W.-J.; Oudmaijer, R. D.; van den Ancker, M. E.; Calvet, N.; Report on the Workshop Herbig Ae/Be Stars: The Missing Link in Star Formation; 157, 50
- de Zeeuw, T.; Tamai, R.; Liske, J.; Constructing the E-ELT; 158, 3

- Dorn, R. J.; Anglada-Escude, G.; Baade, D.; Bristow, P.; Follert, R.; Gojak, D.; Grunhut, J.; Hatzes, A.; Heiter, U.; Hilker, M.; Ives, D. J.; Jung, Y.; Käufl, H.-U.; Kerber, F.; Klein, B.; Lizon, J.-L.; Lockhart, M.; Löwinger, T.; Marquart, T.; Oliva, E.; Origlia, L.; Pasquini, L.; Paufigue, J.; Piskunov, N.; Pozna, E.; Reiners, A.; Smette, A.; Smoker, J.; Seemann, U.; Stempels, E.; Valenti, E.; CRILES+: Exploring the Cold Universe at High Spectral Resolution; 156, 7
- Dorn, R. J.; Aller-Carpentier, E.; Andolfato, L.; Berger, J.-P.; Delplancke-Ströbele, F.; Dupuy, C.; Fedrigo, E.; Gitton, P.; Hubin, N.; Le Louarn, M.; Lilley, P.; Jolley, P.; Marchetti, E.; Mclay, S.; Paufigue, J.; Pasquini, L.; Quentin, J.; Rakich, A.; Ridings, R.; Reyes, J.; Schmid, C.; Suarez, M.; Phan, D. T.; Woillez, J.; NAOMI — A New Adaptive Optics Module for Interferometry; 156, 12

F

- Fomalont, E.; van Kempen, T.; Kneissl, R.; Marcelino, N.; Barkats, D.; Corder, S.; Cortes, P.; Hills, R.; Lucas, R.; Manning, A.; Peck, A.; The Calibration of ALMA using Radio Sources; 155, 19
- Fontana, A.; Dunlop, J. S.; Paris, D.; Targett, T.; Boutsia, K.; Castellano, M.; Galametz, A.; Grazian, A.; McLure, R.; Merlin, E.; Pentericci, L.; Wuyts, S.; Almaini, O.; Caputi, K.; Chary, R.-R.; Cirasuolo, M.; Conselice, C.; Cooray, A.; Daddi, E.; Dickinson, M.; Faber, S. M.; Fazio, G.; Ferguson, H.; Giallongo, E.; Giavalisco, M.; Grogin, N.; Hathi, N.; Koekemoer, A.; Koo, D. C.; Lucas, R.; Nonino, M.; Rix, H.-W.; Renzini, A.; Rosario, D.; Santini, P.; Scarlata, C.; Sommariva, V.; Stark, D. P.; van der Wel, A.; Vanzella, E.; Wild, V.; Yan, H.; Zibetti, S.; When VLT Meets HST: The HUGS Survey; 155, 42

G

- Gadotti, D. A.; Sánchez-Janssen, R.; Report on the Workshop Deconstructing Galaxies: Structure and Morphology in the Era of Large Surveys; 155, 51
- Galametz, M.; Fellows at ESO; 158, 60
- Geier, S.; Fellows at ESO; 157, 54
- Gibson, N.; Fellows at ESO; 156, 60
- Gonté, F.; Smette, A.; Abadie, S.; Alvarez, J. L.; Baksai, P.; Beltran, J.; Boffin, H.; Bourget, P.; Carraro, G.; Castillo, R.; de Wit, W.-J.; Díaz, A.; Gadotti, D.; Girard, J.; Haddad, N.; Hau, G.; Ivanov, V.; Lizon, J.-L.; Mardones, P.; Mérand, A.; Mieske, S.; Monaco, L.; O'Neal, J.; Pallanca, L.; Pompei, E.; Ramirez, A.; Riquelme, M.; Rojas, C.; Schmitobreick, L.; Schmutzer, R.; Smoker, J.; Valenzuela, J. J.; Zins, G.; Ensuring the Reliability and Performance of Instrumentation at the Paranal Observatory; 157, 17
- Grunhut, J.; Fellows at ESO; 157, 54

H

- Hempel, M.; Minniti, D.; Dékány, I.; Saito, R. K.; Lucas, P. W.; Emerson, J. P.; Ahumada, A. V.; Aigrain, S.; Alonso, M. V.; Alonso-García, J.; Amôres, E. B.; Angeloni, R.; Arias, J.; Bandyopadhyay, R.; Barbá, R. H.; Barbuy, B.; Baume, G.; Beamin, J. C.; Bedin, L.; Bica, E.; Borissova, J.; Bronfman, L.; Carraro, G.; Catelan, M.; Clariá, J. J.; Contreras, C.; Cross, N.; Davis, C.; de Grijs, R.; Drew, J. E.; Fariña, C.; Feinstein, C.; Lajús, E. F.; Folkes, S.; Gamen, R. C.; Geisler, D.; Gieren, W.; Goldman, B.; González, O.; Gosling, A.; Gunthardt, G.; Gurovich, S.; Hambly, N. C.; Hanson, M.; Hoare, M.; Irwin, M. J.; Ivanov, V. D.; Jordán, A.; Kerins, E.; Kinemuchi, K.; Kurtev, R.; Longmore, A.; López-Corredoira, M.; Maccarone, T.; Martín, E.; Masetti, N.; Mennickent, R. E.; Merlo, D.; Messineo, M.; Mirabel, I. F.; Monaco, L.; Moni-Bidin, C.; Morelli, L.; Padilla, N.; Palma, T.; Parisi, M. C.; Parker, Q.; Pavani, D.; Pietrukowicz, P.; Pietrzynski, G.; Pignata, G.; Rejkuba, M.; Rojas, A.; Roman-Lopes, A.; Ruiz, M. T.; Sale, S. E.; Saviane, I.; Schreiber, M. R.; Schröder, A. C.; Sharma, S.; Smith, M.; Sodré Jr., L.; Soto, M.; Stephens, A. W.; Tamura, M.; Tappert, C.; Thompson, M. A.; Toledo, I.; Valenti, E.; Vanzi, L.; Weidmann, W.; Zoccali, M.; VISTA Variables in the Vía Láctea (VVV): Halfway Status and Results; 155, 24

J

- Jiménez-Serra, I.; External Fellows at ESO; 157, 56
- Jones, A.; Noll, S.; Kausch, W.; Szyszka, C.; Kimeswenger, S.; An Advanced Scattered Moonlight Model; 156, 31
- Jones, D.; Fellows at ESO; 155, 60

K

- Kabáth, P.; Kawka, A.; Paunzen, E.; Vennes, S.; Report on the Workshop “Seven Years in Chile: The Accomplishments and Goals of Czech Astronomers at ESO”; 156, 58
- Kerber, F.; Kuntschner, H.; Queral, R. R.; van den Ancker, M.; Antarctic Air Visits Paranal — Opening New Science Windows; 155, 17

L

- Lagos, C.; Fellows at ESO; 156, 60
- Le Fèvre, O.; Adami, C.; Arnouts, S.; Bardelli, S.; Bolzonella, M.; Bondi, M.; Bongiorno, A.; Bottini, D.; Cappi, A.; Cassata, P.; Charlot, S.; Ciliegi, P.; Contini, T.; Cucciati, O.; de la Torre, S.; Foucaud, S.; Franzetti, P.; Garilli, B.; Gavignaud, I.; Guzzo, L.; Ilbert, O.; Iovino, A.; Le Brun, V.; Lemaux, B.; López-Sanjuan, C.; Maccagni, D.; McCracken, H. J.; Marano, B.; Marinoni, C.; Mazure, A.; Mellier, Y.; Merighi, R.; Merluzzi, P.; Moreau, C.; Paltani, S.; Pelló, R.; Pollo, A.; Pozzetti, L.; Scaramella, R.; Scoddeggio, M.; Tasca, L.; Tresse, L.; Vergani, D.; Vettolani, G.; Zamorani, G.; Zanichelli, A.; Zucca, E.; The VIMOS VLT Deep Survey: Final Public Release of ~ 35 000 Galaxies and Active Galactic Nuclei Covering 13 Billion Years of Evolution; 155, 33

- Le Fèvre O.; Amorin, R.; Bardelli, S.; Capak, P.; Cassara, L.; Cassata, P.; Castellano, M.; Charlot, S.; Cimatti, A.; Contini, T.; Cuby, J.; Cucciati, O.; Durkalec, A.; de la Torre, S.; Fontana, A.; Fotopoulou, S.; Garilli, B.; Giavalisco, M.; Grazian, A.; Hathi, N.; Ilbert, O.; Le Brun, V.; Lemaux, B.; Lopez-Sanjuan, C.; Maccagni, D.; Mellier, Y.; Moreau, C.; Paltani, S.; Pentericci, L.; Ribeiro, B.; Salvato, M.; Schaerer, D.; Scoddeggio, M.; Scoville, N.; Sommariva, V.; Talia, M.; Taniguchi, Y.; Tasca, L.; Thomas, R.; Tresse, L.; Vanzella, E.; Vergani, D.; Wang, P.; Zamorani, G.; Zucca, E.; The VIMOS Ultra Deep Survey: 10 000 Galaxies to Study the Early Phases of Galaxy Assembly at $2 < z < 6+$; 155, 38
- Lehnert, M.; De Breuck, C.; Kuntschner, H.; Zwaan, M. A.; Report on the ESO/RadioNet Workshop "3D 2014: Gas and Stars in Galaxies: A Multi-wavelength 3D Perspective"; 156, 53
- Lewis, S.; Calia, D. B.; Buzzoni, B.; Duhoux, P.; Fischer, G.; Guidolin, I.; Haimel, A.; Hackenberg, W.; Hinterschuster, R.; Holzlöhrner, R.; Jolley, P.; Pfrommer, T.; Popovic, D.; Alvarez, J.-L.; Beltran, J.; Girard, J.; Pallanca, L.; Riquelme, M.; Gonté, F.; Laser Guide Star Facility Upgrade; 155, 6
- Lopez, B.; Lagarde, S.; Jaffe, W.; Petrov, R.; Schöller, M.; Antonelli, P.; Beckmann, U.; Berio, P.; Bettonvil, F.; Glindemann, A.; Gonzalez, J.-C.; Graser, U.; Hofmann, K.-H.; Millour, F.; Robbe-Dubois, S.; Venema, L.; Wolf, S.; Henning, T.; Lanz, T.; Weigelt, G.; Agocs, T.; Bailet, C.; Bresson, Y.; Bristow, P.; Dugué, M.; Heininger, M.; Kroes, G.; Laun, W.; Lehmitz, M.; Neumann, U.; Augereau, J.-C.; Avila, G.; Behrend, J.; van Belle, G.; Berger, J.-P.; van Boekel, R.; Bonhomme, S.; Bourget, P.; Brast, R.; Clausse, J.-M.; Connot, C.; Conzelmann, R.; Cruzalébes, P.; Csepany, G.; Danchi, W.; Delbo, M.; Delplancke, F.; Dominik, C.; van Duin, A.; Elswijk, E.; Fantei, Y.; Finger, G.; Gabasch, A.; Gay, J.; Girard, P.; Girault, V.; Gitton, P.; Glazenberg, A.; Gonté, F.; Guitton, F.; Guniat, S.; De Haan, M.; Haguenauer, P.; Hanenburg, H.; Hogerheijde, M.; ter Horst, R.; Hron, J.; Hugues, Y.; Hummel, C.; Idserda, J.; Ives, D.; Jakob, G.; Jasko, A.; Jolley, P.; Kiraly, S.; Köhler, R.; Kragt, J.; Kroener, T.; Kuindersma, S.; Labadie, L.; Leinert, C.; Le Poole, R.; Lizon, J.-L.; Lucuix, C.; Marcotto, A.; Martinache, F.; Martinot-Lagarde, G.; Mathar, R.; Matter, A.; Mauclert, N.; Mehrgan, L.; Meilland, A.; Meisenheimer, K.; Meisner, J.; Mellein, M.; Menardi, S.; Menut, J.-L.; Merand, A.; Morel, S.; Mosoni, L.; Navarro, R.; Nussbaum, E.; Ottogalli, S.; Palsa, R.; Panduro, J.; Pantin, E.; Parra, T.; Percheron, I.; Duc, T. P.; Pott, J.-U.; Pozna, E.; Przygodda, F.; Rabbia, Y.; Richichi, A.; Rigal, F.; Roelfsema, R.; Rupprecht, G.; Schertl, D.; Schmidt, C.; Schuhler, N.; Schuil, M.; Spang, A.; Stegmeier, J.; Thiam, L.; Tromp, N.; Vakili, F.; Vannier, M.; Wagner, K.; Woillez, J.; An Overview of the MATISSE Instrument — Science, Concept and Current Status; 157, 5
- Madsen, C.; Jorge Melnick Retires from ESO; 158, 59
- Maguire, K.; External Fellows at ESO; 158, 61
- Marconi, M.; Musella, I.; Di Criscienzo, M.; Cignoni, M.; Dall'Ora, M.; Bono, G.; Ripepi, V.; Brocato, E.; Raimondo, G.; Grado, A.; Limatola, L.; Coppola, G.; Moretti, M. I.; Stetson, P. B.; Calamida, A.; Cantiello, M.; Capaccioli, M.; Cappellaro, E.; Cioni, M.-R. L.; Degl'Innocenti, S.; De Martino, D.; Di Cecco, A.; Ferraro, I.; Iannicola, G.; Moroni, P. G. P.; Silvotti, R.; Buonanno, R.; Getman, F.; Napolitano, N. R.; Pulone, L.; Schipani, P.; STREGA: STRucture and Evolution of the GALaxy with the VST; 158, 39
- Martayan, C.; Mehner, A.; Beccari, G.; Peña, E.; Hummel, W.; Smette, A.; Modigliani, A.; Vernet, J.; Dekker, H.; Neumayer, N.; Mainieri, V.; Moehler, S.; Castillo, R.; Riquelme, M.; The X-shooter Imaging Mode; 156, 21
- Millour, F.; Lagadec, E.; Marco, O. d.; Banerjee, D. P. K.; Mékarnia, D.; Spang, A.; Chesneau, O.; Catching Stellar Mergers at Work with the Very Large Telescope Interferometer; 158, 35
- Miluzio, M.; Search for Supernovae in Starburst Galaxies with HAWK-I; 155, 30
- Moehler, S.; Modigliani, A.; Freudling, W.; Giammichele, N.; Gianninas, A.; Gonneau, A.; Kausch, W.; Lançon, A.; Noll, S.; Rauch, T.; Vinther, J.; Flux Calibration of Medium Resolution Spectra from 300 nm to 2500 nm — Model Reference Spectra and Telluric Correction; 158, 16
- Morel, T.; Castro, N.; Fossati, L.; Hubrig, S.; Langer, N.; Przybilla, N.; Schöller, M.; Carroll, T.; Ilyin, I.; Irrgang, A.; Oskinova, L.; Schneider, F. R. N.; Díaz, S. S.; Briquet, M.; González, J. F.; Kharchenko, N.; Nieva, M.-F.; Scholz, R.-D.; de Koter, A.; Hamann, W.-R.; Herrero, A.; Apellániz, J. M.; Sana, H.; Arlt, R.; Barbá, R.; Dufton, P.; Kholtygin, A.; Mathys, G.; Piskunov, A.; Reisenegger, A.; Spruit, H.; Yoon, S.-C.; The B Fields in OB Stars (BOB) Survey; 157, 27
- Müller, A.; Fellows at ESO; 158, 60
- Mucciarelli, A.; Salari, M.; Bonifacio, P.; Monaco, L.; Villanova, S.; The Abundance of Lithium Measured for the First Time Beyond Our Galaxy; 158, 45
- Muzik, K.; Fellows at ESO; 155, 60
- Obereder, A.; Ramlau, R.; Fedrigo, E.; Mathematical Algorithms and Software for ELT Adaptive Optics — The Austrian In-kind Contributions for Adaptive Optics; 156, 16
- Primas, F.; Tacconi-Garman, L.; Marteau, S.; Mainieri, V.; Rejkuba, M.; Mysore, S.; Dumas, C.; Kaufer, A.; Patat, F.; Sterzik, M.; Fifteen Years of Service Mode Operations: Closing the Loop with the Community; 158, 8
- Randall, S.; Biggs, A.; Davis, T.; Lagos, C.; Stanke, T.; Testi, L.; Zwaan, M.; Report on the ALMA Community Days: Preparing for Cycle 2; 155, 57
- Rengaswamy, S.; Girard, J.; de Wit, W.-J.; Boffin, H.; Speckle Imaging with VLT/NACO No-AO Mode; 155, 12
- Ripepi, V.; Cignoni, M.; Tosi, M.; Marconi, M.; Musella, I.; Grado, A.; Limatola, L.; Clementini, G.; Brocato, E.; Cantiello, M.; Capaccioli, M.; Cappellaro, E.; Cioni, M.-R. L.; Cusano, F.; Dall'Ora, M.; Gallagher, J. S.; Grebel, E. K.; Nota, A.; Palla, F.; Romano, D.; Raimondo, G.; Sabbi, E.; Getman, F.; Napolitano, N. R.; Schipani, P.; Zaggia, S.; STEP: The VST Survey of the SMC and the Magellanic Bridge; 157, 32
- Rosati, P.; Balestra, I.; Grillo, C.; Mercurio, A.; Nonino, M.; Biviano, A.; Girardi, M.; Vanzella, E.; CLASH-VLT Team; CLASH-VLT: A VIMOS Large Programme to Map the Dark Matter Mass Distribution in Galaxy Clusters and Probe Distant Lensed Galaxies; 158, 48
- Royer, F.; Jégouzo, I.; Haigron, R.; Tajahmady, F.; Plassard, F.; The GIRAFFE Archive: Reduced Spectra and Datacubes from the VLT FLAMES GIRAFFE Spectrograph; 158, 21
- Saviane, I.; Bonifacio, P.; Spite, M.; Monaco, L.; Report on the Workshop "Metal Production and Distribution in a Hierarchical Universe"; 156, 47
- Smail, I.; Walter, F.; ALESS: An ALMA Survey of Submillimetre Galaxies in the Extended Chandra Deep Field South; 157, 41
- Spyromilio, J.; Cuby, J.; Lidman, C.; Johnson, R.; Jaunsen, A. O.; Mason, E.; Ivanov, V. D.; Schmidtobreich, L.; ISAAC An Appreciation; 155, 2
- Spyromilio, J.; Liske, J.; Report on the Workshop "Exoplanet Observations with the E-ELT"; 156, 51
- Steffen, W.; Teodoro, M.; Madura, T. I.; Groh, J. H.; Gull, T. R.; Mehner, A.; Corcoran, M. F.; Daminelli, A.; Hamaguchi, K.; The Eta Carinae Homunculus in Full 3D with X-shooter and Shape; 158, 26
- Vanzella, E.; Fontana, A.; Pentericci, L.; Castellano, M.; Grazian, A.; Giavalisco, M.; Nonino, M.; Cristiani, S.; Zamorani, G.; Vignali, C.; The Deepest VLT/FORS2 Spectrum of a $z \sim 7$ Galaxy: An Easy Target for the E-ELT; 157, 46
- Wiklund, T.; Conselice, C. J.; Dahlen, T.; Dickinson, M. E.; Ferguson, H. C.; Grogin, N. A.; Guo, Y.; Koekemoer, A. M.; Mobasher, B.; Mortlock, A.; Fontana, A.; Davé, R.; Yan, H.; Acquaviva, V.; Ashby, M. L. N.; Barro, G.; Caputi, K. I.; Castellano, M.; Dekel, A.; Donley, J. L.; Fazio, G. G.; Giavalisco, M.; Grazian, A.; Hathi, N. P.; Kurczynski, P.; Lu, Y.; McGrath, E. J.; de Mello, D. F.; Peth, M.; Safarzadeh, M.; Stefanon, M.; Targett, T.; Combining ALMA with HST and VLT to Find the Counterparts of Submillimetre Galaxies; 156, 40

ESO, the European Southern Observatory, is the foremost intergovernmental astronomy organisation in Europe. It is supported by 16 countries: Austria, Belgium, Brazil, the Czech Republic, Denmark, France, Finland, Germany, Italy, the Netherlands, Poland, Portugal, Spain, Sweden, Switzerland and the United Kingdom. ESO's programme is focused on the design, construction and operation of powerful ground-based observing facilities. ESO operates three observatories in Chile: at La Silla, at Paranal, site of the Very Large Telescope, and at Llano de Chajnantor. ESO is the European partner in the Atacama Large Millimeter/submillimeter Array (ALMA). Currently ESO is engaged in the design of the European Extremely Large Telescope.

The Messenger is published, in hard-copy and electronic form, four times a year: in March, June, September and December. ESO produces and distributes a wide variety of media connected to its activities. For further information, including postal subscription to The Messenger, contact the ESO education and Public Outreach Department at:

ESO Headquarters
Karl-Schwarzschild-Straße 2
85748 Garching bei München, Germany
Phone +49 89 320 06-0
information@eso.org

The Messenger:
Editor: Jeremy R. Walsh;
Design, Production: Jutta Boxheimer;
Layout, Typesetting: Mafalda Martins;
Graphics: Lorenzo Benassi.
www.eso.org/messenger/

Printed by Color Gruppe
Geretsrieder Straße 10
81379 München, Germany

Unless otherwise indicated, all images in The Messenger are courtesy of ESO, except authored contributions which are courtesy of the respective authors.

© ESO 2015
ISSN 0722-6691

Contents

Telescopes and Instrumentation

Leibundgut B. et al. – SPHERE Science Verification	2
Boffin H. et al. – Making FORS2 Fit for Exoplanet Observations (again)	6
Moehler S. et al. – Improving the Quality of FORS2 Reduced Spectra	10
Käufl H. U. et al. – The Return of the Mid-infrared to the VLT: News from the VISIR Upgrade	15
Martinez P. et al. – The SPEED Project: SPEEDing up Research and Development towards High-contrast Imaging Instruments for the E-ELT	19

Astronomical Science

Ertel S. et al. – An Unbiased Near-infrared Interferometric Survey for Hot Exozodiacal Dust	24
Clark S. et al. – An Astrophysical Laboratory: Understanding and Exploiting the Young Massive Cluster Westerlund 1	30
Zoccali M. et al. – The GIRAFFE Inner Bulge Survey (GIBS)	36
Shahzamanian B. et al. – Variable and Polarised Near-infrared Emission from the Galactic Centre	41
Cantiello M. et al. – VEGAS-SSS: A VST Programme to Study the Satellite Stellar Systems around Bright Early-type Galaxies	46

Astronomical News

Boffin H. et al. – Report on the ESO Workshop “Astronomy at High Angular Resolution”	52
Roche P. – New President of Council	57
Fellows at ESO – B. Husemann, T. Zafar	58
Staff at ESO – K. Tristram	60
Comerón F. – In Memoriam Luis Wendegass	62
Personnel Movements	62
ESO Studentship Programme 2015	63
Annual Index 2014 (Nos. 155–158)	64

Front cover: Colour-composite image of the open cluster NGC 3293 taken with the MPG/ESO 2.2-metre telescope and Wide Field Imager (WFI). Broadband images in *B*, *V* and *I* and a narrowband *H α* image were combined and the image size is 23 by 32 arcminutes. NGC 3293 is a rather well-studied young open cluster in the Milky Way at a distance of about 2800 pc with an age of ~ 8 Myr and still has stars evolving onto the main sequence.
Credit: ESO/G. Beccari

